

ISTANBUL TECHNICAL UNIVERSITY ★ ENERGY INSTITUTE

**INVESTIGATION OF ANODE PROPERTIES AND BATTERY
PERFORMANCES OF METAL MIXED GRAPHITES
FOR LITHIUM ION BATTERIES**

M.Sc. THESIS

Handan BAKALCI

Department of Energy Science and Technology

Energy Science and Technology Programme

JANUARY 2015

ISTANBUL TECHNICAL UNIVERSITY ★ ENERGY INSTITUTE

**INVESTIGATION OF ANODE PROPERTIES AND BATTERY
PERFORMANCES OF METAL MIXED GRAPHITES
FOR LITHIUM ION BATTERIES**

M.Sc. THESIS

**Handan BAKALCI
(301091051)**

Department of Energy Science and Technology

Energy Science and Technology Programme

Thesis Advisor: Prof. Dr. Nilgün KARATEPE YAVUZ

JANUARY 2015

İSTANBUL TEKNİK ÜNİVERSİTESİ ★ ENERJİ ENSTİTÜSÜ

**LİTYUM İYON PİLLERDE METAL İLE KATKILANDIRILMIŞ
GRAFİTLERİN ANOT ÖZELLİKLERİNİN VE
PİL PERFORMANSLARININ İNCELENMESİ**

YÜKSEK LİSANS TEZİ

**Handan BAKALCI
(301091051)**

Enerji Bilim ve Teknoloji Anabilim Dalı

Enerji Bilim ve Teknoloji Programı

Tez Danışmanı: Prof. Dr. Nilgün KARATEPE YAVUZ

OCAK 2015

Handan BAKALCI, a M.Sc. student of ITU Institute of Energy student ID 301091051, successfully defended the thesis entitled “**INVESTIGATION OF ANODE PROPERTIES AND BATTERY PERFORMANCES OF METAL MIXED GRAPHITES FOR LITHIUM ION BATTERIES**”, which she prepared after fulfilling the requirements specified in the associated legislations, before the jury whose signatures are below.

Thesis Advisor : **Prof. Dr. Nilgün KARATEPE YAVUZ**
İstanbul Technical University

Jury Members : **Prof. Dr. Üner ÇOLAK**
İstanbul Technical University

Prof. Dr. Servet TİMUR
İstanbul Technical University

Date of Submission : 15 December 2014

Date of Defense : 23 January 2015

To my lovely mom, dad, sister and my love,

FOREWORD

Firstly, I would like to express my sincere gratitude and thanks to my academic advisor Prof. Dr. Nilgün KARATEPE YAVUZ for her consistent academic supervision, guidance and encouragement through out my research.

I would like to thank Can AKSAKAL and İNCİ AKÜ for supplying raw materials and SEM and galvanostatic analyses.

I would like to thank Res. Ass. Dr. Osman EKSIK and Res. Ass. Esra Şerife PAMPAL for their technical supports and helps.

I am also thankful to Nergis AKIN for her support and friendship.

Finally, I am deeply thankful to my mom, Sevinç, my dad, Recep, my sister, Hicran and my love, Mohan. Without their love, endless support and encouragement, I may not be able to earn this degree.

December 2014

Handan BAKALCI
Chemical Engineer

TABLE OF CONTENTS

	<u>Page</u>
FOREWORD	ix
TABLE OF CONTENTS	xi
ABBREVIATIONS	xv
LIST OF TABLES	xvii
LIST OF FIGURES	xix
SUMMARY	xxiii
ÖZET	xxv
1. INTRODUCTION	1
2. BATTERIES	3
2.1 Introduction to Batteries	3
2.2 Components of Batteries or Cell	4
2.3 Battery Parameters	5
2.3.1 Static battery parameters	5
2.3.2 Dynamic battery parameters	5
2.4 Classification of Batteries	6
2.4.1 Primary batteries	6
2.4.1.1 Zinc primary batteries	6
2.4.1.2 Lithium primary batteries.....	10
2.4.1.3 Specialized primary batteries	11
2.4.2 Secondary batteries	12
2.4.2.1 Lead-acid batteries	13
2.4.2.2 Alkaline batteries	13
3. LITHIUM ION BATTERIES	19
3.1 History and Development of Lithium Ion Batteries	19
3.2 Preference of Lithium Ion Battery Compared to Other Batteries	19
3.3 Lithium Ion Battery Components.....	20
3.3.1 Cathode for lithium ion batteries	20
3.3.1.1 Layered LiCoO_2	21
3.3.1.2 Spinal LiMn_2O_4	21
3.3.1.3 Olivine LiFePO_4	22
3.3.2 Anode for lithium ion batteries	23
3.3.2.1 Lithium metal	23
3.3.2.2 Carbon based.....	23
3.3.2.3 Alloy based	24
3.3.3 Electrolyte	26
3.4 Mechanisms.....	29
3.4.1 Fundamentals	29
3.4.2 Charge and discharge mechanism.....	29

3.4.3 Intercalation and de-intercalation process.....	31
3.4.4 Solid electrolyte interphase formation	33
3.5 Battery Parameters and Performance Criteria	36
3.5.1 Energy density.....	36
3.5.2 Cell voltage and voltage stability	37
3.5.3 Capacity and rate capacity.....	37
3.5.4 Peak current.....	37
3.5.5 Cycle life and shelf life	38
3.5.6 Operating temperature.....	38
3.5.7 Safety.....	39
3.6 Battery Design and Configuration.....	39
3.6.1 Advantages and disadvantages of lithium ion batteries	40
4. CHARACTERIZATION METHODS	41
4.1 Structural Characterization.....	41
4.1.1 X-ray diffraction (XRD).....	41
4.1.2 X-ray photoelectron spectroscopy (XPS).....	42
4.1.3 X-ray fluorescence (XRF).....	44
4.1.4 Fourier transform infrared spectroscopy (FTIR).....	45
4.1.5 Scanning electron microscopy (SEM).....	46
4.1.6 Transmission electron microscopy (TEM).....	48
4.1.7 Raman spectroscopy.....	48
4.1.8 Thermogravimetric analysis (TGA)	49
4.1.9 Brunauer-Emmett-Teller (BET) method.....	51
4.2 Electrochemical Characterization.....	51
4.2.1 Cyclic voltammetry (CV).....	52
4.2.2 Galvanostatic charge and discharge testing	52
4.2.3 Electrochemical impedance spectroscopy (EIS).....	54
5. EXPERIMENTAL STUDIES	57
5.1 Selection and Specification of Materials.....	57
5.2 Preparation of Anode Electrode Material.....	58
5.2.1 Silicon dioxide mixed graphite	58
5.2.2 Tin mixed graphite	59
5.2.3 Aluminium and aluminium oxide mixed graphite	59
5.2.4 Boron mixed graphite.....	60
5.3 Coin Battery Preparation	60
6. RESULTS AND DISCUSSION.....	65
6.1 Results of Silicon Dioxide Mixed Graphite	65
6.1.1 Results of anode material properties	67
6.1.1.1 Results of scanning electron microscopy (SEM)	67
6.1.1.2 Results of thermogravimetric analyses (TGA).....	71
6.1.2 Results of coin battery performances	72
6.2 Results of Tin Mixed Graphite	75
6.2.1 Results of anode material properties	76
6.2.1.1 Results of scanning electron microscopy (SEM)	76
6.2.1.2 Results of thermogravimetric analyses (TGA).....	78
6.2.2 Results of coin battery performances	78
6.3 Results of Aluminum and Aluminium Oxide Mixed Graphite	78
6.3.1 Results of anode material properties	79

6.3.1.1 Results of scanning electron microscopy (SEM).....	79
6.3.1.2 Results of thermogravimetric analyses (TGA)	82
6.3.2 Results of coin battery performances.....	83
6.4 Results of Boron Mixed Graphite Materials	87
6.4.1 Results of anode material properties	88
6.4.1.1 Results of scanning electron microscopy (SEM).....	88
6.4.1.2 Results of thermogravimetric analyses (TGA)	90
6.4.2 Results of coin battery performances.....	90
7. OVERALL RESULTS AND RECOMMENDATION	93
REFERENCES.....	97
CURRICULUM VITAE.....	103

ABBREVIATIONS

ΔG	: Free energy change of reaction
ΔH	: Reaction enthalpy change
ΔS	: Reaction entropy change
3d	: Three-dimensional space
BET	: Brunauer-Emmett-Teller
<i>C</i>	: Dimensionless constant, related to the enthalpy of adsorption
CV	: Cyclic Voltammetry
<i>d</i>	: Distance between two crystalline planes (lattice spacing)
d_{BET}	: Size of the mean primary particle
DEC	: Diethyl carbonate
DMC	: Dimethyl carbonate
E	: Electrochemical voltage
EC	: Ethylen carbonate
EDS	: Energy dispersive spectroscopy
EIS	: Electrochemical impedance spectroscopy
EMC	: Ethyl methyl carbonate
ESR	: Equivalent series resistance
F	: Faraday's constant
FTIR	: Fourier transform infrared spectroscopy
GC	: Gravimetric capacity
GCDT	: Galvanostatic charge and discharge testing
GED	: Gravimetric energy density
HF	: Hydrofluoric acid
I	: Electric current
IR	: Infrared
K, L, ...	: Atom shells beginning with the lowest K
<i>M</i>	: Metallic element
M	: Molar mass of a compound
<i>n</i>	: Number of electrons
<i>n</i>	: Order of reflectance
NMP	: Methyl-2-pyrrolidone
P	: Electrical power
<i>p</i>	: Vapour pressure
p_0	: Saturated pressure of an adsorbate gas
PC	: Propylene carbonate
PVdF	: Polyvinylidene difluoride
R	: Electric resistance
ROCO₂Li	: Lithium alkyl carbonates
ROLi	: Lithium alkoxides
SEI	: Solid electrolyte interphase

SEM	: Scanning electron microscopy
SLI	: Starting/lighting/ignition
SNR	: Signal to noise ratio
SSA	: Specific surface area
STP	: Standard conditions for temperature and pressure
TEM	: Transmission electron microscopy
TG	: Thermogravimetric
TGA	: Thermogravimetric analysis
V	: Electric Voltage
V_a	: Volume of adsorbed gas at standard temperature
V_c	: Operation voltage
V_m	: Volume of adsorbed gas at STP to produce an apparent monolayer
WD	: Width
WDS	: Wavelength dispersive spectroscopy
XPS	: X-ray photoelectron spectroscopy
XRD	: X-ray diffraction
XRF	: X-ray fluorescence
θ	: Angle between the incident beam and plane normal
λ	: Wavelength

LIST OF TABLES

	<u>Page</u>
Table 3.1 : Gravimetric capacity of lithium-alloy forming elements.....	25
Table 3.2 : Conductivity, in mS/cm, of 1M LiPF ₆ solutions in various solvents.....	27
Table 3.3 : Conductivity, in mS/cm, of LiPF ₆ solutions in binary mixture, 1:1 by weight, C: partially crystallized, S: saturated.....	28
Table 3.4 : Energy Density Comparison.	36
Table 3.5 : Rates of discharge.	38
Table 5.1 : Materials details' and its specifications.	57
Table 5.2 : SiO ₂ mixed graphite samples.	58
Table 5.3 : Sn mixed graphite samples.	59
Table 5.4 : Al and Al ₂ O ₃ mixed graphite samples.....	59
Table 5.5 : B mixed graphite samples.	60
Table 5.6 : Materials details' used for slurry preparation.	60
Table 6.1 : TGA results of SiO ₂ mixed graphite samples.	72
Table 6.2 : TGA results of Sn mixed graphite samples.	78
Table 6.3 : TGA results of Al ₂ O ₃ and Al mixed graphite samples.	83
Table 6.4 : TGA results comparison of sample prepared by agate mortar and ball miller.	83
Table 6.5 : Specific discharge capacities of Al and Al ₂ O ₃ mixed graphite and conservation of it.....	87
Table 6.6 : TGA results of B mixed graphite samples.....	90
Table 6.7 : Specific discharge capacities of 5%wt B mixed graphite and conservation of capacity.	92

LIST OF FIGURES

	<u>Page</u>
Figure 2.1 : An illustration of the Voltaic's pile.	3
Figure 2.2 : Schematic of an electrolytic cell with its major components.	4
Figure 2.3 : Illustration of zinc carbon cell.	7
Figure 2.4 : Illustration of alkaline manganese cell.	8
Figure 2.5 : Comparison of AA and D size Zn-C and alkaline cells.	9
Figure 3.1 : Comparison of various types of battery technologies in terms of energy densities.	20
Figure 3.2 : Layered structure of transition metal oxides.	21
Figure 3.3 : Spinal structure of LiMn_2O_4	22
Figure 3.4 : Olivine structure of LiFePO_4	22
Figure 3.5 : Schematics of the structural of three types of carbon.	24
Figure 3.6 : Voltage versus capacity for positive and negative electrode materials for lithium ion batteries.	25
Figure 3.7 : Structural formulas of important co-solvents.	27
Figure 3.8 : Conductivity of 1 M LiPF_6 solutions in various binary mixtures, 1:1 by weight.	28
Figure 3.9 : Charge and discharge mechanism of lithium ion batteries.	30
Figure 3.10 : Insertion mechanism of Li^+ ions into graphite.	31
Figure 3.11 : Illustration of lithium staging in graphite.	32
Figure 3.12 : Voltage plateaus on voltage vs charge curves.	32
Figure 3.13 : In plane structure of graphite in which is fully intercalated with Li^+ ions (LiC_6).	33
Figure 3.14 : The first cycle of graphite/lithium cell cycled in 1 M LiPF_6 EC/DEC (2:1) electrolyte.	34
Figure 3.15 : Representative structure of SEI layer with different components.	35
Figure 3.16 : SEM images of (a) natural graphite, (b) natural graphite after charge, (c) doped natural graphite after charge.	35
Figure 3.17 : Cell discharge curve.	37
Figure 3.18 : Illustration of different Li-Ion battery configuration with shape and component. a, cylindrical; b, coin; c, prismatic; d, thin and flat.	40
Figure 4.1 : Schematic of the Bragg diffraction by crystal planes.	42
Figure 4.2 : Electron emission process after the absorption of X-rays from the inner shell K.	43
Figure 4.3 : XPS spectrum of an oxidized aluminum surface as a function of binding energy.	43
Figure 4.4 : Comparison of a) wavelength dispersive spectroscopy b) energy dispersive spectroscopy.	44
Figure 4.5 : Comparison of measurement spectra (left) vs. WDS (right) EDS.	45

Figure 4.6 : Schematic of the Michelson interferometer.....	45
Figure 4.7 : (left) Interferogram (right) IR spectrum.	46
Figure 4.8 : Final spectrum of the investigated material obtained with FTIR.	46
Figure 4.9 : Comparison of two photographs taken with light microscope and SEM.	47
Figure 4.10 : Tescan Vega3 SBU device.	48
Figure 4.11 : TEM Photograph of single crystal. Electron diffraction pattern can be seen. The transmitted beam is brighter than the diffracted beams.	48
Figure 4.12 : Raman shift in wave number is given as a function of ratio between Si and Ge in a thin film made of Si _{1-x} Ge _x	49
Figure 4.13 : Decomposition starting temperature T _i and finish temperature T _f obtained with TGA.	50
Figure 4.14 : TA Q600 SDT termogravimetric device.	50
Figure 4.15 : Cyclic voltammogram of a deposited insoluble film during electro- reduction and reoxidation process.	52
Figure 4.16 : TI BST8-WA 8 channel battery analyzer.	53
Figure 4.17 : Pseudo-linear part of a non-linear voltage current characteristic.	55
Figure 5.1 : IKA universal mill M20.	58
Figure 5.2 : Hi-Quality natural agate mortar and pestle.....	58
Figure 5.3 : WiseClean ultrasonic bath.	60
Figure 5.4 : MSK-AFA-III automatic thick film coater.....	61
Figure 5.5 : Binder vacuum drying ovens.	61
Figure 5.6 : Anode material coated on copper foil.....	61
Figure 5.7 : Precision disc cutter MSK-T-06.	62
Figure 5.8 : Cylindrical shaped anode material coated on copper foil.....	62
Figure 5.9 : Innovative technology IL-2 GB glove box.....	62
Figure 5.10 : Coin battery components and sequence.....	63
Figure 5.11 : MTI Corporation - MSK - 110 hydraulic crimping machine.	63
Figure 6.1 : SEM images of artificial graphite: a) 2.5kx, b) 1.0kx, c) 500x, d) 250x.	67
Figure 6.2 : SEM images of SiO ₂ : a) 2.0kx, b) 1.0kx, c) 500x, d) 250x, e) 101x.....	68
Figure 6.3 : SEM images of Sn powder: a) 1.01kx, b) 500x, c) 200x, d) 100x.	68
Figure 6.4 : SEM images of MgO: a) 2.5kx, b) 1.0kx, c) 500x, d) 250x.....	69
Figure 6.5 : SEM images of SiO ₂ :graphite composite at 50:50 wt%: a) 1000x, b) 500 x, c) 250x.	69
Figure 6.6 : SEM images of SiO ₂ :graphite composite at 70:30 wt%: a) 2.5kx, b) 1.0k x, c) 500x, d) 250x.....	70
Figure 6.7 : SEM images of SiO ₂ :graphite composite at 80:20 wt%: a) 500x, b) 250x	70
Figure 6.8 : SEM images of SiO ₂ :graphite:Sn composite = 70:20:10 wt%: a) 1.0kx, b) 500x, c) 250x.....	71
Figure 6.9 : SEM images of SiO ₂ /MgO/graphite composite: a) 1.0kx, b) 500x, c) 250x.	71
Figure 6.10 : Normalized specific capacity comparison of SiO ₂ mixed graphite.....	73
Figure 6.11 : Specific capacity vs voltage for SiO ₂ :graphite = 80:20 wt%.	74
Figure 6.12 : Specific capacity vs voltage for SiO ₂ :graphite:Sn = 70:20:10 wt%....	74
Figure 6.13 : SEM images of AgNO ₃ powder: a) 2.5kx, b) 1.02kx, c) 500x, d) 200x.	76

Figure 6.14 : SEM images of Sn:graphite composite = 50:50 wt%: a) 1.0kx, b) 500x, c) 250x.....	76
Figure 6.15 : SEM images of Sn:graphite composite = 60:40 wt%: a) 1.0kx, b) 500x, c) 250x.....	77
Figure 6.16 : SEM images of Sn:graphite:AgNO ₃ composite = 60:30:10 wt%: a) 1.0kx, b) 500x, c) 250x.....	77
Figure 6.17 : SEM images of Sn:graphite:AgNO ₃ composite = 45:45:10 wt%: a) 1.0kx, b) 500x, c) 250x.....	77
Figure 6.18 : SEM images of Al: a) 5.0kx, b) 2.5kx, c) 1.0kx, d) 500x, e) 250x.....	80
Figure 6.19 : SEM images of Al ₂ O ₃ : a) 1.0kx, b) 500x, c) 250x, d) 100x.....	80
Figure 6.20 : SEM images of Al ₂ O ₃ :SiO ₂ :graphite composite at 54:15:31 wt%: a) 5.0kx, b) 1.5kx, c) 500x.....	81
Figure 6.21 : SEM images of Al ₂ O ₃ :SiO ₂ :graphite composite at 27:39:33 wt%: a) 1.0kx, b) 501x, c) 251x.....	81
Figure 6.22 : SEM images of Al:graphite = 67:33 wt% by using Al ₂ O ₃ : a) 1.0kx, b) 500x, c) 250x.....	82
Figure 6.23 : SEM images of Al:graphite = 67:33 wt% by using Al: a) 2.0kx, b) 1.0kx, c) 500x, d) 210x.....	82
Figure 6.24 : Normalized specific capacity comparison of Al ₂ O ₃ mixed graphite... 84	84
Figure 6.25 : Specific capacity vs voltage for Al ₂ O ₃ :SiO ₂ :graphite = 54:15:31 wt%.	85
Figure 6.26 : Specific capacity vs voltage for Al ₂ O ₃ :SiO ₂ :graphite = 27:39:33 wt%.	85
Figure 6.27 : Specific capacity vs voltage for Al:graphite = 67:33 wt% by using Al.	86
Figure 6.28 : SEM images of B powder: a) 10kx, b) 5.0kx, c) 2.5kx.....	88
Figure 6.29 : SEM images of B:graphite = 2.5:97.5 wt%: a) 5.0kx, b) 1.5kx, c) 500x.	89
Figure 6.30 : SEM images of B:graphite = 5:95 wt%: a) 5.0kx, b) 1.5kx, c) 500x..	89
Figure 6.31 : SEM images of B:graphite = 7.5:92.5 wt%: a) 2.5kx, b) 1.0kx, c) 496x, d) 250x.....	89
Figure 6.32 : Normalized specific capacity comparison of B mixed graphite samples.	91
Figure 6.33 : Specific capacity vs voltage for 5 wt% B mixed graphite.....	91

INVESTIGATION OF ANODE PROPERTIES AND BATTERY PERFORMANCES OF METAL MIXED GRAPHITES FOR LITHIUM ION BATTERIES

SUMMARY

Reliable and sustain energy storage is crucial for modern portable electronics, such as mobile phones, laptop computers, MP3 players, other electronic devices, and potential applications for automobile industry. In this sense, lithium ion batteries provide an attractive solution. In addition, the later will bring significant contribution to reduce greenhouse gas emission and address global warming. Even though, lithium ion batteries offer advantages, there is a constant demand for higher energy density, higher power density, longer cycle life batteries which has motivated research into new battery materials for next generation of advanced lithium ion batteries.

In lithium ion batteries, graphite is the most widely used anode materials. Even though, metallic materials like silicon, tin, boron etc. have higher specific capacity, due to severe volume changes during charge/discharge, graphite is preferred more compared to metallic materials. However, specific capacity of graphite needs to be improved which is only 372 mAh/g. Intensive researches continue on developing new anode materials with graphite and metals to improve cyclability and specific capacity of lithium ion batteries.

This thesis mainly focused on development of metal mixed anode material for lithium ion batteries and assessment of their electrochemical and structural characteristics. The materials investigated are graphite and metals such as silicon dioxide, aluminum, boron and tin. For material characterization, scanning electron microscopy and thermogravimetric analyses were applied. For electrochemical characterization, galvanostatic measurements have been conducted.

Compared to carbon based material, silicon has higher theoretical capacity, which is around 4200 mAh/g. Considering its high capacity, silicon is promising material to be used as composite for anode material for lithium ion battery. However, during intercalation/de-intercalation process with lithium, composite structure is changed during large volume expansion/contraction of Si. In this work, to minimize the volume expansion, silicon dioxide was used with graphite. Moreover, additives like tin and magnesium oxide were used to enhance to battery performance. After fabrication of coin lithium ion batteries, galvanostatic measurements were examined. According to results, it can be concluded that even though the initial discharge capacity of battery was improved compared to artificial graphite, due to loss of active matter and SEI formation at the initial cycles, stable discharge capacity cannot be met for all samples.

Tin has also higher theoretical capacity, which is 992 mAh/g, compared to graphite. In this study, to improve the battery performance tin/graphite composites, which were prepared with different mass ratios, were used as anode material. Furthermore, addition of silver nitrate to composites were investigated. At the galvanostatic measurement of Sn mixed graphite, no reading can be recorded resulting from using a mean diameter of about 600 μm particle sized Sn powder, which leads flaking at every coating of the tin mixed slurry. Since the diameter of the tin particles could not be reduced further with agate mortar, the qualitative research of tin mixed graphite could not be performed.

Recent studies showed that cycling could be improved by addition of aluminum and aluminum oxide to anode material. Eventhough, aluminium reacts with one lithium atom with moderate volume increase where tin reacts with 4.4 lithium atoms, gravimetric capacity of aluminium (990 mAh/g) is comparable versus tin (990 mAh/g). To enhance battery performance, aluminum or aluminum oxide/graphite composite were also investigated. Furthermore, silicon was used as additive in the composites to utilize and to maintain good capacity during cycle. Prepared samples showed higher initial discharge capacity compared to artificial graphite. However, none of the samples showed proper running battery profile due to the irreversible capacity losses during first cycle.

Recent researchers also showed that boron addition to anode material has increase the discharge capacity and decrease the irreversible capacity of lithium ion battery. In this study, different boron additions were examined to find out optimum addition level of boron mixed graphite. In the battery performance analysis of boron mixed graphite, it can be clearly observed that all samples showed superior initial capacity compared to that of artificial graphite. In addition to that, after irreversible capacity loss at the first cycle, the capacity stayed stable at the following cycles with minor changes.

LİTYUM İYON PİLLERDE METAL İLE KATKILANDIRILMIŞ GRAFİTLERİN ANOT ÖZELLİKLERİNİN VE PİL PERFORMANSLARININ İNCELENMESİ

ÖZET

Günümüzde gelişen teknoloji ile birlikte cep telefonu, dizüstü bilgisayar, MP3 çalar gibi taşınabilir elektronik cihazlar ile otomobil endüstrisindeki potansiyel yaklaşımlar için güvenli ve sürdürülebilir enerji depolanması hayati bir öneme sahiptir. Bu kapsamda, lityum iyon pilleri birçok avantajlı özelliği ile çözüm sunmaktadır. Bunun yanı sıra çevreye verilen zararın azalmasında da büyük bir öneme sahiptir. Lityum iyon piller diğer piller ile karşılaştırıldığında, birçok noktada avantajlı özellikleri sahip olsa da gelişen teknoloji ve modern hayatın gereksinimleri düşünüldüğünde, daha yüksek enerji ve güç yoğunluğuna, daha uzun çevrim döngüsüne ihtiyaç vardır. Bu sebeplerle, yeni nesil lityum iyon piller için yeni pil malzemelerinin geliştirilmesi konusunda araştırmalar devam etmektedir.

Yüksek depolama kapasitesi, yüksek şarj/deşarj verimi, kendiliğinden boşalmanın ve kapasite kayıplarının az olması, uzun ömür, ucuzluk, enerji yoğun olması (kWh/kg veya kWh/l) ve enerjiyi en az hacimde ve ağırlıkta depolayabilmesi lityum iyon bataryalarda aranan özelliklerdendir. Genel olarak halihazırda kullanılan pillerin ağırlığının ve boyutunun azaltılması, pil kapasitesinin, ömrünün ve şarj-deşarj oranlarının varolandan iyileştirilmesi için yeni elektrot malzemelerinin ve yeni elektrot yapı tasarımlarının geliştirilmesine gerek vardır. Birçok gelişmiş ülkede bu konular üzerine yaygın araştırmalar yapılmaktadır.

Lityum iyon pillerde anot malzemesi olarak ticari birçok malzeme kullanılmakla birlikte en yaygın kullanılanı grafitir. Silikon, bor, kalay gibi metaller, grafit ile karşılaştırıldığında daha yüksek spesifik kapasiteye sahip olmalarına rağmen şarj/deşarj sırasında yüksek oranda hacimsel değişime uğradıklarından grafitte göre daha az tercih edilmektedirler. Bunun yanı sıra, 372 mAh/g'lık spesifik kapasiteli grafit için ise, düşük spesifik kapasitesini iyileştirmeye yönelik çalışmalar yapılmaktadır.

Tez çalışması kapsamında, İstanbul Teknik Üniversitesi – Enerji Enstitüsü, Malzeme Üretim ve Hazırlama Laboratuvarı'nda anot malzemesi metal ve metal oksitler ile karıştırılan grafitin anot özellikleri ve pil performansı incelenmiştir. Bu amaçla, metal ve metal oksit olarak silikon dioksit, alüminyum, bor ve kalay kullanılmıştır. Metal ile karıştırılan grafit anot malzemelerinin, taramalı elektron mikroskobu (SEM) ve termogravimetrik analiz (TGA) sistemleri ile karakterizasyonları gerçekleştirilmiştir. Ayrıca galvanostatik ölçümler yapılarak pil performansları incelenmiştir.

Karbon yapılı maddelerle karşılaştırıldığında, silisyumun ilk çevrimdeki spesifik kapasitesi oldukça yüksek olup 4200 mAh/g'dır. Bu yüksek kapasite nedeniyle silisyumun lityum iyon pillerde anot malzemesi olarak kullanımı gelecek vaad etmektedir. Fakat interkalasyon/deinterkalasyon prosesi sırasında yüksek oranda hacimsel değişiklik nedeniyle yapısında büyük değişiklikler meydana gelmektedir. Tez çalışması kapsamında; hacim değişimini azaltmak için farklı oranlarda silisyum dioksit ile grafit karıştırılarak anot malzemesi üretilmiş ve pil performansı incelenmiştir. Ayrıca, anot malzeme üretiminde; silisyum dioksit ile karıştırılmış grafitte, hacim değişimi azalmak ve pil performansını artırmak için magnezyum oksit ile kalay da ilave edilmiştir. Numuneler mekanik olarak karıştırılarak hazırlanmıştır. Karışım, istenilen viskozite özelliklerine getirilerek bakır folya üzerine kaplanmış ve sonrasında kurutularak düğme pil boyutunda kesilmiştir. Üretilen anot malzemesi, düğme pil yapımında kullanılarak lityum iyon pilin performansı belirlenmiştir. Elde edilen pil ölçüm sonuçlarına göre, numunelerin ilk deşarj kapasiteleri grafitte oranla daha yüksek olmasına rağmen, ilk çevrimdeki aktif madde kaybı ve katı elektrolit faz oluşumundan dolayı kararlı deşarj kapasiteye ulaşamamıştır. Magnezyum oksit katkılı anot malzemesi ile hazırlanan pillerden ölçüm alınmadığından, magnezyum oksitin pil performansına olan etkisi incelenememiştir.

Lityum iyon pillerde; karbon yapılı malzemelerle karşılaştırıldığında, kalayın da spesifik kapasitesi yüksektir (992 mAh/g). Fakat silisyumda olduğu gibi, kalay da interkalasyon/deinterkalasyon prosesi sırasında hacimsel değişikliklere uğramakta ve pil performansını olumsuz yönde etkilemektedir. Tez çalışması kapsamında; kalay, grafit ile değişik oranlarda karıştırılarak anot malzemesi üretilmiş ve pil performansı incelenmiştir. Numuneler mekanik olarak karıştırılarak hazırlanmıştır. Karışım, istenilen viskozite özelliklerine getirilerek bakır folya üzerine kaplanmış ve sonrasında kurutularak düğme pil boyutunda kesilmiştir. Üretilen anot malzemesi, düğme pil yapımında kullanılarak lityum iyon pilin performansı belirlenmiştir. Çalışmada kullanılan kalay tozunun tanecik boyutunun büyük olmasından dolayı üretilen kaplama malzemesi ile bakır folya arasında düşük yüzey gerilimi oluşmuş, bu durum kaplamanın bakır folyadan kalkmasına neden olmuştur. Bu nedenle, pil ölçümlerinden sonuç alınamamıştır. Ayrıca pil performansını artırmak amacı ile kullanılan gümüş nitratin etkisi ölçüm alınmadığından incelenememiştir.

Son yıllarda gerçekleştirilen çalışmalarda; grafit anotun alüminyum ve alüminyum oksit ile katkılanması sonucunda pil veriminin artabileceği gözlenmiştir. Kalayın 4.4 lityum iyonu ile etkileşmesine rağmen alüminyumun bir lityum iyonu ile etkileşerek aynı spesifik kapasitesine (990 mA/h) sahip olması önemlidir. Tez çalışması kapsamında; grafit, alüminyum ve alüminyum oksit ile farklı oranlarda karıştırılarak anot malzemesi üretilmiş ve pil performansı incelenmiştir. Numuneler mekanik olarak karıştırılarak hazırlanmıştır. Karışım, istenilen viskozite özelliklerine getirilerek bakır folya üzerine kaplanmış ve sonrasında kurutularak düğme pil boyutunda kesilmiştir. Üretilen anot malzemesi, düğme pil yapımında kullanılarak lityum iyon pilin performansı belirlenmiştir. Ayrıca karışımlara silisyum oksit eklenerek pil verimine olan etkileri incelenmiştir. Elde edilen karışımlarla hazırlanan anot malzemeleri, grafit ile karşılaştırıldığında daha yüksek başlangıç deşarj kapasite değeri verse bile ilk çevrimde oluşan tersinmez kapasite kaybı pillerin uzun ömürlü olmasını engellemiştir.

Son yıllarda gerçekleştirilen çalışmalarda, bor katkılı karbonların tersinir kapasitelerinin karbon yapılarına göre daha yüksek olduğu görülmüştür. Tez çalışması kapsamında, grafitte kütlece farklı oranlarda bor karıştırılarak pil verimini artıracak en uygun bor oranı tespit edilmiştir. Numuneler mekanik olarak karıştırılarak hazırlanmıştır. Karışım, istenilen viskozite özelliklerine getirilerek bakır folya üzerine kaplanmış ve sonrasında kurutularak düğme pil boyutunda kesilmiştir. Üretilen anot malzemesi, düğme pil yapımında kullanılarak lityum iyon pilin performansı belirlenmiştir. Elde edilen karışımlarla hazırlanan grafit anot malzemelerin grafitte göre daha yüksek başlangıç deşarj kapasitelerine sahip olduğu tespit edilmiştir. Ayrıca, ilk çevrimdeki tersinmez kapasite kaybından sonra küçük değişiklikler olmasına rağmen kararlı kapasite ölçümleri elde edilmiştir.

1. INTRODUCTION

With recent technological developments and rising population, energy demand is increasing rapidly in the 21st of century. Presently, energy needs are supplied from fossil fuels, which is at risk due to the decrease in non-renewable sources. Furthermore, CO₂ emission, which is main reason of global warming, is associated with use of fossil fuels. Therefore, it is becoming an issue in global energy politics.

Search for sustainable and environmentally friendly energy sources continues. The renewable energy sources like solar and wind energy are known as environmentally friendly, but they depend on nature conditions. Thus, energy storage is needed for continuous use. Batteries are electrochemical storage devices, which can store energy in the form of chemical potential difference and convert it to electrical energy whenever or wherever it is needed.

Considering the increase in usage of portable electronic devices like mobile phones, laptops, MP3 players and other electronic devices, and potential applications for automobile industry, intensive researches are undertaken on lithium ion batteries worldwide.

Providing very high energy density, and featuring high capacity, low weight and high open circuit voltage are the main drivers of using lithium ion batteries technology. Despite their advantages, lithium ion battery has room for improvement in terms of cost, cycling life and safety.

The general goal of this work is to improve cyclability and specific capacity of lithium ion battery by modifying the anode material by metal doping. Furthermore, impact of metal mixed graphite on solid electrolyte interphase (SEI) formation and its effect on battery performance are investigated.

Chapter 2 presents literature review on the basics of batteries. Chapter includes an overview of the general background, history, basic parameters on batteries, followed by the classification of batteries.

Chapter 3 is dedicated to the literature review related to lithium ion batteries. The section includes an overview of general background, a brief history and developments, general components of rechargeable lithium ion batteries, mechanisms, battery parameters and performance criteria, and battery design and configuration, followed by advantages and disadvantages.

Chapter 4 presents the characterization methods, both structural and electrochemical.

Chapter 5 presents the experimental studies performed at this work. It includes structural and electrochemical characterization of addition of silicon, aluminum, alumina, boron and tin to graphite, which are used as anode in the battery.

Chapter 6 offers the results of characterization analyses done for this work. It includes analyses results obtained for anode material preparation and characterization steps where additions of Si, Al, Al₂O₃, B and Sn to graphite. Furthermore, battery performance results are shared by comparing addition of Si, Al, Al₂O₃, B and Sn to graphite vs. bare graphite. By combining high capacity elements, Si, Al, Al₂O₃, B and Sn, and carbon, the composite anode materials can deliver much higher capacity than pure carbon and maintain good cyclability.

The overall results for this study are given in Chapter 7.

2. BATTERIES

2.1 Introduction to Batteries

There are technical and economical limitations for the direct storage of electrical energy with electrolytic capacitors or superconducting coils. Therefore, storage of electrical energy requires its conversion into another form of energy. It can be stored by converting to potential, kinetic, thermal or chemical energy.

A battery is a chemical device for storage of electrical energy. The energy of chemical compounds in batteries acts as storage medium and while discharge, battery converts the chemical energy into electrical energy by means of electrochemical reaction [1-3].

Alessandro Volta, a Professor of Natural Philosophy at the University of Pavia in Italy, invented the first battery 200 years ago, in 1800. The “Volta’s Pile” (Figure 2.1), which is known as first galvanic battery, consists of different metals separated by an acidic; ion conduction medium and the current was generated by the chemical reactions through this system. Modern batteries are built on the same basic principle of the “Voltaic’s pile” [3, 4].



Figure 2.1 : An illustration of the Voltaic’s pile [5].

2.2 Components of Batteries or Cell

Even though the term “cell” is used for the basic electrochemical unit, the term “battery” is more widely accepted. Depending on required output voltage or capacity, cells are connected in series, parallel or both. Two or more electrically joined cells are called a battery.

The cell consists of three major components: cathode, anode and electrolyte.

The cathode is positively charged electrode, which accepts electrons from the external circuit and is reduced during the electrochemical reaction. It is also known as the oxidizing electrode.

The anode is negatively charged electrode, which releases electrons to the external circuit and is oxidized during the electrochemical reaction. It is also known as the reducing electrode.

The electrolyte or ionic conductor provides the medium for the charge transfer, as ion, inside the cell between anode and cathode. Typically, an electrolyte is in liquid form but solid form of electrolytes is also used in some batteries. Salt, acids or alkalis dissolved water, or solvents are used as liquid electrolyte to convey the ionic conductivity. Solid electrolytes are ionic conductors, which operate at the temperature of cell.

Additionally, a separator material is used to separate anode and cathode electrodes physically to avoid any internal short circuit, which is permeable to electrolyte in order to assure the required ionic conductivity [1, 3]

A schematic of an electrolytic cell is shown in Figure 2.2 with its major components.

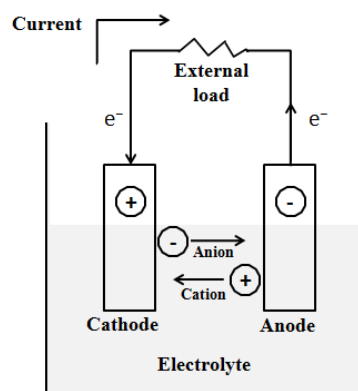


Figure 2.2 : Schematic of an electrolytic cell with its major components.

2.3 Battery Parameters

The battery parameters are divided into two main groups as the static and dynamic battery parameters.

2.3.1 Static battery parameters

Physical characteristics of battery are known as static battery parameters. Manufacturer sets these parameters and tests them accordingly. After the completion of chemical development, battery is programmed with static information. The definition of important static battery parameters will be given in this section.

Theoretical voltage is calculated with the help of electrode materials. Nominal voltage is the value achieved in the practice, whereas theoretical voltage cannot be achieved in practice due to the battery properties. Specific energy is the stored energy per unit mass. It is expressed as Watt-hours per kilogram. Cut-off voltage is the term that used for minimum voltage of battery referring to empty state. Capacity is the amount of charge that can be drawn from fully charged battery to fully discharged battery. It is measured in Ampere-hour (Ah). Capacity rate is a measure of rate, at which a battery is discharged relative to its maximum capacity. Cycle life is the term used for the number of charge-discharge cycles that battery sustains. Generally, the number of charge-discharge before the capacity drops by 80%, is used as cycle life. Self-discharge rate is the rate of energy reduction without load. Battery discharges its energy slowly due to electrochemical reactions. Shelf life is the storage period of battery in an inactive position, before the capacity drops by 80%. This is mainly occurred due to the loss of active materials [4, 6, 7].

2.3.2 Dynamic battery parameters

Battery runtime usage, environmental condition, in which the battery operates, and operating circumstances are designated by dynamic battery parameters. The definition of important variables will be given in this section

State of charge gives the capacity of the battery in percentages. State of discharge or depth of discharge is the percentages of battery capacity that has been discharged, expressed as a percentage of maximum capacity. Terminal voltage gives the voltage between battery terminals with load. Open circuit voltage defines the voltage

between battery terminals without load. Internal resistance gives the resistance in the battery. More heat is produced with increasing resistance, which reduces the battery efficiency. Service life gives the length of time, during which a battery is expected to operate. During discharge, capacity and voltage are affected by the battery temperature. As the temperature increases in the battery, the chemical activity of the battery also increases and the internal resistance sinks. Accordingly, capacity and power rise. On the other hand, self-discharge grows with increasing temperature, which reduces the capacity. State of health is a value used for health of battery. The battery condition is ideal when the state of health value is 100% [4, 7].

2.4 Classification of Batteries

Mainly batteries are classified as primary (non-rechargeable) or secondary (rechargeable) batteries in terms of their reuseability. Regarding to particular structures and/or designs, further classifications are also used to identify the batteries, e.g., aqueous/non-aqueous, low/high power and according to their size. In this section, primary and secondary batteries are described.

2.4.1 Primary batteries

Primary batteries, which are also called non-rechargeable batteries, utilize the chemicals only once. After first discharge, they are discarded.

Having good shelf life, high energy density at low to moderate discharge rate, mostly small and ease of use are the general advantages of primary batteries. In addition to the mentioned advantages, they are also cheap and light, which makes them a convenient power source for portable electric and electronic devices [2, 3].

2.4.1.1 Zinc primary batteries

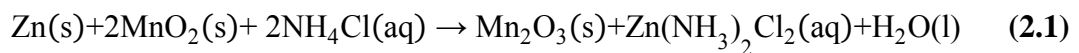
Commonly, zinc-manganese-dioxide electrochemical couples are used in consumer batteries. They are classified under four main groups, i.e., zinc-carbon, alkali-manganese, zinc-silver oxide, and zinc-air batteries.

Zinc-carbon batteries

The first zinc-carbon batteries are invented in the middle of 19th century. In the cell, zinc can is the negative terminal and carbon rod is the positive terminal. Carbon rode is surrounded by manganese oxide and carbon powder. The main reason of using

carbon powder is to increase the electrical conductivity of the positive mass. An aqueous solution of ammonium chloride (NH₄Cl) or zinc chloride (ZnCl) is used as an electrolyte. This aqueous solution is absorbed into paste type separator and metal oxide, for example manganese dioxide, and carbon mixture. Thus, the electrolyte formation is gelled. Therefore, it is called “dry cell”. In addition, a seal is used in the cell to prevent the contact of positive carbon rod with negative zinc can. Finally, outer surface of the cell is covered by cardboard, where manufacturer and other information are printed [3, 8].

The overall reaction with ammonium chloride electrolyte is simply



The nominal cell voltage of the cell is 1.5V.

The overall reaction with zinc chloride electrolyte is simply



The nominal cell voltage of the cell is 1.5V.

A zinc- carbon cell is shown schematically in Figure 2.3.

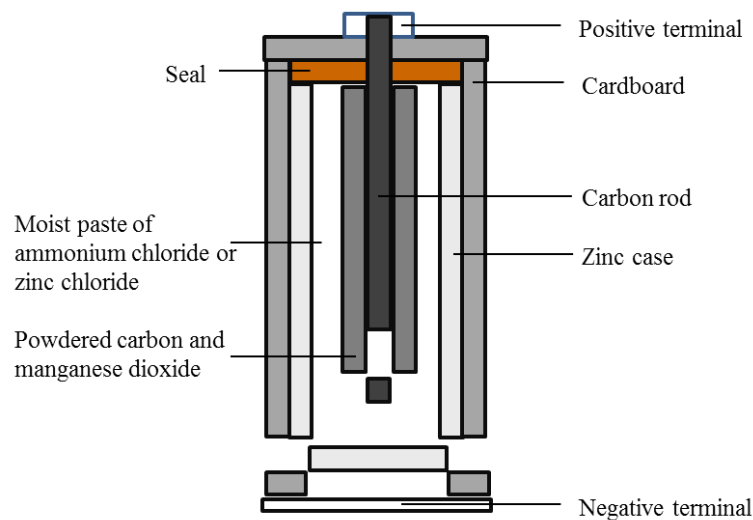


Figure 2.3 : Illustration of zinc carbon cell [3].

Alkali-manganese cells

Alkali manganese cells are the upgrade version of zinc carbon cells, which differ in electrolyte type, nature of negative electrode and cell configuration from zinc carbon cells. First alkaline zinc manganese dioxide cell was introduced in early 1960s [3].

Zinc powder is used as the negative electrode, which surrounds the current collector that is placed at the center of cell. This negative current collector is in the form of a brass pin. Manganese dioxide and carbon powder mix is used as a positive electrode, which surrounds the separator and contacts with nickel-plated steel can. Potassium hydroxide (KOH) is used as electrolyte, which has a high electrical conductivity [3].

The total reaction is simply



The nominal cell voltage is 1.5V.

An alkaline manganese cell is shown schematically in Figure 2.4.

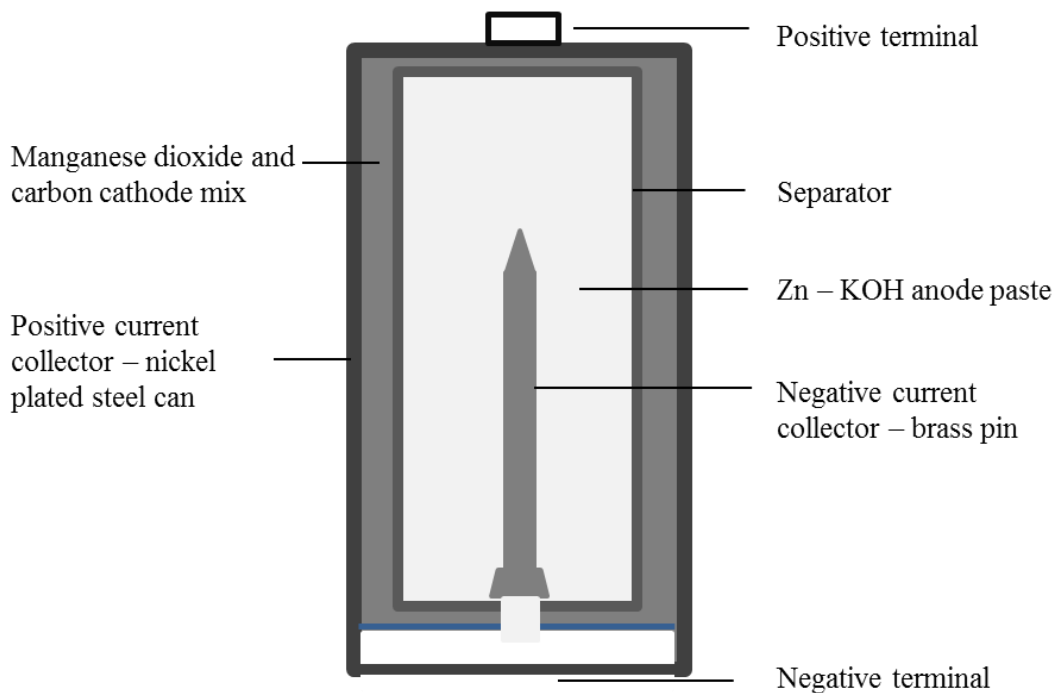


Figure 2.4 : Illustration of alkaline manganese cell [3].

Both zinc carbon cells and alkaline manganese cells have nominal voltage of 1.5 V and can be produced in a variety of sizes. However, alkaline manganese cells have longer shelf life; higher drain discharge, lower self-discharge and better leakage resistance compared to zinc carbon cells [3, 9].

A comparison of the performance of the two batteries is shown in Figure 2.5. It is easy to see that the runtime through 3 Ω resistance is 3 hours for a D size zinc carbon cell and 45 hours for a D size alkaline cell [9].

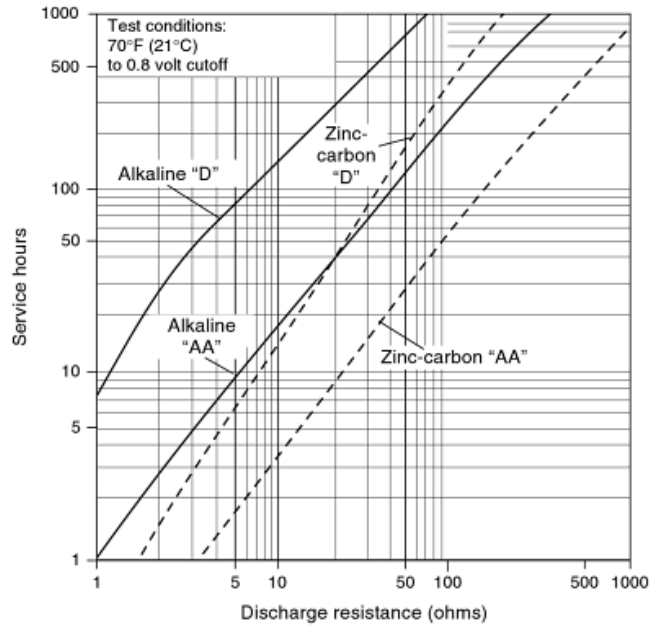


Figure 2.5 : Comparison of AA and D size Zn-C and alkaline cells [7].

Zinc-silver oxide batteries

In zinc silver oxide batteries; zinc powder is used as negative electrode and silver monoxide (Ag_2O) is used as positive electrode. Potassium hydroxide (KOH) or sodium hydroxide (NaOH) aqueous solution is used as an electrolyte.

The total reaction is simply



The nominal cell voltage is 1.5V.

High energy and a flat potential are the advantages of these kinds of batteries. Moreover, their performances are good at low temperatures and they have a good shelf life. Considering their characteristics, they are appropriate for use in electronic devices, but only in button sizes considering the high cost of silver [9].

Zinc-air batteries

In zinc-air batteries, oxygen (O_2) in air is used as positive electrode. Potassium hydroxide (KOH) is used as electrolyte.

The total reaction is simply



The nominal cell voltage is 1.4V.

Oxygen availability in the battery affects the current that battery can support. There are air holes at the bottom of the button battery, which allow the air to flow. When the air flows through the battery, air diffuser layer distributes the oxygen uniformly and reach to Teflon layer. Through Teflon layer, only oxygen can get through, where water vapour has a limitation. This mechanism prevents the battery to discharge quickly.

Primary zinc-air batteries have high energy density with a good shelf life at low cost. Mostly they are used in hearing aid application [9].

2.4.1.2 Lithium primary batteries

First lithium primary batteries were introduced to market in the 1970s. Lithium is used as a negative electrode. Lithium is the lightest metal in the periodic table with high specific energy. These two unique properties provide advantages, while using as an anode in the battery. There are many alternatives, which can be used as positive electrode in lithium primary batteries, e.g., CuO, CuS, CF_x, FeS₂, MnO₂, MoO₃, Ag₂CrO₄ and V₂O₅. Mostly, CF_x, MnO₂, FeS₂ and CuO are used in the primary cell, where first two metals provide 3V cells and latter two metals provide 1.5V cells. Lithium is highly reactive with water, so electrolyte used in the battery should not be in aqueous form. Solution of lithium salts in polar organic liquids, solution of lithium salts in polar inorganic liquids, fused lithium salts, ionically conduction polymers and ionically conduction ceramics are the groups of non-aqueous electrolyte that can be used in lithium primary batteries. In most cases, solution of lithium salts in polar organic liquids is used as an electrolyte. Even though, lithium is not stable with regard to organic liquids thermodynamically; passivating layer is formed on the surface of the lithium metal, when the lithium is exposed to air, hence preventing the self-discharge of the battery. Therefore, the layer formation allows the organic liquid to be used as an electrolyte. In addition, ionic conductivity of the electrolyte is very important to define the internal resistance of the cell. Compared to aqueous electrolytes, e.g., zinc chloride, potassium hydroxide, conductivity of organic electrolytes is low. Polar solvents can be used to maximize the conductivity, which has an ability to dissolve lithium salts. LiClO₄, LiAlCl₄, LiBF₄, LiPF₆, LiAsF₆, LiCF₃SO₃ and LiN(CF₃SO₂)₂ are examined as dissolved salts in the battery.

Considering the market applications, LiPF_6 and LiAsF_6 are preferred as a solute and dimethoxyethane or diethyl carbonate are preferred as solvent [3, 9].

Lithium primary batteries have high energy and power, long shelf life. In addition, they can be worked in a wide range of temperature. They can be also performed in different forms like button, coin, cylindrical, prismatic, very thin with small variations in capacities [9].

Most common and commercialized types of lithium batteries are lithium/sulphur dioxide, lithium/thionyl chloride, lithium/manganese dioxide and lithium/carbon monofluoride batteries. For a more detailed review about different types of lithium primary batteries, further reading of [9] is recommended.

2.4.1.3 Specialized primary batteries

In some applications for batteries, the needs are very specific, so batteries need to be designed distinctively.

The specialized primary batteries can be splitted into four main groups regarding to their special requirements. These are batteries in medical applications, seawater activated batteries, torpedo batteries and thermal batteries.

Medical applications

Batteries in medicine can be categorized under three groups, which are the batteries implanted in the body, devices that are worn by the patient and devised used by medical staff. Mostly, lithium cells are preferred, which offers high gravimetric and volumetric energy densities with high voltage and flat discharge curves. Additionally, it is very light.

Seawater activated batteries

Seawater activated batteries are mostly preferred for usage in emergency cases or military equipments like rescue lights on life jacket, navigation lights on buoys, divers' searchlight or torpedo propulsion and underwater defense systems. Normally, battery is dry and it is activated by contacting with seawater, which accommodates sufficient salinity to electrolyte. This particular feature gives the battery long or indefinite shelf life, which is very important considering availability in emergency condition. Those kinds of batteries are also called as "reserve batteries" as well.

Generally, magnesium is used as negative electrode and silver chloride is used as positive electrode.

Torpedo batteries

Torpedo batteries are employed in military so a very high power output needs to be produced for just a few minutes. The power density is another key parameter with endurance, safety in usage, long shelf life and resistance to shock and vibration. Since the 1970s, zinc-silver-oxide or magnesium-silver-chloride reserve batteries are used in military torpedo batteries.

Thermal batteries

Thermal batteries are also employed in military as torpedo batteries do. They are reserve batteries and are activated with application of heat. Usually, metallic salt is used as electrolyte. It is in solid form at ambient temperature so it is not conductive. When heat is applied, it is molten and it provides distinctive conductivity, which provides indefinite shelf life to the battery. Additionally, when they are activated, very high power output is generated for short periods. The mixture of lithium and potassium chlorides is used as an electrolyte. As a negative electrode, lithium is used and as a positive electrode, iron sulfide is used [3].

2.4.2 Secondary batteries

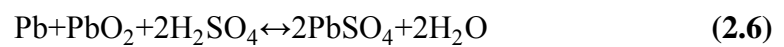
Secondary batteries, which are also called rechargeable batteries, can be recharged electrically after discharge rather than being discarded. While recharging, current is passed through the opposite direction of discharge current. Since electrical energy is stored, it is also known as “storage batteries” or “accumulators”.

In terms of usage of secondary batteries, it is classified under two subgroups. First application is to use it as an energy storage device. There is a need of primary energy source for charging and the device is mostly connected to this source. When there is demand, energy is delivered. These types of secondary batteries are used in automotive and aircraft systems. Second application is to use it as a primary battery while discharging and but can be recharged after usage rather than replace. This type of secondary battery is used in portable consumer electronics, power tools, electric vehicles etc.

Having high power density, flat discharge curve, and good low-temperature performance are the properties of the secondary batteries in addition to their rechargeability [1, 3].

2.4.2.1 Lead-acid batteries

Lead acid batteries are the oldest secondary batteries that widely used and well know which was developed in 1859. Lead is used in both electrodes as active material. Lead (Pb) is used a negative electrode and lead oxide (PbO₂) is used as a positive electrode. As an electrolyte, sulphuric acid (H₂SO₄) aqueous solution is used. The total reaction is simply



The nominal cell voltage is around 2V.

While discharging; in negative electrode, lead (Pb) is oxidized into the divalent ion Pb⁺² in sulphuric acid (H₂SO₄) and forms lead sulphate (PbSO₄); and in positive electrode, the charged active material fourvalent ions (Pb⁺⁴) is reduced to Pb⁺².

Lead-acid batteries have several advantages, which can be summarized as high rate capability, moderately good performance at varied temperature, good float service and low cost. On the other hand, its main disadvantages can be summarized as limited specific energy and energy density, relatively low cycle life and poor charge retention and storageability in the discharge state.

Applications of lead acid batteries can be categorized under three main groups which are starting/lighting/ignition (SLI) or automotive, traction, and stationary. Each device has its own design feature and operating duty [1-3, 10, 11].

For more detail information, further reading of [1-3, 10, 11] is recommended.

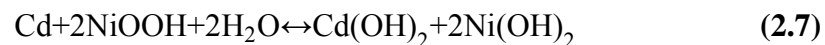
2.4.2.2 Alkaline batteries

In alkaline batteries, an aqueous alkaline solution like potassium hydroxide (KOH) or sodium hydroxide (NaOH) is used as the electrolyte. In rechargeable batteries, one of the three metals (cadmium, iron, or zinc) is used as negative electrode. As for positive electrode, oxide of metals in a higher valence state is used and mostly one of the three metals (manganese (IV) oxide, nickel (III) oxide, or silver (II) oxide) is used as a positive electrode [1, 3].

Nickel-cadmium batteries

Nickel cadmium secondary batteries are the most common and popular in alkaline secondary battery segment which has varied cell designs and broad range of sizes. It was used in portable devices up to 1990. It is also known as “nicads”.

Cadmium (Cd) is used as a negative electrode and trivalent nickel oxyhydroxide (NiOOH) is used as a positive electrode. Mostly potassium hydroxide (KOH) is used as an electrolyte rather than sodium hydroxide (NaOH) considering its higher electrical conductivity. The total cell reaction is simply



The nominal cell voltage is 1.3V.

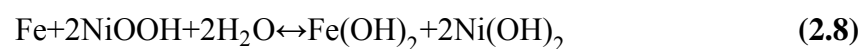
Nickel cadmium batteries can be employed in cylindrical, prismatic or button shapes where first two shapes are commonly used in the market. The advantages of nickel cadmium batteries can be summarized as having sustained high current, low internal resistance either at low or high temperature, storage at varied temperature like -30 °C to 60°C without any significant performance deterioration. On the other hand, there are several disadvantages of these batteries, which can be summarized as having lower voltage than primary cells, lower capacity, slow overnight recharge, relatively high self-discharge rate and memory effect [1, 3, 10].

For more detail information on nickel cadmium batteries, further reading of [1, 3, 10] is recommended.

Nickel-iron batteries

The commercialization of nickel iron batteries were started at the beginning of 20th century.

Iron (Fe) is used as negative electrode and trivalent nickel oxyhydroxide (NiOOH) is used as a positive electrode. Potassium hydroxide (KOH) is used as an electrolyte with the addition of lithium hydroxide to stabilize the capacity of cathode during charge/discharge cycle. The total cell reaction is simply



The nominal cell voltage is 1.37V.

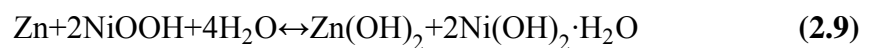
The advantages of nickel iron batteries can be summarized as having extremely rugged construction, long shelf life and endurance. On the other hand; high self-discharge, low coulombic efficiency, poor energy and powder density, poor low temperature performance and higher cost compared to lead acid batteries are the main disadvantages of nickel iron batteries [1, 3, 9].

For more detail information on nickel cadmium batteries, further reading of [1, 3, 9] is recommended.

Nickel-zinc batteries

In nickel-zinc batteries; zinc (Zn) is used as negative electrode where trivalent nickel oxyhydroxide (NiOOH) is used as a positive electrode. Since zinc has high electrode potential, nickel zinc batteries have relatively high voltage.

The total cell reaction is simply



The nominal cell voltage is 1.78V.

The energy density of nickel zinc batteries are two times more than nickel cadmium batteries. Being environmental friendly, relatively cheap, and good rate capacity are the advantages of the nickel zinc batteries. However, zinc has a good solubility in potassium hydroxide (KOH) which causes reduction in cycle-life due to shape change at zinc electrode. By using additives at negative electrode and using diluted solution of KOH were extended the cycle-life of the nickel zinc batteries but not enough for using them in electric cars [1, 3, 9].

Nickel-hydrogen-electrode batteries

In hydrogen electrode batteries, hydrogen is used as negative electrode while the positive electrode is trivalent nickel oxyhydroxide (NiOOH).

The total cell reaction is simply



The nominal cell voltage is 1.32V

This system is exclusively developed for aerospace applications, which require long cycle life at low depth of discharge. However, their practices are very limited considering its high cost [1, 7].

The further extension of these type batteries is nickel-metal hydride batteries where hydrogen is stored in metal hydride form. The total cell reaction is simply



The nominal cell voltage is 1.32V

Compared to nickel cadmium batteries; nickel metal hydride batteries have greater specific energy and energy density. Also considering the recycling, they are environmental friendly. However; they are more costly and have higher self-discharge rate compared the nickel cadmium batteries. Also at higher temperatures, they do not have promising charge acceptance [1, 3, 9, 10].

Silver-oxide batteries

In silver-oxide batteries; zinc or cadmium is used as negative electrode and as positive electrode, either silver peroxide (Ag_2O) or silver monoxide (AgO) can be used. Since silver peroxide (Ag_2O) is not stable in the battery and is prone to react with silver (Ag) to give silver monoxide (AgO); silver monoxide (AgO) is preferably used as positive electrode even its cell voltage is lower than the silver peroxide cell voltage.

Due to high energy density, low internal resistance, and flat second discharge, zinc silver oxide batteries are used in submarines, military and space application. But they are commercialized batteries due to their high cost, limited cycle and activated life.

Cadmium silver oxide batteries have longer cycle life compared to zinc silver oxide batteries but their energy density is between nickel cadmium and zinc silver oxide batteries. Since they are also expensive as zinc silver oxide batteries, they are not commercialized as well [1, 9, 12].

Zinc-manganese dioxide batteries

Zinc manganese dioxide batteries are the rechargeable version of primary alkaline manganese cells. Eventhough they have higher capacity compared to well-known secondary batteries and low cost, its cycle life and rate capacity are not promising [1].

Lithium ion batteries

Since this work deals with lithium ion batteries and its modification, detail information on lithium ion batteries will be given in Chapter 3.

3. LITHIUM ION BATTERIES

3.1 History and Development of Lithium Ion Batteries

First rechargeable lithium batteries were introduced in the 1980s, after primary lithium ion batteries were commercialized in early 1970s, which was mentioned in Section 2. Lithium metal was used as anode, which provides high voltage and distinctive capacity. High energy density is attained lithium metal but violent chemical reactions are taken place due to temperature changes which causes safety concerns. Considering that, the researchers were focused on using lithium ions rather than lithium metal, which is relatively safer.

In 1986, reversible intercalation of lithium into graphite in a lithium/polymer electrolyte/graphite half-cell was shown by Rachid Yazami et al. Intercalation means that metal ions are reversibly taken into or out from host without giving significant changes to it [13].

After few years, Goodenough et al. showed that lithium ions can be intercalated (taken into) and extracted (taken out) from its host by electrochemically when Li_xMO_2 is used as a host. M can be cobalt, manganese or nickel. They also made a research on alternative material for lithium metal anodes [14]. Graphitic carbon was found as an alternative material for lithium as anode since it is dimensionally stable for lithium intercalation and extraction. In addition, it does not have safe concern compared to lithium. Considering these points, graphite was started to be used as anode in lithium ion rechargeable batteries [15].

Based on Goodenough et al. studies, first commercialized lithium ion rechargeable batteries was introduced to market by Sony in 1991 [16].

3.2 Preference of Lithium Ion Battery Compared to Other Batteries

The usage of portable electronic devices such as mobile phones and laptop computers is grown exponentially in last decades. Therefore, there is a demand for storage sources, which is compacted, light weighted and having high energy

densities. In addition, there is a demand for advanced batteries for electric vehicles considering the increasing global environmental concerns [17].

Considering lithium ion batteries characteristics, the usage and proposal of it for portable electronic devices and large devices appears to be logical. In Figure 3.1, in terms of energy densities, various types of battery technologies are compared [18].

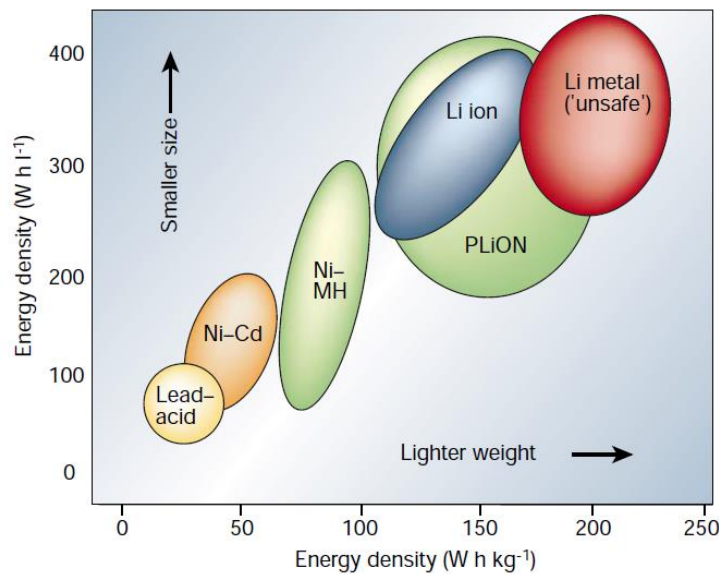


Figure 3.1 : Comparison of various types of battery technologies in terms of energy densities [18].

As shown in Figure 3.1, lithium ion batteries outperform other battery chemistries from both volumetric and specific energy density perspective. Having high energy density and design flexibility is the main motivation for using lithium ion batteries.

3.3 Lithium Ion Battery Components

Lithium ion battery is composed of mainly four compounds, which are the cathode, anode and electrolyte.

3.3.1 Cathode for lithium ion batteries

A variety of positive electrode materials have been developed and many of these are commercially available. A good positive electrode of a lithium ion battery should have high free energy of reaction with lithium and good structure stability that can prevent significant structural change after charge/discharge process. It should have high lithium ion diffusivity. Additionally, it should show good electronic conductivity and insoluble in electrolyte. Moreover, it should be produced from

inexpensive reagents and synthesized with low cost. The widely used materials, which show the good positive electrode properties, are the lithium transition metals oxides in lithium ion battery [1, 19].

3.3.1.1 Layered LiCoO₂

Widely used cathode materials for lithium ion batteries are layered lithium transition metal oxides, which are represented as LiMO₂ (M=Co, Ni or Mn). These are used as intercalation compounds.

LiCoO₂ has α -NaFeO₂ structure with oxygen in cubic closed packed arrangement. With the removal of lithium from the structure completely, the oxygen layers rearrange themselves to give hexagonal close packing of oxygen in CoO₂. Figure 3.2 shows the layered structure of transition metal oxides.

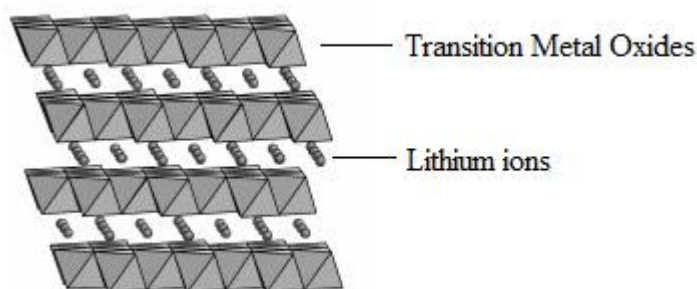


Figure 3.2 : Layered structure of transition metal oxides. Modified from [20].

Li_{1-x}CoO₂ is widely used as cathode in the market due to its cycling stability over thousands of cycles when x is changed from zero to 0.5. The theoretical capacity of Li_{1-x}CoO₂ is 140 mAh/g when x is 0.5. Without any capacity loss over 70 cycles, capacity can be increased from 140 mAh/g from 170 mAh/g between 2.75 to 4.4 V.

Considering its limited availability, cobalt is expensive to use. It has also safety issue due to its thermal stability. Therefore, it is used in only small cell. An alternative cathode material development is a need to for big scale applications [13, 14, 19].

3.3.1.2 Spinal LiMn₂O₄

The most well known spinal oxide is LiMn₂O₄, and its structure is shown in Figure 3.3. AB₂X₄ is the general formula for spinals and original crystal is based on the structure of MgAl₂O₄.

The discharge of LiMn_2O_4 occurs in two steps, one is around 4V and another is around 3V. Only 4V plateau is used with capacity around 120 mAh/g to avoid Jahn-Teller instability, which is related with Mn (III) instability.

The theoretical specific charge of the spinal $\text{Li}_{1-x}\text{Mn}_2\text{O}_4$ is 148 mAh/g when x is changed from zero to one. However, in commercial usage, it varies from 115 to 125 mAh/g when cycled between 3.5 and 4.3 V vs Li/Li^+ .

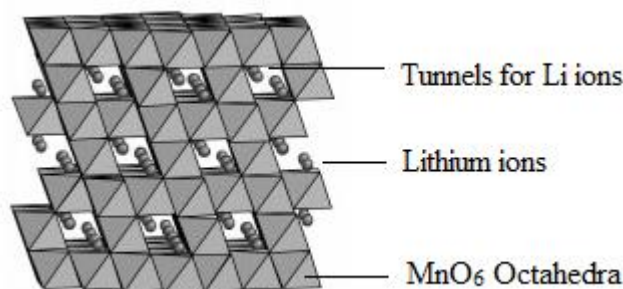


Figure 3.3 : Spinal structure of LiMn_2O_4 . Modified from [20].

Compared to layered LiCoO_2 ; spinal LiMn_2O_4 has lower cost, has higher electrochemical potential and is relatively less toxic. Nevertheless, it is unstable at elevated temperatures. However, recent studies show that there might be possible solutions to overcome this issue [13, 14, 19].

3.3.1.3 Olivine LiFePO_4

Among the phosphate based positive electrode, LiFePO_4 is the most promising one and the olivine structure of it can be seen in Figure 3.4.

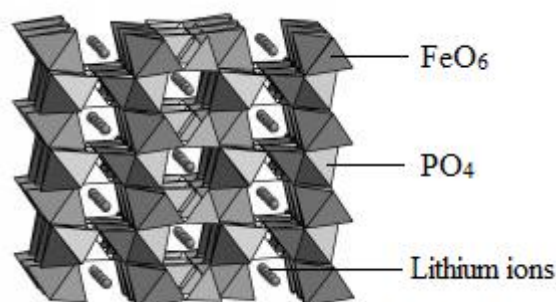


Figure 3.4 : Olivine structure of LiFePO_4 [20].

Similar to spinel LiMn_2O_4 , LiFePO_4 is inexpensive and has lower toxicity compared to LiCoO_2 .

The theoretical specific charge of LiFePO_4 is about 170 mAh/g. However, the practical specific charge is about 130 mAh/g.

The discharge occurs at 3.5 V vs. Li/Li^+ which is lower than LiCoO_2 . Therefore, it is not attractive for high power applications. However, since it is less reactive to electrolytes, it reduces the specific charge fading [13, 14, 19].

3.3.2 Anode for lithium ion batteries

A good negative electrode of a lithium ion battery should have high lithium chemical potential, high capacity, high electronic conductivity and low lithium diffusion barrier. Additionally, to prevent significant structural change after charge/discharge process, it should have good structure stability [19].

3.3.2.1 Lithium metal

With the properties of having largest theoretical specific capacity of any metal, the most electropositive metal vs. standard hydrogen electrode and the lightest metal, lithium metal is the ultimate anode material for lithium ion batteries. The highest possible gravimetric density and highest cell voltage against cathode material observed for any element are generated with lithium metal properties. However, dendrites are formed due to uneven distribution of lithium metal that is linked with non-uniform current distribution. These dendrites cause short-circuiting which is major handicap to use lithium metal as anode in lithium ion batteries [21].

3.3.2.2 Carbon based

Carbon based materials are used as anode material in commercial lithium ion batteries. Lithiated carbon potential is close to the one with lithium metal. Therefore, whole cell voltage of lithium ion battery is similar to the one using lithium metal as the anode. Considering that, different types of graphitized carbon are the most widely used anode materials. It can be found in different crystalline and amorphous forms. Natural graphite, oil, pitch, coal tar, benzene, hydrocarbons etc can be used as sources to produce carbon based anode materials. In general, carbon anode can be divided into three main groups, which are graphite, soft carbon and hard carbon depending on carbon with sp^2 bonding between carbon atoms. Soft carbon can be changed with heat treatment. Hard carbon cannot be graphitized even it is treated to

elevated temperatures [15, 23, 24]. The schematics of the structural of three types of carbon can be seen in Figure 3.5.

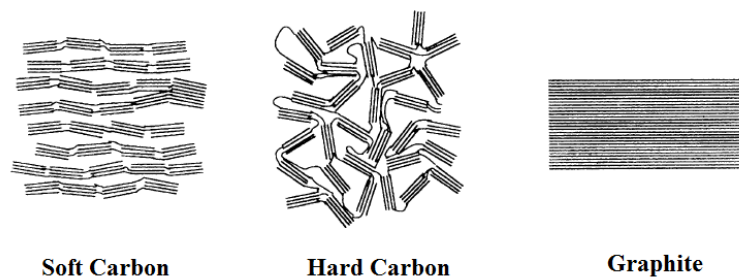


Figure 3.5 : Schematics of the structural of three types of carbon [22].

Graphite consists of stacked graphene layers. The space between planes is around 0.335 nm. There is about 10% volume expansion upon lithium intercalation. The theoretical capacity of graphite is 372 mAh/g. Soft carbon consists of graphene layers, which are neatly stacked, but there is less long-range order. The space between planes is around 0.375 nm. Soft carbons have low density, large irreversible capacity in the first cycle and poor cycleability. Hard carbon consists of graphene layers, which are not neatly stacked. The space between layers is above 0.38 nm, which means no volume change upon intercalation and potentially better cycleability. Hard carbons have similar disadvantages with soft carbon but still promising candidates as anode for high capacity batteries [21, 24].

To improve specific capacity and cycle life, the investigation on carbon based anode materials is still going on.

The specific capacity (Ah/kg) for lithiated carbon (LiC_6) and lithium metal anodes are 372 Ah/kg and 3862 Ah/kg respectively [1]. The theoretical capacity of metallic lithium is much higher than lithiated carbon material, which has composition of LiC_6 .

3.3.2.3 Alloy based

Many metallic elements (M) can react with lithium to form Li_xM_y alloys. Table 3.1 shows the specific capacity of some lithium-alloy forming metal elements. Lithium metal has the largest specific capacity among all metallic elements. Silicon has also very high specific capacity when $\text{Li}_{4.2}\text{Si}$ alloy is formed. Nevertheless, dramatic volume change is happened in metal when it reacts with lithium. This change leads to

cracking and failure of electrode. To overcome volume change upon lithium intercalation, alloy powders with small particle size have been proposed.

Table 3.1 : Gravimetric capacity of lithium-alloy forming elements. Modified from [15].

Components	Specific Capacity, mAh/g
LiC ₆	372
Li	3861
Li ₂₁ Si ₅	4199
Li ₃ As	1073
LiAl	993
Li ₂₁ Sn ₅	994
Li ₃ Sb	660
Li ₂₂ Pb ₅	569

Desirable cycling performance has been demonstrated with fine-grained alloy elements. There are many pores and cavities in a loosely packed small size metallic matrix, which have buffer effect on expansion of individual particles. Overall dimension of electrode does not change during cycling since expanded particles do not contact very much during extraction of lithium from Li_xM_y particles [15].

Figure 3.6 shows the positive and negative electrode materials with their voltage vs. capacity values, which are presently used, or under consideration for the next generation of rechargeable lithium ion batteries [18].

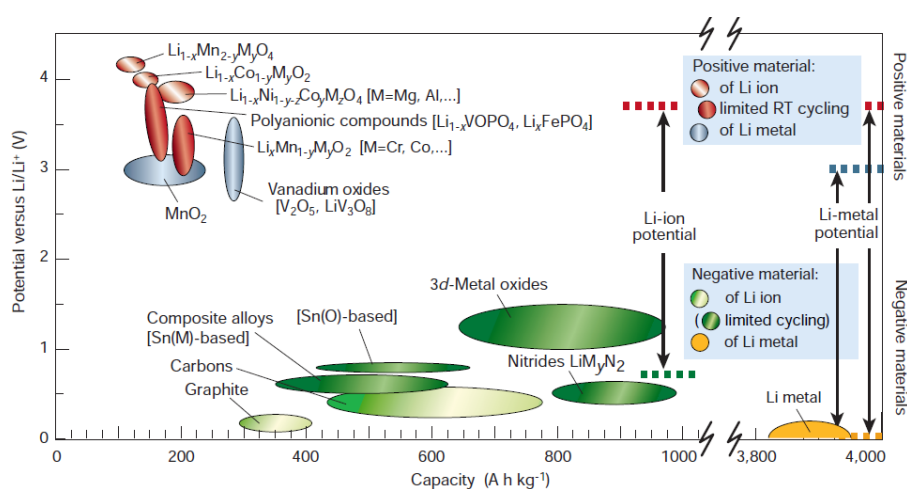


Figure 3.6 : Voltage versus capacity for positive and negative electrode materials for lithium ion batteries [18].

3.3.3 Electrolyte

The main function of the electrolyte is to provide steady flow of electrons via an external circuit and prevent direct electron change between electrodes. The main property of the electrode is to be an ionic conductor to secure the internal charge transfer. Additionally, it should be remain inert during operation so it can show electrochemical stability. These two main properties can only be achieved either by the electrolyte components being thermodynamically stable under operating conditions or by effective passivation of electrode surface, preventing sustained decomposition of electrolyte components. In lithium ion batteries, second option is mostly preferred. To have low melting point and high boiling temperature, electrolyte should include wide range of liquid and have a good thermal stability up to 70 °C. Moreover, it should be compatibility with other cell components, safe to use, has low toxicity and low cost [1, 21].

The electrolyte used in lithium ion batteries can be classified under four main groups, which are polymer electrolytes, gel electrolytes, ceramic electrolytes and liquid electrolyte. Liquid electrolytes are the most commonly used in lithium ion batteries, which are composed of lithium salts dissolved in multiple non-aqueous organic solvents. The key reason for mixing several solvents is to obtain desired ion conductivity.

LiClO_4 , LiAsF_6 , LiPF_6 , LiO_3CF_3 , $\text{LiN}(\text{SO}_2\text{C}_2\text{F}_5)_2$, LiBF_4 are the candidates for lithium salts. Most common salt used in marketed lithium ion batteries is LiPF_6 , which has a high conductivity and good safety properties. However, it is expensive, hygroscopic. In addition, it gives hydrofluoric acid (HF) when react with water so needs to be handled in a dry environment. The solution with $\text{LiN}(\text{SO}_2\text{C}_2\text{F}_5)_2$ also offers high conductivity, it is stable to water and easily dries and does not cause any aluminum corrosion. Considering these promising properties, it has received significant attention [1].

Two to four solvents are used in current lithium ion batteries. Using multiple solvents provide better cell performance, higher conductivity and a broader temperature range than possible compared to single solvent electrolyte. Almost all solvents in current lithium ion batteries are esters due to their oxidative stability and ability to form stable passivating products after reaction.

The dieters of carbonic acid (carbonates) are most commonly used. Binary mixture of linear and cyclic carbonates is used as electrolytes, which has low viscosity and high electric constant respectively. Common cyclic carbonates are made of ethylene carbonate (EC) and propylene carbonate (PC). The common linear carbonates are diethyl carbonate (DEC), dimethyl carbonate (DMC) and ethyl methyl carbonate (EMC). Figure 3.7 shows the structural formulas of these important solvents.

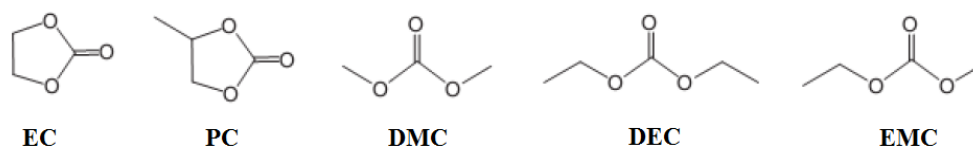


Figure 3.7 : Structural formulas of important co-solvents [21].

The conductivity of of 1 M LiPF_6 solutions in common solvents, which are shown in Figure 3.7, is shown in Table 3.2.

Table 3.2 : Conductivity, in mS/cm, of 1M LiPF_6 solutions in various solvents. Modified from [1].

Solvent	0.0 °C	20.0 °C	40.0 °C	60.0 °C	80.0 °C
DEC	2.1	2.9	3.6	4.3	4.9
EMC	3.2	4.3	5.2	6.2	7.1
PC	2.8	5.2	8.4	12.2	16.3
DMC	4.7	6.5	7.9	9.1	10.0
EC	-	6.9	10.6	15.5	20.6

Different salt concentration and temperatures gives different variety of conductivity. The conductivity of binary 1:1 mixtures of EC with common solvents for different salt concentration and temperatures are summarized in Table 3.3.

In addition, the conductivity of 1 M LiPF_6 binary solutions with EC is plotted over temperature in Figure 3.8. As shown, EC:DMC solution offers biggest conductivity with low capacity fade [1].

Table 3.3 : Conductivity, in mS/cm, of LiPF₆ solutions in binary mixture, 1:1 by weight, C: partially crystallized, S: saturated. Modified from [1].

Solvent	Concentration	0.0 °C	20.0 °C	40.0 °C	60.0 °C	80.0 °C
EC:DEC	0.25 M	1.7 (C)	4.2	5.8	7.3	8.8
	0.50 M	3.0	6.4	8.7	11.1	13.6
	1.00 M	4.2	7.0	10.3	13.9	17.5
	1.25 M	3.6	6.4	9.7	13.6	17.4
	1.50 M	-	5.6	-	-	-
	1.75 M	-	4.8 (S)	-	-	-
EC:DMC	0.25 M	4.2	5.8	7.8	9.7	11.5
	0.50 M	6.5	9.3	12.8	16.0	19.1
	1.00 M	6.9	10.3	14.0	17.9	21.6
	1.25 M	7.0	-	15.0	19.5	24.0
	1.50 M	5.6	9.3	13.7	18.4	23.3
	1.75 M	5.4	9.3	14.1	19.2	24.7
EC:EMC	0.25 M	3.7	5.3	7.2	9.1	10.9
	0.50 M	5.1	7.5	10.2	12.8	15.4
	1.00 M	5.3	8.5	12.2	16.3	20.3
	1.25 M	4.7	8.0	12.0	16.2	20.6
	3.50 M	-	0.9 (S)	-	-	-

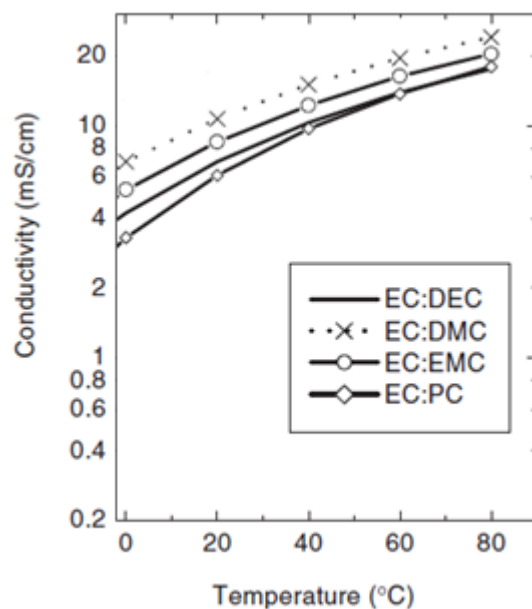


Figure 3.8 : Conductivity of 1 M LiPF₆ solutions in various binary mixtures, 1:1 by weight. Modified from [1].

3.4 Mechanisms

3.4.1 Fundamentals

The design of lithium ion battery system requires careful choice of battery materials to obtain high operating voltage (V_c). The operation of lithium ion battery obeys thermodynamic laws. Therefore, the electrochemical chemical reaction in lithium ion battery follows Gibbs-Helmholtz equation:

$$\Delta G = \Delta H - T\Delta S \quad (3.1)$$

, where ΔG is the free energy change of reaction, ΔH is the reaction enthalpy change and ΔS is the reaction entropy change.

The free energy change, ΔG , of a cell reaction is also related to its electrochemical voltage, E , based on Faraday's law;

$$\Delta G = -nFE \quad (3.2)$$

, where n is the number of electrons transferred in the reaction and F is the Faraday's constant (96487 C/mol).

The gravimetric energy density (GED) of a battery in mWh/g is given as:

$$GED = V_c \times GC \quad (3.3)$$

, where V_c is the operating voltage in volt and GC is gravimetric capacity in mAh/g.

The theoretical gravimetric capacity, GC in mAh/g, for a compound is given as:

$$GC = ((1/M) \times nF) / 3.6 \quad (3.4)$$

, where M is the molar mass of a compound and F is Faraday's constant.

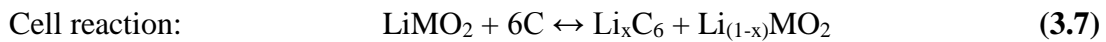
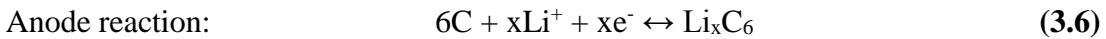
3.4.2 Charge and discharge mechanism

Lithium ion battery is composed of mainly three compounds, which are the cathode, anode and electrolyte. Variety of materials can be used for these compounds, which was explained in detail at Section 3.3.

As cathode, typically lithium containing transition metal oxide ($LiMO_2$) is used. As anode, carbon based material is used. Electrolyte can be a liquid, a gel or a solid polymer. The electrodes are separated from each other via separator but electrically connected by electrode, which allows ions to flow.

In lithium ion battery, energy is stored through red-ox reactions. Reduction reaction takes place at cathode where oxidation reaction takes place at anode. The electrons which are released during oxidation reaction is used while reduction reaction. The direction of external electron flow is from anode to cathode during the cell operation.

The reactions take place at electrode and also total cell reaction for a standard $\text{LiMO}_2/\text{graphite}$ cell are shown as follow;



For the reaction in equations (3.5)-(3.7), the arrows to the right indicate charging and those to the left indicate discharging [13, 21].

The mechanism of charge and discharge can be seen from Figure 3.9 [25].

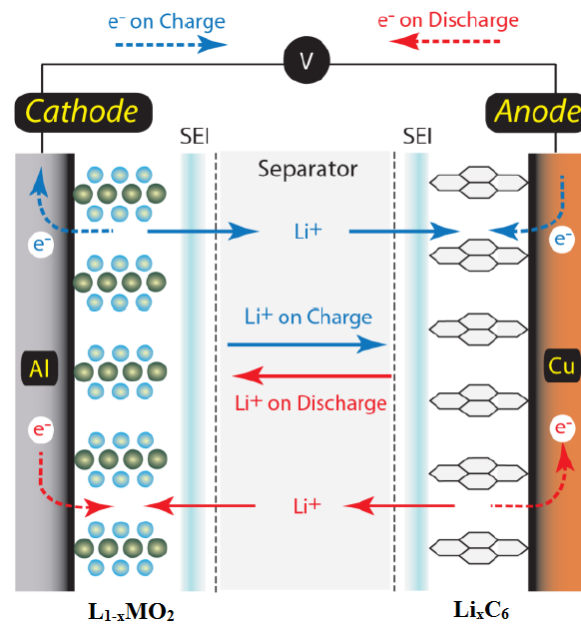


Figure 3.9 : Charge and discharge mechanism of lithium ion batteries [25].

As shown in Figure 3.9, depending on whether cell is being charged or discharged, the electrodes behaves as cathode and anode. During the discharge, electrons flow from the negative electrode, which is anode, to positive electrode, which cathode. However; during charging, negative electrode acts as cathode while positive electrode acts as anode since internal electrochemical potential difference is lower than the voltage supplied from externally. Considering that, electrodes are named as cathode or anode according to their functionality during discharge [21].

3.4.3 Intercalation and de-intercalation process

During discharging and charging of lithium ion batteries, Li^+ ions move back and forth between cathode and anode. Therefore, the processes of Li^+ ions entering and leaving of electrodes are called intercalation and de-intercalation respectively. Sometimes, it is also called “rocking chair battery” where in both electrodes, there is no change at host materials and its structure nearly but Li^+ ions shuttle between cathode and anode. Ions are reversibly inserted or removed from the host during intercalation and de-intercalation process. During that, often, volume change at host material can be seen. However, the structure of the material is not significantly changed. The host material’s crystal structure and its orientation, and ions’ properties affect the intercalation process. Intercalation of Li^+ ions into a common anode, graphite, can be shown in Figure 3.10. Li^+ ions should use the edge plane path between graphene layers in order to enter graphite structure.

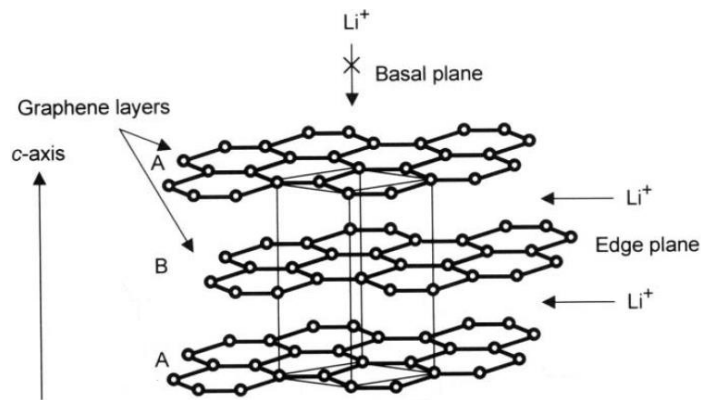


Figure 3.10 : Insertion mechanism of Li^+ ions into graphite. Modified from [26].

During charge of lithium ion battery, Li^+ ions are de-intercalated from cathode and intercalated into anode, please see equations (3.5) - (3.7). Based on the equation (3.6), x can be changed from zero to one depending on Li^+ ions’ intercalation level in the graphite structure. During the intercalation process, different phases or stages are formed. In Figure 3.11, the classical model of lithium staging in graphite can be shown. These stages can be seen as voltage plateaus on voltage vs. charge curves, which is illustrated on Figure 3.12. Typically, the main intercalation and de-intercalation of lithium takes place at potentials below 0.25 V vs Li^+/Li with three potential plateaus formation.

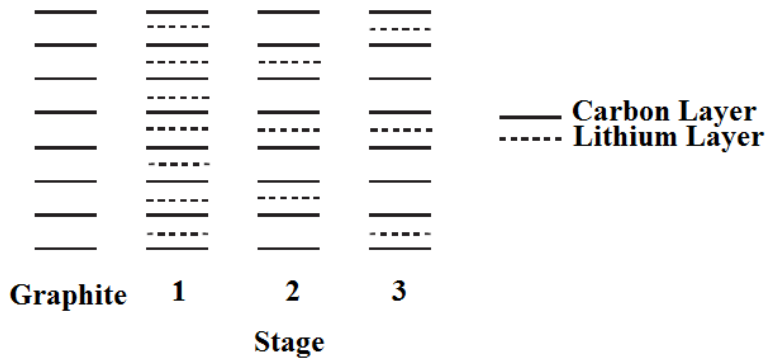


Figure 3.11 : Illustration of lithium staging in graphite [1].

During first charging, certain amount of charge is consumed which is not fully recovered during following discharging. This none-recovered capacity is called irreversible capacity, which is seen at first charge/discharge cycle of carbon-based materials. Following cycles, good rechargeability is shown by graphite, which is called reversible capacity rate.

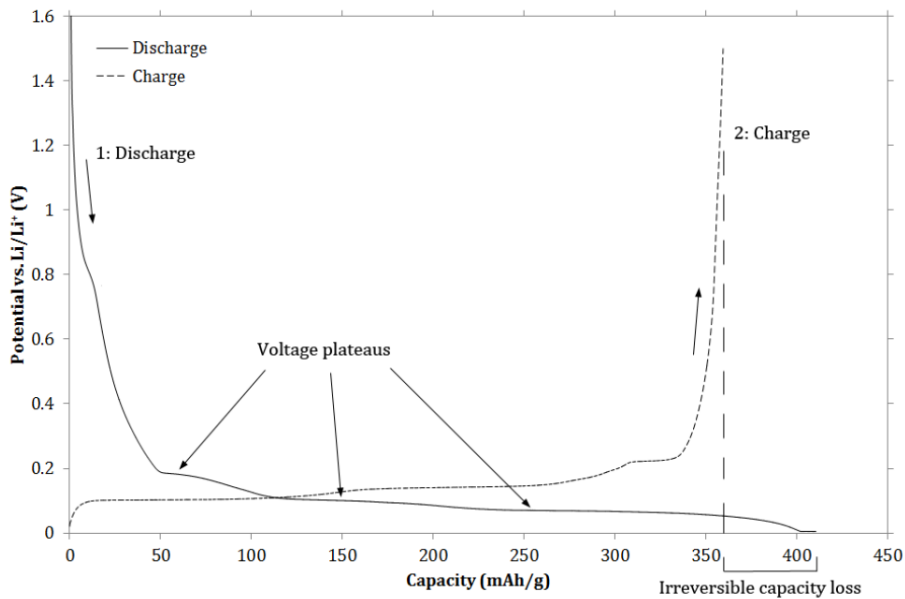


Figure 3.12 : Voltage plateaus on voltage vs charge curves. Modified from [19].

The theoretical maximum capacity of Li^+ ions in the graphite structure is one Li^+ per six carbon atoms, which corresponds to LiC_6 . This can be achieved in stage 1 shown in Figure 3.11, which is the most lithium rich stage. In-plane structure of graphite, which is fully intercalated with Li^+ ions at stage 1, can be shown in Figure 3.13. In terms of electric energy, the theoretical capacity of graphite in lithium ion battery is 372 mAh/g [1, 13, 21, 26].

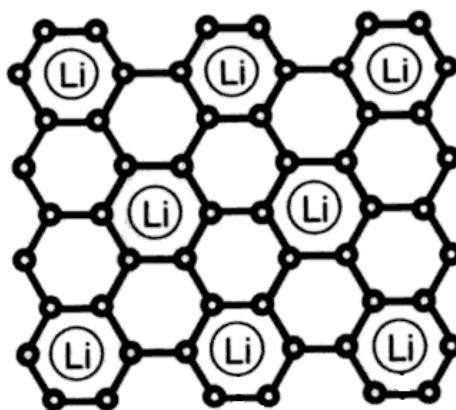


Figure 3.13 : In plane structure of graphite in which is fully intercalated with Li^+ ions (LiC_6). Modified from [25].

3.4.4 Solid electrolyte interphase formation

Solid electrolyte interphase (SEI) formation is the most important parameter that affects the battery performance. SEI formation is occurred due to degradation of electrolyte and other solid materials in electrolyte. Since it affects the battery performance, it has been searched for many years. SEI is formed after battery is performed so it is very difficult to analyze it during its formation. Considering that there is no clear understanding on its compounds, structure and general properties [21].

During first charge cycle, electrolyte and its solid materials are degraded and formed a layer on negative electrode. This layer is called SEI. This process is irreversible and performance loss is observed at first cycle due to this formation as shown in Figure 3.14. The amount of irreversible capacity depends on electrolyte formulation, electrode materials, and carbon types used as anode. If the reaction takes place at particle surface, materials with low specific surface area normally give lower irreversible capacity [1].

As shown in Figure 3.14, lithium starts intercalation process with around 0.2V vs. Li/Li^+ . During first discharge, due to electrolyte reduction, reactions take place at voltage 0.8V vs. Li/Li^+ and SEI layer is formed on graphite surface. This layer acts as passivating layer and prevents solvent to co-intercalate but let lithium ions to flow through. Due to solvent co-intercalation with lithium into graphite, exfoliation of graphite sheet happens and this effects the intercalation of lithium process. SEI layer acts also as electronic insulator that prevents further reduction of electrolyte as cycling continues [5].

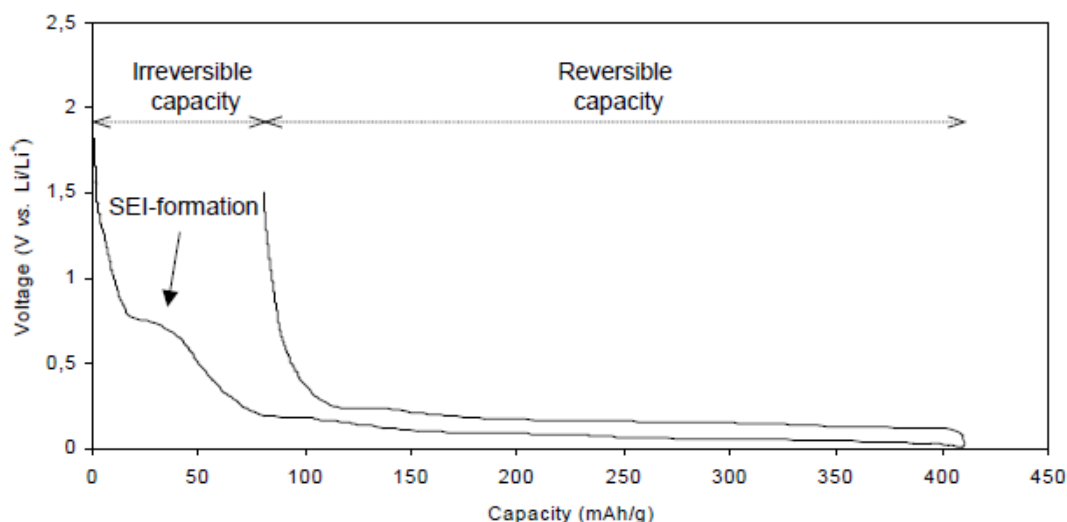


Figure 3.14 : The first cycle of graphite/lithium cell cycled in 1 M LiPF_6 EC/DEC (2:1) electrolyte [5].

Formation of SEI layer is irreversible and it is charge-consuming reaction. Depending on both carbon material and electrolyte formulation, irreversible capacity constitutes around 20% of total capacity.

Even though many factors affect the SEI layer's composition and morphology, most important factor is electrolyte formulation. Generally, this layer composed of many inorganic and organic materials in an inhomogeneous fashion and has a complex nature. Lithium fluoride (LiF), lithium oxide (Li_2O), lithium carbonate (Li_2CO_3), lithium alkyl carbonates (ROCO_2Li) and lithium alkoxides (ROLi) are the most common SEI components. Figure 3.15 shows a representative structure of SEI layer with different components.

Different types of electrolytes are used in lithium ion batteries. It is very crucial to have stable electrolyte at anodic and cathodic potentials in lithium ion battery, which are changed from 0V to 4.2V vs. lithium. Practically, there is no solvent, which is thermodynamically stable with lithium near 0V vs. lithium. But many solvents form passivation film on electrode surface with limited reaction. Therefore, thermodynamically stable SEI layer helps to improve battery performance and also stands for many years without significant degradation [1].

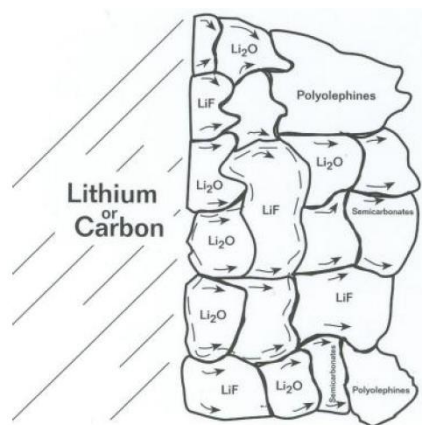


Figure 3.15 : Representative structure of SEI layer with different components [21].

During charge and discharge, gas formation is observed which is affected mainly by SEI formulation. Therefore, it is crucial to control the SEI formation. Control mechanism can be generated by modifying or doping the anode. These treatments can help to optimize charge speed in the battery. To obtain SEI formation, charge/discharge can be done at optimized speed. After completion of cycles, charged batteries can be stored at room temperature for several days and then SEI layer formation can be observed.

The comparison of SEM images of natural graphite, natural graphite after charge and doped natural graphite after charge can be seen in Figure 3.16.

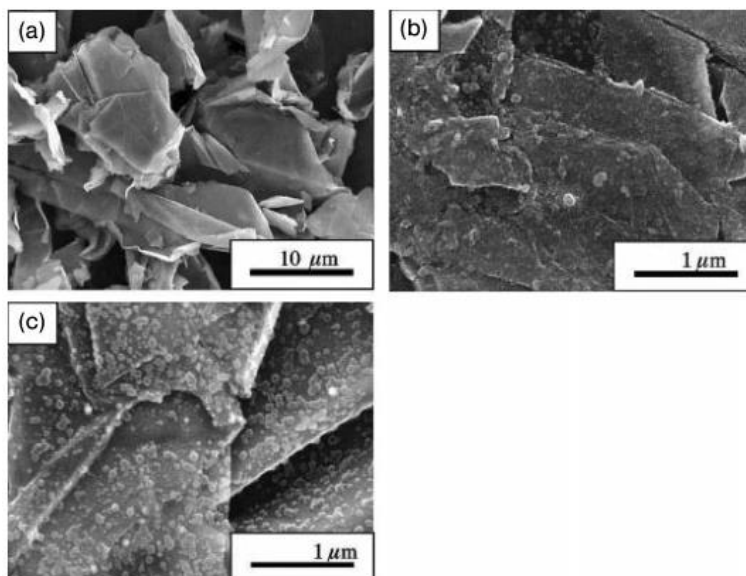


Figure 3.16 : SEM images of (a) natural graphite, (b) natural graphite after charge, (c) doped natural graphite after charge [20].

It is obviously seen that SEI formation is inhomogeneous on graphite surface. A large number of small spots were observed on graphite, which is due to doping. So

having adequate SEI formation on the electrode is very important to have safe operation of lithium ion battery [20].

Graphite plays important role on SEI formation. As graphite's specific surface area is increased, the capacity loss caused by SEI formation is also increased. Based on numerous studies proven; that surface area increase on non-basal plane increases irreversible capacity loss [5].

3.5 Battery Parameters and Performance Criteria

Basic parameters and performance criteria of lithium ion batteries will be given compared to Ni-Cd and Ni-MH.

3.5.1 Energy density

The energy density of battery can be given in two ways, per weight or per volume. The gravimetric energy density of battery is expressed in Watt-hours per kilogram (W-hr/kg). The volumetric energy density of battery is expressed in Watt-hours per liter (W-hr/l).

Energy density comparison of lithium ion battery versus Ni-Cd and Ni-MH can be seen in Table 3.4. It is clearly seen that; in terms of gravimetric energy densities, lithium ion battery is almost doubling the Ni-Cd and Ni-MH, which provides much lighter battery formation without compromising run time. Alternatively, the run time will be doubled if the battery weight is kept as same. This explains why lithium ion batteries is used for mobile phones and laptop computers instead of Ni-MH [27].

Table 3.4 : Energy Density Comparison. Modified from [27].

Cell Type	Ni-MH	Ni-Cd	Li-Ion
Gravimetric Energy Density (W-h/kg)	55	50	90
Volumetric Energy Density (W-h/l)	180	140	210

3.5.2 Cell voltage and voltage stability

To power the load, cell voltage is the key parameter. The Ni-Cd and Ni-MH have 1.25 V nominal cell voltages whereas lithium ion cell has 3.6V nominal cell voltage. The cell discharge curves can be seen in Figure 3.17. Considering that to achieve equal voltage of a single lithium ion cell, three series of connected Ni-Cd or Ni-MH are required.

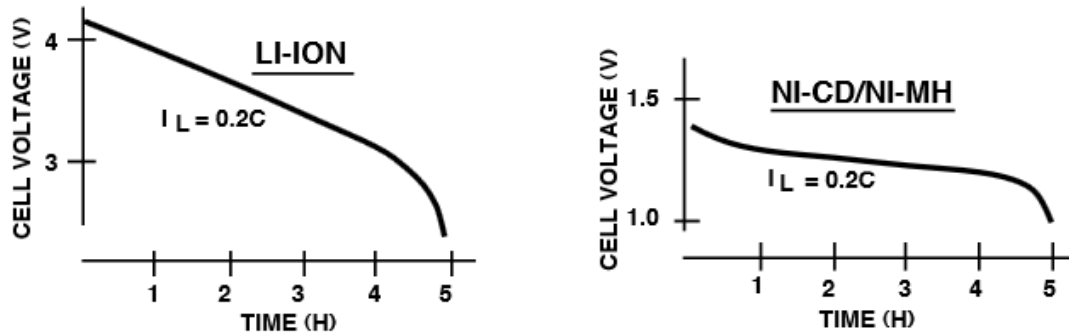


Figure 3.17 : Cell discharge curve [27].

However, as seen in Figure 3.17, the discharge curve of Ni-Cd or Ni-MH is very flat which is similar to ideal battery. So they can be easily used with linear regulators. Nevertheless, for lithium ion batteries, switching convertors are required to obtain good energy conversion efficiency in the power supply [27].

3.5.3 Capacity and rate capacity

The amount of energy that can be stored in a given amount of volume or mass is defined as specific capacity. It is measured as Amper-hour (Ah). The rate capability is the rate, which the cell is being charged [13].

3.5.4 Peak current

Internal equivalent series resistance (ESR) of a battery determines the maximum current can be delivered from that battery.

The battery voltage will be reduced by an amount equal to ESR multiplied with the load current which pass through ESR.

$$V = I \times R \quad (3.8)$$

In addition, the current passing through ESR will cause power dissipation within the battery which can be expressed by the ESR multiplied the current squared. This can cause significant heating within battery when there is high rate of discharge.

$$P = I^2 \times R \tag{3.9}$$

Both Ni-Cd and Ni-MH batteries have low ESR like below 0.1 Ω, which means that ESR is never a problem for peak charge for these kinds of batteries. Besides, lithium ion batteries have higher ESR compared to Ni-Cd and Ni-MH but mostly it is a problem for lithium ion batteries for most applications [27].

3.5.5 Cycle life and shelf life

High cycle lives of batteries are preferred due to economical and ecological reasons. The number of cycles illustrates how often the battery can be charged and discharged before it reaches to lower limit. Eighty percent of nominal capacity can be set as cycle life value.

Additionally, cell design, temperature, the electrochemical system and the charge state affect the shelf life of battery [28].

Shelf life of a battery depends on self-discharge, which occurs in all batteries. Table 3.5 shows the typical self-discharge of Ni-MH, Ni-Cd and Li-Ion batteries. However, these values may be varied with manufacturing specifications.

Table 3.5 : Rates of discharge. Modified from [27].

Cell Type	Ni-MH	Ni-Cd	Li-Ion
Self -Discharge @ 20 °C (%/Month)	20-30	15-20	5-10

When the discharge rates are compared, lithium ion battery is the most promising. However, it is important to note that temperature affects the self-discharge rate. As the battery temperature is increased, the self-discharge rate is also increased [27].

3.5.6 Operating temperature

Operating temperature is important parameter for battery regarding to charging characteristics and A-hr capacity. While designing the battery, it has to be ensured that chargers have temperature sensor to assure that the battery works in allowable temperature limit.

The safe charging temperature for Li-Ion battery is between 0 °C to 45 °C. The safe discharging temperature for Li-Ion battery is between -20 °C to 60 °C [27].

3.5.7 Safety

Thermal runaway and cell rupture can be occurred due to over heating or overcharging which are the main safety concerns for lithium ion batteries. This is the major disadvantages of this technology and laptops or mobile phones explosions cases were happened which have caused injuries. Approximately 80% of recent researches were focused on safety issues to operate Li-Ion batteries in safe [13].

3.6 Battery Design and Configuration

Battery design should be chosen depending on the requirement of application field. To give adequate capacity, power and safety feature, electrochemical potential and capacity of cathodes and anodes should be considered first while designing the battery. The current collection method, basic battery safety and electrode kinetics are the other factors that should be considered.

Depending on type of electrode/electrolyte configuration, electrolyte, and packaging; battery can be categorized. Electrode/electrolyte configuration can be grouped under two types which are winding type and stack type. Lithium polymer batteries require polymer electrode so liquid electrodes are used in lithium ion batteries. Can types and pouch types are the packaging classification.

Depending on designed voltage range, the electric capacity of battery can be changed. Battery voltage is changed proportionally to its state of charge. Also total electric capacity of the cathode is identical to that of anode during charging and discharging. These are the basic principle of a battery which are not changed eventhough battery desing may change depending on shape and function [28, 29].

The basic configuration of nearly all lithium ion batteries can be categorized under 4 main parts. The cathode is usually transition metal oxide (LiMO_2) which is coated onto an aluminum foil. The anode is used carbon based material, which is coated on a copper foil. As electrolyte, liquid type is used which is ionically good conducting. Also to prevent touch of cathode and anode, insulating separator is used.

As shown in Figure 3.18; cylindrical, coin, prismatic, and thin and flat battery configurations are the main four different configurations of lithium ion batteries, which can be found in the market depending on their usage.

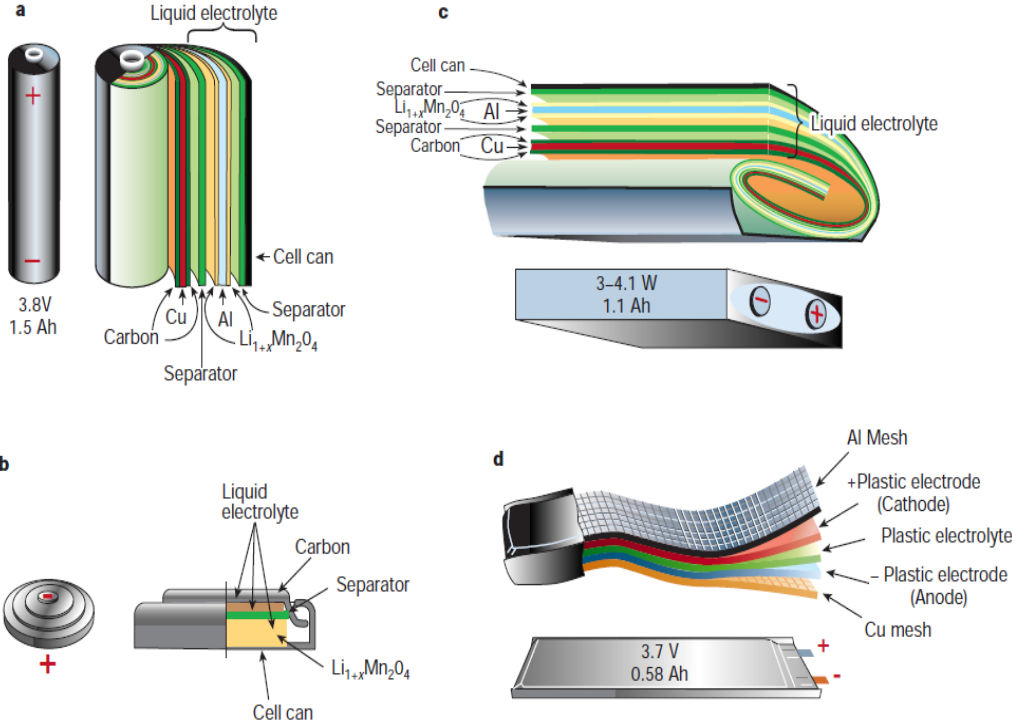


Figure 3.18 : Illustration of different Li-Ion battery configuration with shape and component. a, cylindrical; b, coin; c, prismatic; d, thin and flat [18].

3.6.1 Advantages and disadvantages of lithium ion batteries

Lithium ion batteries offer several advantages compared to other types of batteries. They have high specific energy and energy densities up to 150 Wh/kg. They have low self-discharge rate and longer shelf life up to 5 to 10 years. They have rapid charge capability. Moreover, they have higher cell voltage up to about 4V per cell, high coulomb and energy efficiency. Additionally, there is no need for maintenance and memory effect. They operate fairly wide operating temperatures. In addition, there is a possibility of miniaturization and very thin form production.

In contrast, lithium ion batteries have some disadvantages. They have relatively high initial cost. They are degraded at high temperatures. In addition, there is a need of a protection circuit to avoid overcharge, over discharge and excessive temperature rise. Additionally, they offer lower power than Ni-Cd and Ni-MH, especially at low temperatures [1, 7, 30].

4. CHARACTERIZATION METHODS

The performance of lithium-ion batteries is defined by its properties such as capacity, power, charge/discharge rate and safety, which can be directly influenced by adopting electrode materials with different electrochemical characteristics. Additionally, charge/discharge cycles cause irreversible changes in the microstructure of the electrodes, which may result in capacity drop [31]. Hence, the detailed analyses of structural and electrochemical properties of electrode materials and batteries respectively are of utmost importance for development of high performance batteries.

This section gives a brief review on the characterization methods of electrode materials and batteries for lithium-ion batteries. In section 4.1, the structural characterization methods are explained, while section 4.2 is dedicated to the electrochemical analysis.

4.1 Structural Characterization

Most widely used methods for structural characterization can be summarized in the following 6 categories.

4.1.1 X-ray diffraction (XRD)

Although, Nobel Prize winner Wilhelm Conrad Rontgen discovered the X-rays in the end of 19th century, Max von Laue did not discover the X-ray diffraction (XRD) by crystals until 1912 [32]. This discovery resulted in the development of two new sciences: X-ray crystallography and X-ray spectroscopy, which is widely used for the identification of bulk crystalline structures [32, 33].

The X-rays are electromagnetic waves in the wavelength range between 0.01 and 10 nm, corresponding to energy of 100 eV up to 100 keV. Small wavelengths result in a good penetrating ability and are used for imaging applications in medicine and science. The penetrated waves can also interact with the internal structure of the

investigated solid, such as crystals. This interaction results in a constructive interference, if the incident wave is reflected from the crystalline plane with an angle θ (angle between the incident beam and plane normal), which can be calculated by

$$n\lambda=2d \sin \theta \quad (4.1)$$

, where λ is the wavelength of the X-rays, n is the order of reflectance and d is the distance between two crystalline planes (lattice spacing) causing the constructive interference according to Bragg's law [14]. Figure 4.1 shows the Bragg diffraction by crystal planes.

By sweeping the incident angle, a spectrum of diffraction intensities is obtained as a function of incident angle. Thus, the crystal structure can be analyzed by comparing the measured spectrum with spectra of known origin. Databases containing more than 60000 spectra exist today [34].

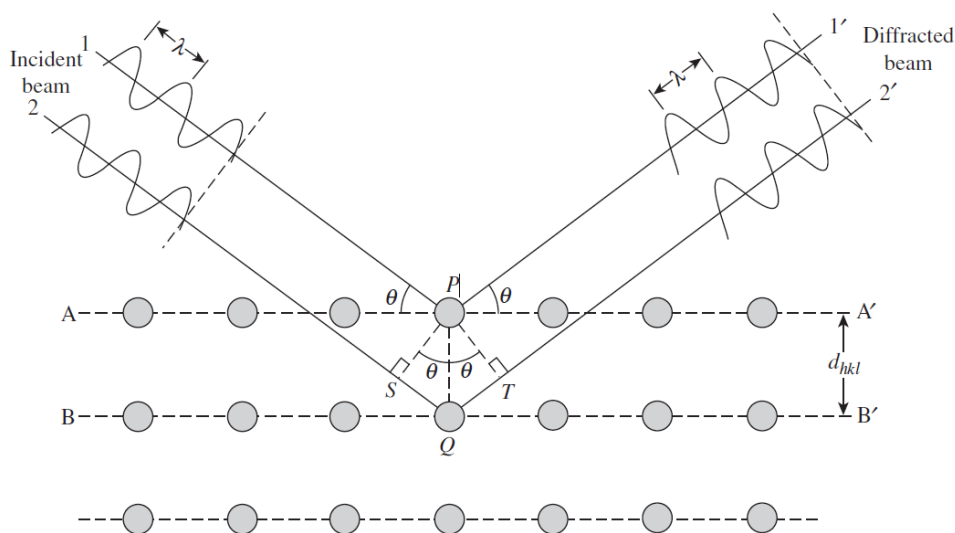


Figure 4.1 : Schematic of the Bragg diffraction by crystal planes [34].

In summary, XRD is used to characterize the crystallographic structure, crystallite size and preferred orientation in polycrystalline or powdered solid samples [30].

4.1.2 X-ray photoelectron spectroscopy (XPS)

When an atom absorbs an X-ray photon, an electron is ejected from one of the inner electron shells (the lowest shell is marked as K, the second lowest shell as L etc.) of the atom, since the X-ray photons are highly energetic. Figure 4.2 presents the electron emission process from the inner shell K after the absorption of highly energetic X-ray photons. The energy needed for an electron to escape the atoms

surface (binding energy) depends on the investigated material and escaped electron shell. This unique energy can be used to identify the investigated material. Figure 4.3 shows the XPS spectrum of an oxidized aluminum surface as a function of binding energy. Each peak is assigned not only to an element but also to a specific electron shell. Electron shells are addressed with the quantum numbers, e.g., principal quantum number and azimuthal quantum number. For example, Al 2p corresponds the second subshell of the second electron shell.

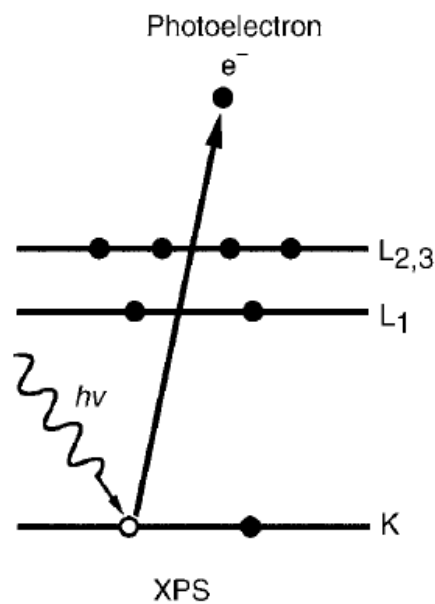


Figure 4.2 : Electron emission process after the absorption of X-rays from the inner shell K [34].

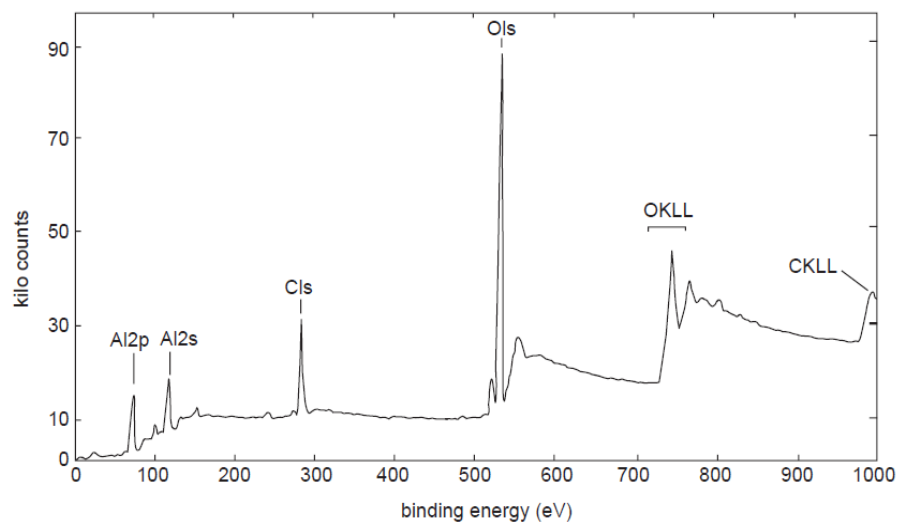


Figure 4.3 : XPS spectrum of an oxidized aluminum surface as a function of binding energy [34].

4.1.3 X-ray fluorescence (XRF)

XRF is used to analyze the chemical properties of the investigated materials by detecting the characteristic X-rays emitted from the material after radiated and excited by high-energy X-rays. The characteristic attributes of the material can be obtained from either the wavelength or the energy of the emitted radiation. Hence, two types of XRF exist, i.e., wavelength dispersive spectroscopy (WDS) and energy dispersive spectroscopy (EDS). A visual comparison of operation mode of both types is presented in Figure 4.4 [34].

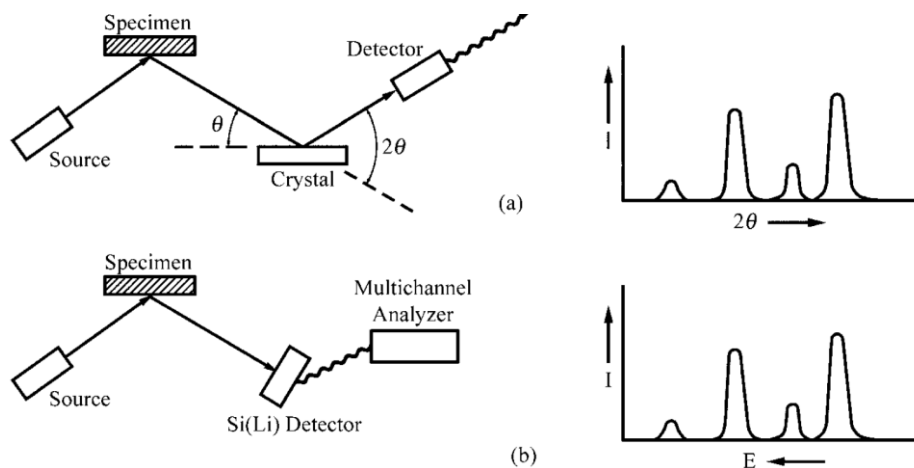


Figure 4.4 : Comparison of a) wavelength dispersive spectroscopy
b) energy dispersive spectroscopy [34].

A basic XRF-spectrometer consists of an X-ray source, a detection system and data collection part. The first part is responsible for the generation of excitation radiation. In a wavelength dispersive spectrometer, the fluoresced radiation is detected via a single crystal, since only a specific wavelength is diffracted with a given angle, at which the detector is positioned, according to the Bragg's law. In contrast to that, energy dispersive spectrometer features a photon detector, which can separate the incident X-ray photons according to their energies. WDS features a better resolution than the EDS. However, the technique is harder to employ, since the instrumentation is more complicated. A comparison of spectra obtained with WDS and EDS is shown in Figure 4.5. On the left hand side, WDS spectrum is presented as a function of wavelength in \AA , while on the right hand side, the EDS is given as a function of energy in eV. It should be kept in mind, that the obtained values via WDS are relative with respect to the background. The characteristic lines are assigned to the corresponding materials.

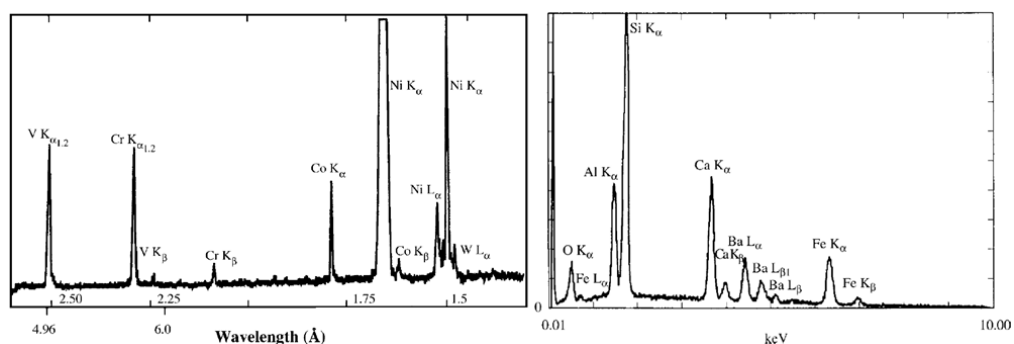


Figure 4.5 : Comparison of measurement spectra (left) vs. WDS (right) EDS [34].

4.1.4 Fourier transform infrared spectroscopy (FTIR)

FTIR is most widely used spectroscopic technique in IR-range. In contrast to dispersive spectroscopy, the whole spectrum is obtained at once using a Fourier transform method. The main part of FTIR spectrometer is the so called Michelson interferometer, as given in Figure 4.6. The incident IR radiation from the source enters the interferometer and with the help of a beam splitter, one half of the radiation is transmitted to a fixed mirror, while the other half is reflected to a moving mirror. After the reflection at both mirrors, the beams collide once again at the beam splitter. By changing the distance of the moving mirror, interference is generated between two beams, which results in constructive and destructive interference periodically as a function of distance. The combined beams are then transmitted through the investigated material to the detector. The resulting image at the detector is called interferogram, which is the sum of superposed sinusoidal signals. After the Fourier transformation of the interferogram, an IR-spectrum is obtained. An example of interferogram can be seen in Figure 4.7.

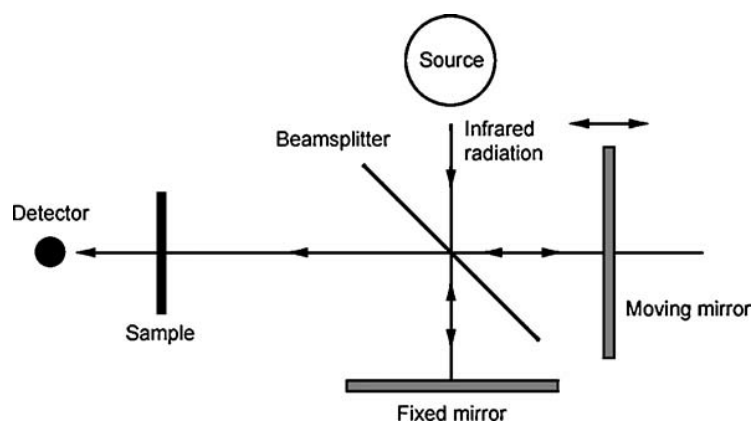


Figure 4.6 : Schematic of the Michelson interferometer [34].

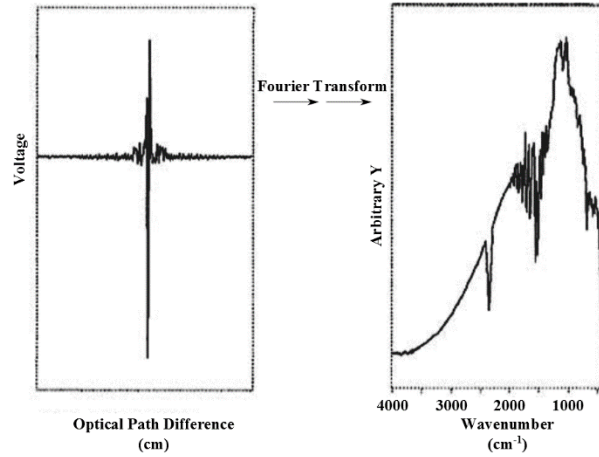


Figure 4.7 : (left) Interferogram (right) IR spectrum [34].

However, the obtained IR-spectrum also contains data from the background, e.g., detector, beam splitter, mirror, IR source, disturbing contribution of water vapor and carbon dioxide in the atmosphere. A reference measurement should be undertaken without the investigated material to eliminate the contribution of the background. Figure 4.8 shows the final transmission spectrum of the investigated material. Transmission is the ration of the incident and transmitted radiation.

FTIR can also be used to measure the reflectance, but the signal to noise ratio (SNR) is better by the transmission measurements. Like X-rays, the absorption lines of materials in IR range are unique and can be used to analyze samples.

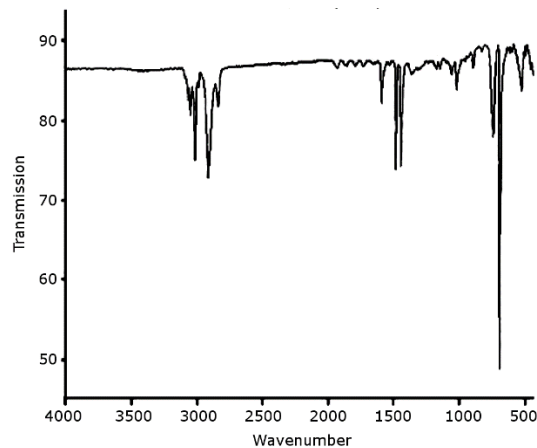


Figure 4.8 : Final spectrum of the investigated material obtained with FTIR [34].

4.1.5 Scanning electron microscopy (SEM)

Manfred Ardenne first invented the scanning electron microscope in 1937. An electron gun, containing a cathode mostly made of tungsten, generates a beam of

thermions, thermionically generated electrons, with energy in the range between 0.2 keV and 40 keV. The beam is focused to a spot with a diameter in the orders of 10^{-9} m, and is swept in a raster across the surface of the investigated material. The interaction of high-energy electron beam with the surface may cause in the reflection of electrons by elastic scattering, emission of secondary electrons and emission of characteristic electromagnetic radiation, mostly X-rays. The interactions are monitored with an appropriate detector and allocated to a spatial position. The variations of the electron scattering and generation of secondary electrons indicates changes in elevations, thus allowing generating a tomographic image of the surface [35, 36]. A comparison of photographs taken with a light microscope and SEM can be seen in Figure 4.9. SEM photograph contains the topographic data as well as features the same in-plane resolution [34].

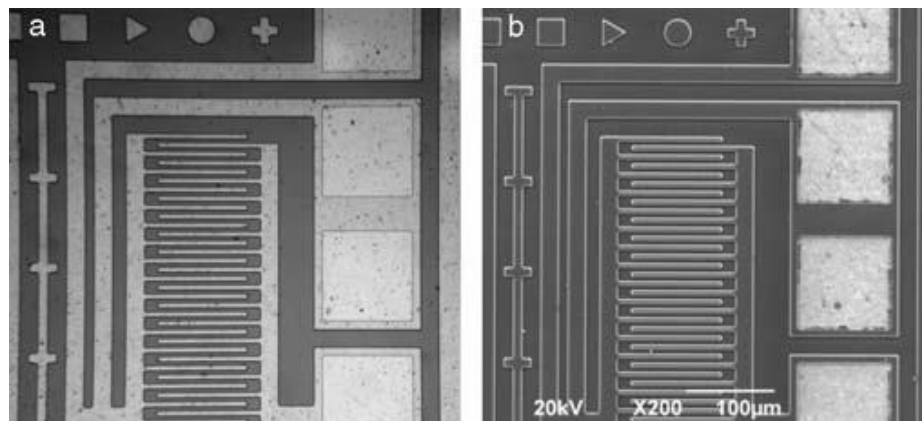


Figure 4.9 : Comparison of two photographs taken with light microscope and SEM [34].

Additionally, the characteristic X-rays are used to identify of the investigated material. Thus, SEM is used to analyze the topography and morphology of powder samples.

In this study, sample morphologies were investigated using Tescan Vega3 SBU (Figure 4.10). Tungsten heated cathode is used as electron gun. The resolutions at high and low vacuum mode are 3 nm at 30 kV/8 nm at 3 kV and 3.5 nm at 30 kV respectively. Magnification varies from 3x to 1000000x. The maximum field of view is 25 mm at WD 30 mm [37].



Figure 4.10 : Tescan Vega3 SBU device [37].

4.1.6 Transmission electron microscopy (TEM)

Two scientists Max Knoll and Ernst Ruska invented transmission electron microscope in 1931 [38]. In contrast to SEM, by TEM, the electrons are transmitted through the investigated material, if it is transparent to the electron beam at the adopted wavelength. The tunneling electrons interact with the internal structure of the material like in XRD, which results in diffraction, since the electrons can also be assumed as waves due to the wave-particle dualism. In Figure 4.11, a TEM photograph of a single crystal is shown. The transmitted beam is brighter than the diffracted beams [34].

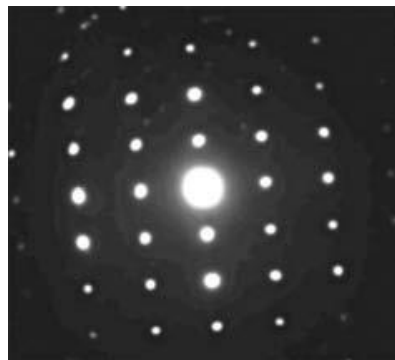


Figure 4.11 : TEM Photograph of single crystal. Electron diffraction pattern can be seen. The transmitted beam is brighter than the diffracted beams [34].

4.1.7 Raman spectroscopy

Raman spectroscopy is based on the Raman effect named after C. V. Raman which describes inelastic scattering of a monochromatic excitation source such as electromagnetic radiation [39]. The photons are absorbed by the investigated material and then re-emitted again. The wavelength of the re-emitted radiation is shifted up or

down in respect to the absorbed radiation. The shift contains information about the internal structure of a molecule such as vibrational and rotational energy states. Materials in solid, liquid or gaseous state can be investigated with Raman spectroscopy. In Figure 4.12, the Raman shift is given as a function of ratio between Si and Ge in a thin film. The thickness of the film affects directly the shift [40].

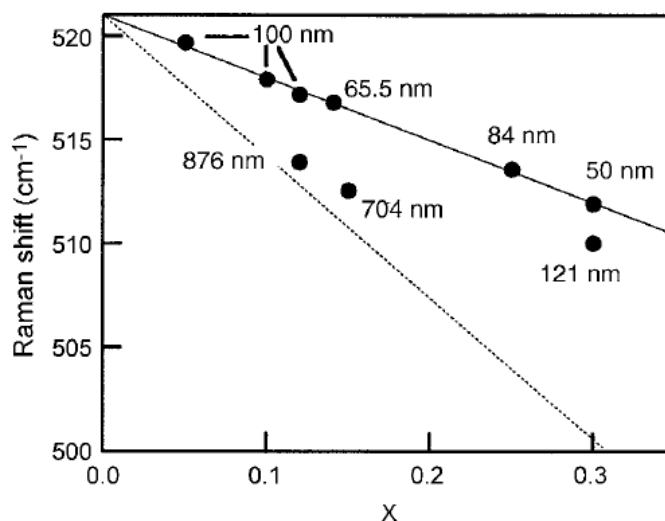


Figure 4.12 : Raman shift in wave number is given as a function of ratio between Si and Ge in a thin film made of Si_{1-x}Ge_x [34].

The polarization of the Raman radiation with respect to the crystal and the polarization of the excitation radiation can be used to find the orientation of the crystal, if the crystal structure is known. Thus, Raman spectroscopy is only a complementary method to XRD.

4.1.8 Thermogravimetric analysis (TGA)

Thermogravimetric analysis (TGA) is an analytical method used to determine the material's thermal stability and its fraction of volatile components by monitoring the change of its mass as a function of increasing temperature with constant heating rate, or as a function of time with constant temperature. The investigated material is subjected to the heat normally in a controlled atmosphere.

The obtained data can give insight about the thermally activated physical processes including second-order phase transitions, including vaporization, sublimation, absorption, adsorption, and desorption. Additionally, chemical processes such as chemisorption, desolvation, decomposition and solid-gas reactions. Electrode

materials can be characterized by the weight of the disordered carbon content using this technique [30].

Figure 4.13 illustrates a typical TG curve in which the mass change is plotted against increasing temperature. Decomposition of a sample is represented by two characteristic temperatures: T_i and T_f . T_i is the lowest temperature when the onset of mass change is detected and T_f is the lowest temperature when the mass change is completed.

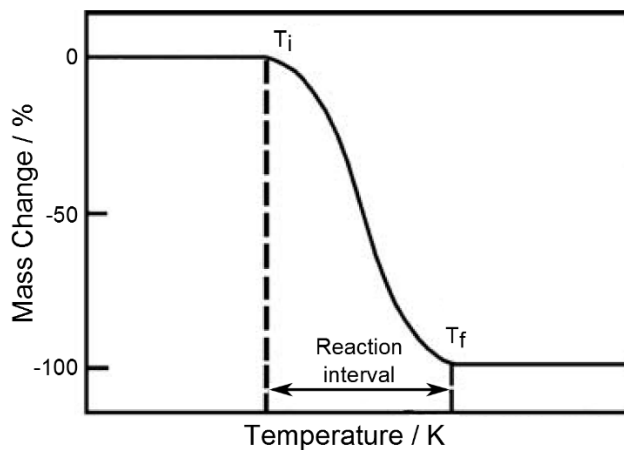


Figure 4.13 : Decomposition starting temperature T_i and finish temperature T_f obtained with TGA [34].

In this study, thermogravimetric analyses were conducted at ITU Energy Institute Material Production and Preparation Laboratory by using TA Q600 SDT thermogravimetric device (Figure 4.14) to analyze the composition of samples. Sample capacity is maximum 200 mg and balance sensitivity is 0.1 μg . Temperature range is ambient to 1500 $^{\circ}\text{C}$. Heating rate range at ambient to 1000 $^{\circ}\text{C}$ is 0.1 to 100 $^{\circ}\text{C}/\text{min}$. The maximum vacuum pressure can be applied is 7P [41].



Figure 4.14 : TA Q600 SDT thermogravimetric device [41].

4.1.9 Brunauer-Emmett-Teller (BET) method

In 1938, Brunauer, Emmett and Teller have introduced the so-called Brunauer-Emmett-Teller (BET) theory to explain the physical adsorption of gas molecules on a solid surface. The BET method is based on this theory and serves for the measurement of the specific surface area of a material. In other words, the specific surface area of a powder may be determined by physical adsorption of a gas on the surface of the solid and by calculating the amount of adsorbate gas corresponding to a monomolecular layer on the surface, since the physical adsorption is a result of the weak van der Waals forces between the adsorbed gas molecules and the adsorbing surface area of the investigated powder. The well-known BET adsorption isotherm equation is given by

$$\frac{1}{V_a \left(\frac{p_0}{p} - 1 \right)} = \frac{C-1}{V_m C} \times \frac{p}{p_0} + \frac{1}{V_m C} \quad (4.2)$$

, where p is partial vapour pressure of adsorbate gas in equilibrium with the surface at 77.4 K (boiling point of liquid nitrogen), p_0 is saturated pressure of adsorbate gas, V_a is volume of gas adsorbed at standard temperature and pressure, V_m is volume of gas adsorbed at STP to produce an apparent monolayer on the sample surface and C is dimensionless constant that is related to the enthalpy of adsorption of the adsorbate gas on the powder sample. With the assumption of spherical, non-porous, smooth and monodisperse particles, the size of the mean primary particle can be approximated as

$$d_{\text{BET}} = 6 \times (\rho \text{SSA})^{-1} \quad (4.3)$$

, where ρ is the bulk density of the powder, SSA is the specific surface area and d_{BET} is the mean particle diameter [30, 42].

4.2 Electrochemical Characterization

Most widely used methods for electrochemical characterization can be summarized in the following three categories.

4.2.1 Cyclic voltammetry (CV)

Cyclic voltammetry (CV) can be used to investigate the chemical reactivity of species. It is the most widely used and most versatile electro analytical technique to obtain qualitative information about electro active species [43].

This method gives insight about the electrochemical behavior of a voltaic cell by providing valuable data on the thermodynamics of redox processes and on the kinetics of heterogeneous electron transfer reactions. Since the obtained data about the voltammetric behavior is unique, this method is sometimes called as electrochemical spectroscopy [14].

In CV, a voltage is applied between a so-called working electrode and reference electrode in a voltaic cell. The potential between these two electrodes can be assumed as an excitation signal. The potential is then swept in a given range as a function of time. The resulting current is monitored and is considered as response signal to the excitation signal. It is called cyclic voltammetry, since the applied voltage is inverted after the given potential limit is reached. The resulting voltage-current characteristic is considered as electrochemical fingerprint [14, 43]. Figure 4.15 shows the cyclic voltammogram of a deposited insoluble film during electro-reduction and re-oxidation process, triggered with the applied voltage [1].

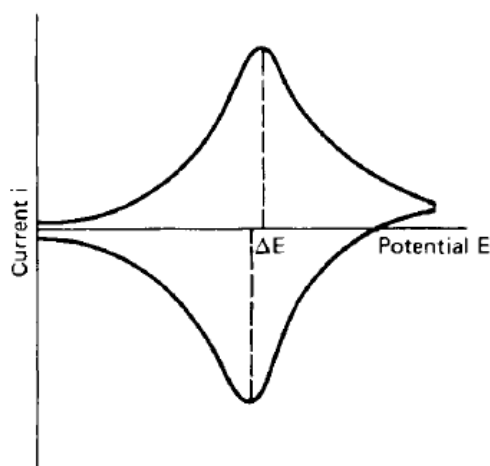


Figure 4.15 : Cyclic voltammogram of a deposited insoluble film during electro-reduction and reoxidation process [1].

4.2.2 Galvanostatic charge and discharge testing

Galvanostatic charge and discharge testing (GCDT), also known as chronopotentiometry, is the reciprocal method to characterize a battery cell. During

the GCDT test, a constant current is applied to an electrode and the voltage response is monitored. In batteries and chemical cells, this method is used to evaluate the efficiency and capacity of differing anode, cathode, and electrolyte materials [1].

In this study, electrochemical characterization of coin battery were done both in Inci Akü Laboratory placed in İTÜ Energy Institute and in TEMAG Laboratory placed in İTÜ Faculty of Mechanics by using MTI BST8-WA 8 channel battery analyzer (Figure 4.16). BST8-WA is an eight-channel battery analyzer to analyze small coin cells and cylindrical batteries from 0.002 mA to 1 mA, up to 5V. Each channel of the analyzer has independent constant-current and constant-voltage source, which can be programmed and controlled by computer software. This system provides most applications in battery testing fields such as electrode materials research, battery performance test, small-scale battery formation, capability grading, battery pack testing etc. Brand new laptop with MS Window 8, MS Excel 2013 and latest version testing software are installed and calibrated for immediate use. Up to 20 sets of analyzers can be simultaneously controlled by one laptop [44].

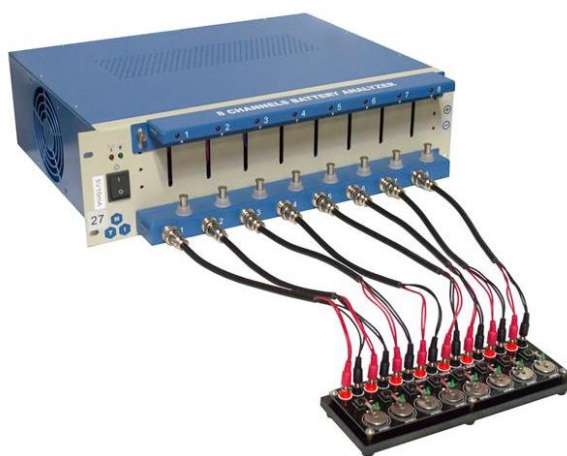


Figure 4.16 : TI BST8-WA 8 channel battery analyzer [44].

The weight of the active anode material was considered for the determination of the measurement configurations. During the early investigation of the irreversible cycles, charge and discharge steps were conducted at a constant current. This value is equal to the one tenth of the charge/discharge ratio ($C/10$), which corresponds to the specific capacity of graphite 372 mAh/g. It was chosen to realize a regular and slow transition of lithium ions into the anode. After the first discharge, charging was undertaken at the same speed. Afterwards, the next charge cycle was conducted with

a ratio of C/4 and discharge cycle was conducted with a ratio of C/3 to investigate the capacity losses.

The charging process, also known as the lithium intercalation, was undertaken against the lithium cathode with a voltage of 0.01 V, while the voltage for discharge process was set as 4.5 V.

4.2.3 Electrochemical impedance spectroscopy (EIS)

EIS is a powerful tool to investigate the mechanisms of electrochemical reactions by measuring the dielectric and transport properties of materials. In other words, EIS is a method to characterize a chemical process in terms of electrical measurements by exploiting the Faraday's law [45].

The properties of porous electrodes and passive surfaces can be analyzed.

The well-known Ohm's law is only valid for ideal resistors. The resistance of an ideal resistor is also frequency independent and current-voltage characteristic is in phase, if an AC signal is applied to the ideal resistor. In contrast to ideal resistors, the real resistors feature a more complex behavior. Thus, the concept of impedance is adopted instead of resistance. Although, impedance implies a resistance to the flow of electrical current, it also leads to a phase shift between current and voltage as a response to the applied AC signal. Thus, impedance has real and imaginary parts. Real part corresponds to the energy dissipation, while the imaginary part represents the energy storage.

EIS is a linear technique and the results are interpreted in terms of linear system theory. However, electrochemical cells are not linear systems, which means that the doubling the voltage will not be result in a doubled current. Additionally, the current response will contain harmonics of the excitation frequency. Thus, a small (1 to 10 mV) AC signal is applied to the cell in a normal EIS. With such a small excitation signal, the system will be pseudo-linear and easier to characterize. Figure 4.17 shows the pseudo-linear part of a non-linear voltage current characteristic.

During the measurement, the investigated material must be in a steady state. External interferences such as adsorption of impurities, growth of an oxide layer, building up of reaction products, coating degradations and temperature changes may also falsify the measurement, since they disrupt the state of the material [45].

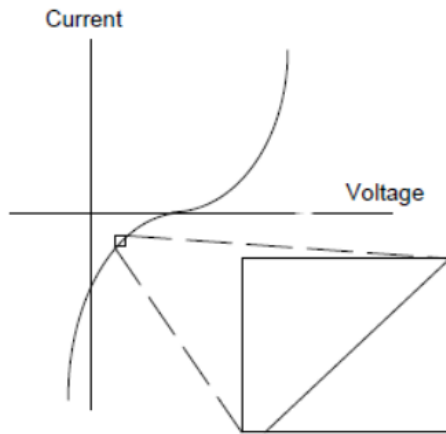


Figure 4.17 : Pseudo-linear part of a non-linear voltage current characteristic [45].

5. EXPERIMENTAL STUDIES

5.1 Selection and Specification of Materials

As stated previously in section 3.3.2.3, metals have high theoretical specific capacity compared to graphite. However, high volume expansion is occurred when they react with lithium. Yet, the studies show that carbon matrix buffers the volume expansion, when metals are used as composite with graphite. In addition, use of nano-sized particles mitigates the effects of the volume change and promotes cycling stability [24, 46-48].

In this study; different metals and metal oxides were selected to improve cyclability and specific capacity of lithium ion battery by mixing with graphite anode material. The materials details' and its specifications are summarized in Table 5.1.

Table 5.1 : Materials' details and its specifications.

Material Name	Supplier Name	Product Name	Purity, %	Particle Size
Graphite	MTI Corporation	Artificial graphite powder for Li-ion battery anode	> 99.5	119.0 - 23.0 μ m (D50)
Silicon dioxide (SiO ₂)	Sigma Aldrich Chemistry	Silicon dioxide, nano powder	99.5	10-20 nm (BET)
Magnesium oxide (MgO)	Merck Millipore	Magnesium oxide, light extra pure, Ph Eur, BP, E 530	98 - 100	n.a.
Aluminum (Al)	Anachemia Canada Co - A VWR Company	Aluminum, powder, 200 mesh	n.a.	44 μ m
Aluminum oxide (Al ₂ O ₃)	Sigma Aldrich Chemistry	Aluminum oxide, nanoparticles	n.a.	30-60 nm (TEM)
Tin (Sn)	Sigma Aldrich Chemistry	Tin	> 99.5	< 600 μ m
Silver nitrate (AgNO ₃)	Merck Millipore	Silver nitrate GR grade	n.a.	n.a.
Boron (B)	Pavezyum Kimya Sanayi	PVZ Boron 95	95-97	< 1 μ m

5.2 Preparation of Anode Electrode Material

5.2.1 Silicon dioxide mixed graphite

Silicon dioxide (SiO_2) and graphite were mixed with different weight percentages to find out the optimum mixing ratio. Tin (Sn) was added to promote the utilization of silicon and improve the electrochemical performance of the anode [49]. Additionally, magnesium oxide (MgO) was added to silicon dioxide and graphite composite to maintain superior capacity retention and rate capability [47]. Table 5.2 summarizes the samples' content used for this study.

Table 5.2 : SiO_2 mixed graphite samples.

Sample Name	Sample Content
Si 1	SiO_2 :Graphite = 50:50 wt%
Si 2	SiO_2 :Graphite = 70:30 wt%
Si 3	SiO_2 :Graphite = 80:20 wt%
Si 4	SiO_2 :Graphite:Sn = 70:20:10 wt%
Si 5	SiO_2 : MgO:Graphite = 30:20:50 wt%

Samples were prepared by mixing physically via either using IKA Universal mill or Agate mortar for 30 minutes, which are shown in Figure 5.1 and Figure 5.2 respectively.



Figure 5.1 : IKA universal mill M20 [50].



Figure 5.2 : Hi-Quality natural agate mortar and pestle [51].

5.2.2 Tin mixed graphite

To find out impact of addition of tin (Sn) to graphite, different weight percentages of tin mixing with graphite were examined. Moreover, addition of silver nitrate (AgNO_3) to tin/graphite composite were also investigated. AgNO_3 is used as buffer for volume change of Sn during cycling [52]. Table 5.3 summarizes the samples' contents.

Table 5.3 : Sn mixed graphite samples.

Sample Name	Sample Content
Sn 1	Sn:Graphite = 50:50 wt%
Sn 2	Sn:Graphite = 60:40 wt%
Sn 3	Sn:Graphite:AgNO ₃ = 60:30:10 wt%
Sn 4	Sn:Graphite:AgNO ₃ = 45:45:10 wt%

Samples were prepared by mixing physically via either IKA Universal mill or Agate mortar for 30 minutes.

5.2.3 Aluminium and aluminium oxide mixed graphite

To find out impact of addition of aluminium (Al) and aluminium oxide (Al_2O_3) to battery performance, different weight percentages of Al and Al_2O_3 addition to graphite were examined. To utilize and to maintain good capacity during cycle, SiO_2 addition to Al_2O_3 /graphite composites were also investigated [53]. Table 5.4 summarizes the samples' content used for this study.

Table 5.4 : Al and Al_2O_3 mixed graphite samples.

Sample Name	Sample Content
Al 1	Al_2O_3 : SiO_2 :Graphite = 54:15:31 wt%
Al 2	Al_2O_3 : SiO_2 :Graphite = 28:39:33 wt%
Al 3	Al:Graphite = 67:33 wt% by using Al_2O_3
Al 4	Al:Graphite = 67:33 wt% by using Al

Samples were prepared by mixing physically via either IKA Universal mill or Agate mortar for 30 minutes.

Sample Al 4 was also prepared by mixing via ball miller to compare the samples' compositions, which were prepared by Agate mortar. Sample was mixed at 160 rpm for 5 hours via ball miller, which was placed in Mechanical Metallurgy Laboratory, in Istanbul Technical University Metallurgical and Materials Engineering Department.

5.2.4 Boron mixed graphite

To improve the battery performance, different weight percentage of boron mixing with graphite were examined. Table 5.5 summarizes the samples' contents.

Table 5.5 : B mixed graphite samples.

Sample Name	Sample Content
B 1	B:Graphite = 2.5:97.5 wt%
B 2	B:Graphite = 5:95 wt%
B 3	B:Graphite = 7.5:92.5 wt%

Samples were prepared by mixing physically. Samples were mixed with either IKA Universal mill or Agate mortar for 30 minutes.

5.3 Coin Battery Preparation

Firstly, slurry was made with 10 g active material, 0.44 g carbon black, 15 g N-Methyl-2-pyrrolidone (NMP) and 1.76 g polyvinylidene difluoride (PVDF). Materials' details are summarized in Table 5.6.

Table 5.6 : Materials details' used for slurry preparation.

Material Name	Supplier Name	Product Name
Carbon Black	TIMCAL Graphite & Carbon	Conductive carbon black EQ-Lib-SuperC45
N-Methyl-2-pyrrolidone (NMP)	Sigma Aldrich Chemistry	N-Methyl-2-pyrrolidone, Reagent Plus
Polyvinylidene difluoride (PVDF)	MTI Corporation	PVDF binder for Li-ion battery electrodes

This mixture was stirred via ultrasonic batch (Figure 5.3).



Figure 5.3 : WiseClean ultrasonic batch.

Secondly, MSK-AFA-III Automatic Thick Film Coater was used for coating (Figure 5.4) [54]. Machine surface was cleaned with NMP followed by placing copper foil on the surface and vacuumed. To remove impurities on foil copper, it was also cleaned with NMP. Then, slurry was placed in front of blade on the coating machine, which was set to 120 μm thickness and 3.3 mm/sec speed. Then the coating machine was run for homogenous coating.



Figure 5.4 : MSK-AFA-III automatic thick film coater [54].

Finally, after coating, machine was set to 70 $^{\circ}\text{C}$ and coated copper foil was dried for 30 minutes under vacuum. Following, coated copper foil was dried at 120 $^{\circ}\text{C}$ for 12 hours in Binder vacuum drying oven (Figure 5.5) to remove the solvent from the system.



Figure 5.5 : Binder vacuum drying ovens [55].

Figure 5.6 presents anode material coated copper foil.



Figure 5.6 : Anode material coated on copper foil.

Anode material coated on copper foil was cut in cylindrical shape and cell size by using Precision Disc Cutter MSK-T-06 (Figure 5.7) [56].



Figure 5.7 : Precision disc cutter MSK-T-06 [56].

Figure 5.8 presents the cylindrical shaped anode material coated on copper foil.



Figure 5.8 : Cylindrical shaped anode material coated on copper foil.

Fabrication of coin battery was taken place in Innovative Technology IL-2 GB glovebox (Figure 5.9). It works at 1.7 mbar pressure with argon gas. It contains zero moisture content and 0.2 ppm oxygen gas to prevent oxidation of materials and samples. Each anode material was weighted and then all were taken into glove box where argon gas flows inside. Figure 5.9 presents the glove box where the coin batteries were fabricated.



Figure 5.9 : Innovative technology IL-2 GB glove box.

In battery fabrication; 1M LiPF₆ salt was used as electrolyte which as dissolved in 1:1:1 volumetric solution of ethylene carbonate (EC), diethyl carbonate (DEC) and ethyl methyl carbonate (EMC), as cathode material LiCoO₂ was used and as anode samples were used which were described in section 5.1.

Battery fabrication was done based on defined sequence, which is shown in Figure 5.10 from bottom to top.

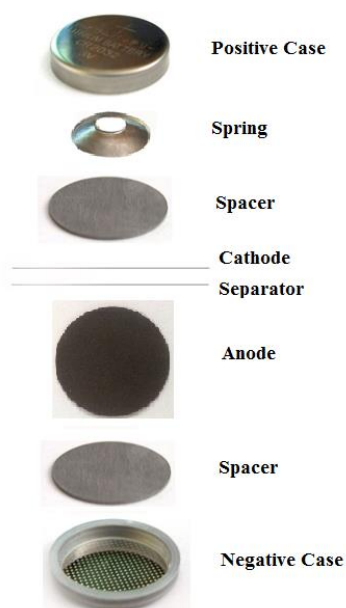


Figure 5.10 : Coin battery components and sequence. Modified from [57].

To prevent short circuit, separator was placed onto anode which was then soaked with electrolyte. Whatman - Glass microfiber filters, Grade GF/D was used as separator in this study. Following lithium, spacer and spring were placed and battery was closed by placing positive case. To ensure that battery was sealed well and prevent electrolyte leakage, coin battery was compressed via MTI Corporation - MSK - 110 Hydraulic Crimping machine (Figure 5.11) in glove box.



Figure 5.11 : MTI Corporation - MSK - 110 hydraulic crimping machine [58].

6. RESULTS AND DISCUSSION

The research on lithium ion batteries until now was focused on increasing battery performance and cycle time, and maximization of specific capacity by stabilizing SEI layer. These studies contain optimization and development of battery components and other parameters, which affect the battery performance, but especially on the anode, the cathode and the electrolyte.

The general goal of this work is to improve cyclability and specific capacity of lithium ion battery by mixing the anode material by metal.

The research on developing anode material for lithium ion battery shows that using high capacity metals with the commercialized anode material graphite delivers promising results in terms of battery cyclability and specific capacity. In this work, to find a post-promising metal to be used for anode preparation, recent researches done in this field have been reviewed. Based on literature review, most promising metals and metal oxides were identified and anode material preparations were carried out. At the final stage, coin batteries were fabricated with metal mixed graphite anode materials and battery performances were analyzed.

6.1 Results of Silicon Dioxide Mixed Graphite

Recently, there has been much interest on metal-based materials for developing lithium ion batteries with high energy density. Silicon has very high theoretical capacity (4200 mAh/g) in comparison with traditional carbonaceous material (372 mAh/g for graphite) and possesses the potential for alternative anodes for lithium ion batteries. However, there is a large volume change during alloying/dealloying with lithium, which causes capacity loss during cycle [47].

The studies show that carbon matrix buffers the volume expansion, when metals are used as composite with graphite. In addition, use of nano-sized particles mitigates the effects of the volume change and promotes cycling stability [24, 46-48].

Sun et al. [59] investigated electrochemical properties of nano structured SiO₂ thin film in lithium ion batteries. In their study, it was found out that SiO₂ is electrochemically active and shows good cycle performance and reactive mechanism with lithium. For the first 100 cycles, reversible discharge capacities were found in the range of 416 to 510 mAh/g, where the SiO₂/Li cells were cycled between 0.01 and 3.0 V.

Guo et al. [60] explored the performance of nano-SiO₂ and hard carbon composite as electrode in lithium ion batteries. The specific capacity of SiO₂ is 1675 mAh/g. In the composite, hard carbon was used as the host of SiO₂. Their study showed that the nano-SiO₂ in the composite is highly active electrochemically and delivers stable cycling performance. The reversible capacity of SiO₂/hard carbon composite was found around 630 mAh/g, which is much higher than reversible capacity of carbon (300 mAh/g), where the voltage profiles were between 0.0 and 3.0 V.

Zuo et al. [61] investigated the improvement of cycle performance for Si/carbon composite used as anode in lithium ion batteries. The composite electrode of silicon/carbon features an initial reversible capacity of 575 mAh/g and still maintained a high reversible capacity of 506 mAh/g after 40 cycles with capacity loss of around 0.3% per cycle.

Wu et al. [49] explored the effect of Sn addition to Si/graphite composite in terms of increasing the silicon utilization and improving electrochemical performance. The results showed that reversible capacity of silicon/graphite/tin composite is around 1592 mAh/g, which is relatively very high, with voltage arrangement from 0.03 to 1.5 V. Moreover, composite showed stable cycling performance and had excellent rate capability.

Zhou et al. [47] investigated the impact of MgO addition to Si/graphite composite on specific capacity. It was found out that Si/MgO/graphite composite exhibits excellent capacity retention and superior rate capability. Even though the MgO inside the composite is not involved in the electrochemical reaction, it maintains the composite structure during large volume expansion/contraction of Si, as well as protecting the Si particles. The results showed that it delivered 630 mAh/g capacity after 74 cycles, where it has around 700 mAh/g initial capacity.

In this study, SiO₂ was mixed with graphite with different mass ratio. Furthermore, the addition of MgO and Sn to composites was investigated. Anode material characterization has been undertaken by means of SEM and TGA analyses. Then, galvanostatic tests were conducted for battery performances. Results were presented and discussed in detail in Sections 6.1.1 and 6.1.2 Results of coin battery performances

6.1.1 Results of anode material properties

6.1.1.1 Results of scanning electron microscopy (SEM)

Figure 6.1 shows SEM images of artificial graphite. Mean particle size of graphite is about 119 μm . As showed in Figure 6.1, graphite has heterogen surface, which is composed prismatic layers and includes defects and surface disorders.

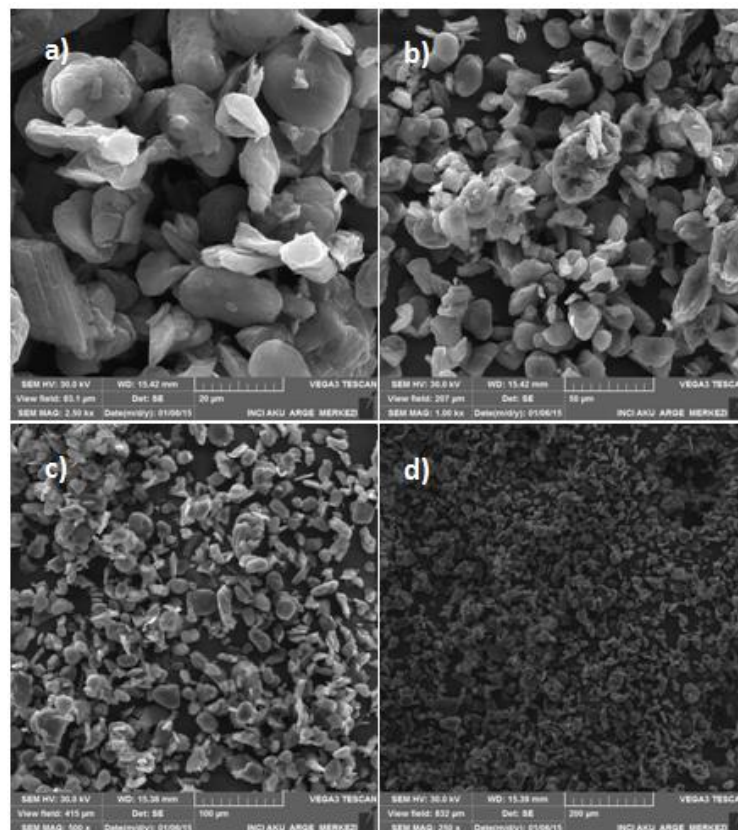


Figure 6.1 : SEM images of artificial graphite: a) 2.5kx, b) 1.0kx, c) 500x, d) 250x.

Figure 6.2 shows SEM images of silicon dioxide. Silicon dioxide has heterogen surface. It is composed of different size of grains and has agglomeration structure.

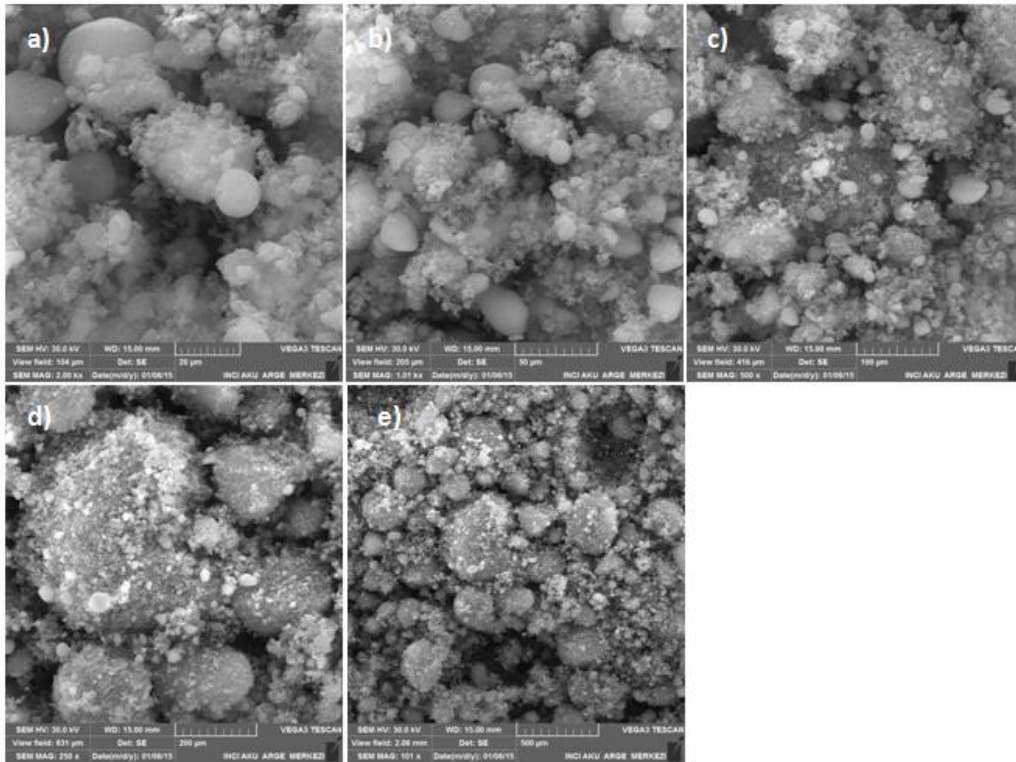


Figure 6.2 : SEM images of SiO₂: a) 2.0kx, b) 1.0kx, c) 500x, d) 250x, e) 101x.

Figure 6.3 shows the SEM images of tin powder. Tin powder consists of spherical grains with a smooth surface and of similar size.

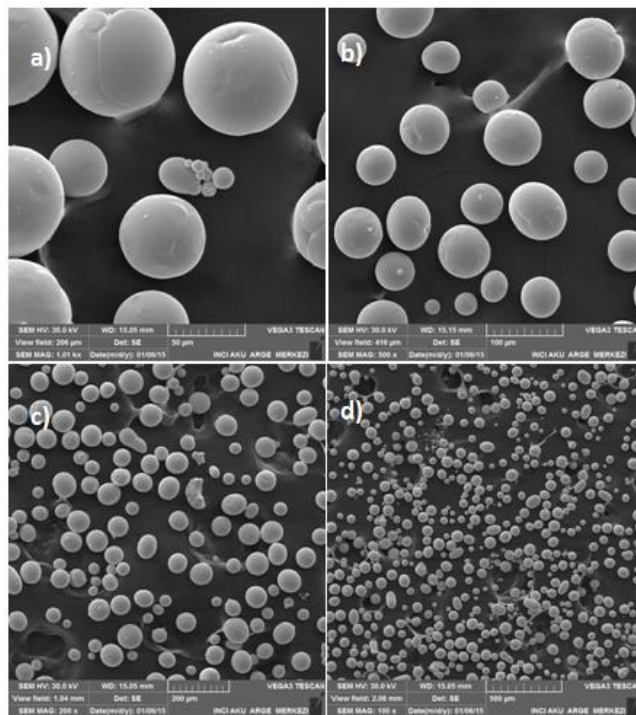


Figure 6.3 : SEM images of Sn powder: a) 1.01kx, b) 500x, c) 200x, d) 100x.

Figure 6.4 shows the SEM images of magnesium oxide. As compared to silicon dioxide, magnesium oxide has smaller grains and more agglomeration structure.

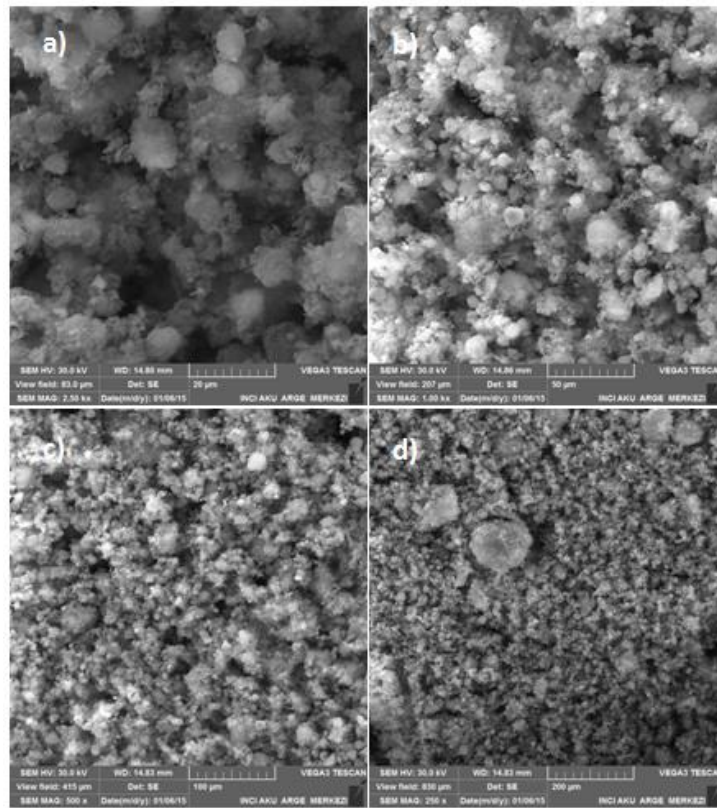


Figure 6.4 : SEM images of MgO: a) 2.5kx, b) 1.0kx, c) 500x, d) 250x.

Figure 6.5 - Figure 6.7 exhibit SEM images of silicon dioxide/graphite composite with mixing ratios of 50:50, 70:30 and 80:20 wt%, respectively. SEM images show that silicon dioxide and graphite were evenly mixed, eventhough agglomeration of silicon dioxide was observed on SEM images.

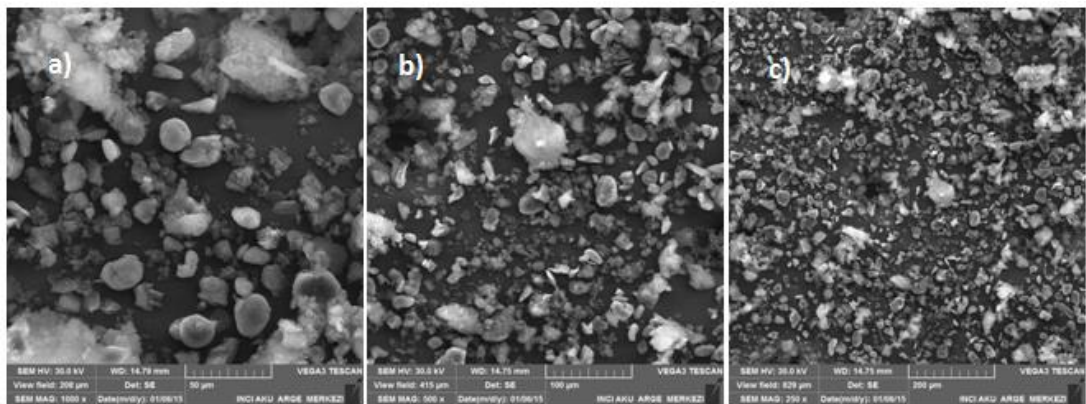


Figure 6.5 : SEM images of SiO₂:graphite composite at 50:50 wt%:
a) 1000x, b) 500x, c) 250x.

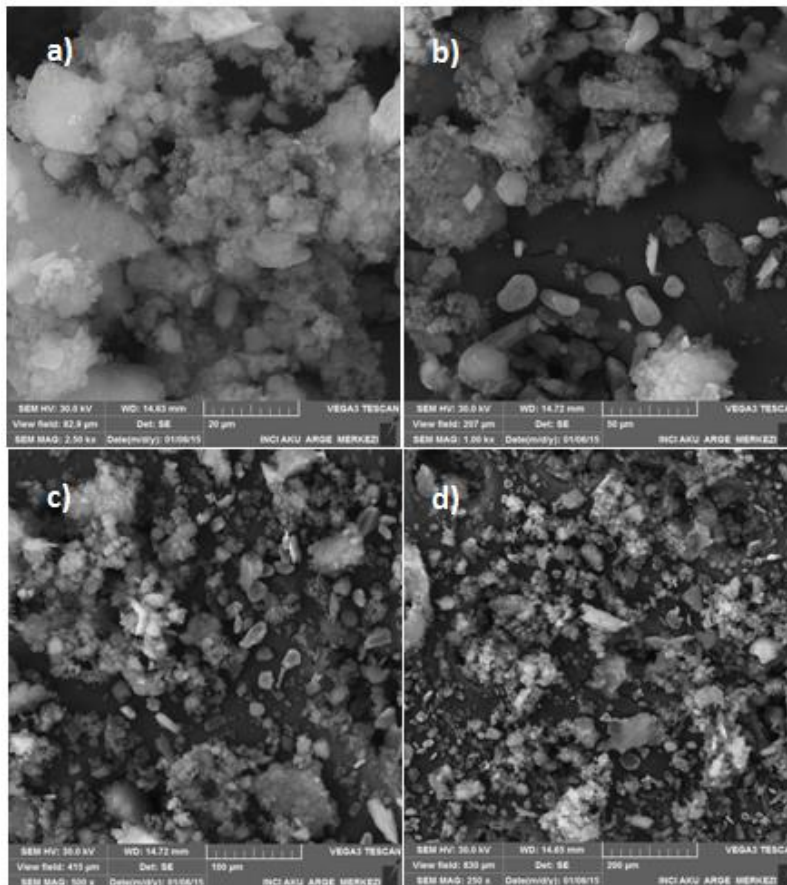


Figure 6.6 : SEM images of SiO₂:graphite composite at 70:30 wt%: a) 2.5kx, b) 1.0kx, c) 500x, d) 250x.

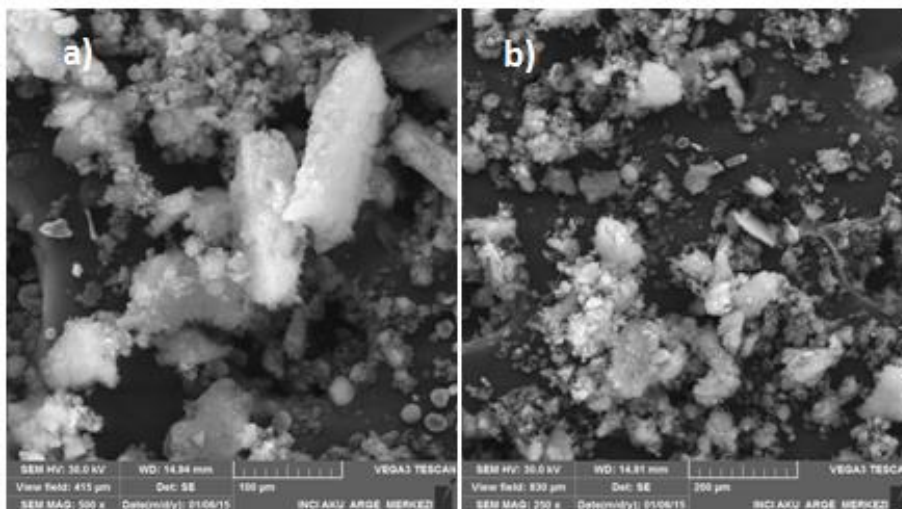


Figure 6.7 : SEM images of SiO₂:graphite composite at 80:20 wt%: a) 500x, b) 250x.

Figure 6.8 shows the SEM images of silicon dioxide/graphite/tin composite with a mixing ratio of 70:20:10 weight percentages, respectively. As can be seen in the images, agglomerated structure of silicon dioxide covered the tin grains and this structure is evenly distributed on graphites.

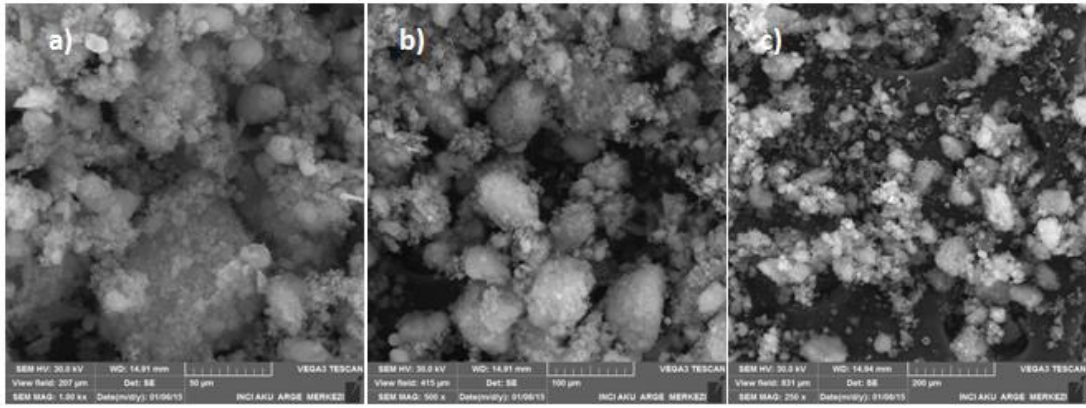


Figure 6.8 : SEM images of SiO₂:graphite:Sn composite = 70:20:10 wt%: a) 1.0kx, b) 500x, c) 250x.

Figure 6.9 shows the SEM images of silicon dioxide/magnesium oxide/graphite composite. Silicon dioxide and magnesium oxide were monitored on graphite surface. Due to the structure of silicon dioxide and magnesium oxide, agglomerations were observed on graphite and these lead to different size of grains in the composite.

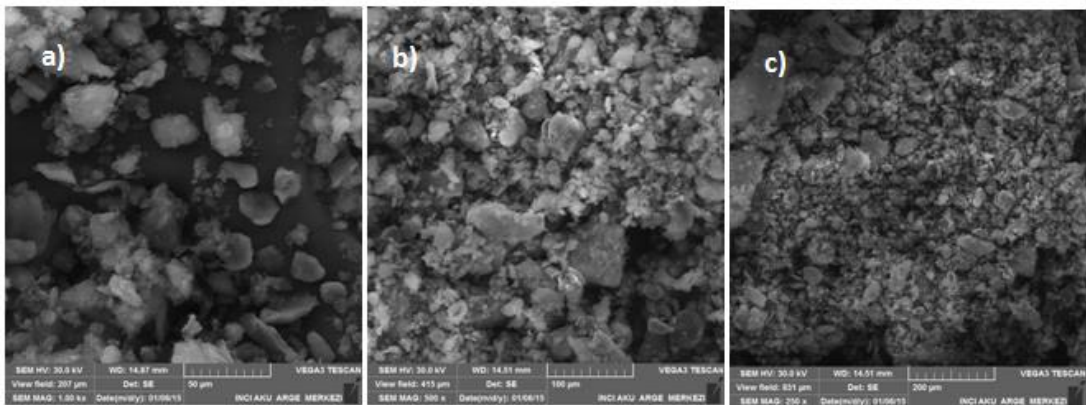


Figure 6.9 : SEM images of SiO₂/MgO/graphite composite: a) 1.0kx, b) 500x, c) 250x.

6.1.1.2 Results of thermogravimetric analyses (TGA)

Silicon dioxide contents of the silicon dioxide/graphite composites were also determined from TGA measurements. The weight loss at a temperature between 300-950 °C in the TGA graphs was attributed to the oxidation of graphite in the composite and the results were given in Table 6.1 by comparing targeted inclusion levels. TGA results show that the inclusion levels of silicon dioxide, and silicon dioxide and magnesium oxide mixture are higher than expected for sample Si 1 and Si 4, respectively. These samples were mixed with IKA universal mill M20 and it may be possible that graphite loss from the composite occurred during milling. For

sample Si 5, total silicon dioxide and magnesium oxide content was found by TGA analyses.

Table 6.1 : TGA results of SiO₂ mixed graphite samples.

Sample Name	Sample Content	SiO ₂ Content, %	SiO ₂ +SnO ₂ Content, %	SiO ₂ +MgO Content, %
Si 1	SiO ₂ :Graphite = 50:50 wt%	61	-	-
Si 2	SiO ₂ :Graphite = 70:30 wt%	76	-	-
Si 3	SiO ₂ :Graphite = 80:20 wt%	76	-	-
Si 4	SiO ₂ :Graphite:Sn = 70:20:10 wt%	-	84	-
Si 5	SiO ₂ : MgO:Graphite = 30:20:50 wt%	-	-	70

6.1.2 Results of coin battery performances

At the galvanostatic measurement of some samples, systematic measurement errors occurred. Thus, the measured values exceed the theoretical limits in some cases. Although the absolute values of some samples cannot be used directly, conservation of specific capacity can be compared for all samples by normalizing measurement data to their corresponding start value.

The comparison of capacity decrease slope of different mixing mass ratio of silicon dioxide/graphite composites was shown in Figure 6.10 with regard to artificial graphite as reference.

Figure 6.10 shows discharge capacities of 70 wt% and 80 wt% SiO₂ mixed graphite samples for the first 5 cycles, which were charged at C/4 ratio and discharged at C/3 ratio. Moreover, specific discharge capacity of MgO and Sn added SiO₂/graphite composites as well as of artificial graphite was also shown for comparison.

Accordingly, it can be concluded that with 80 wt% SiO₂ mixed graphite and Sn added SiO₂/graphite composite shows higher initial specific capacity than artificial graphite, which agrees with the data from literature [49, 59, 60]. Additionally, the benefit of adding Sn to composite, which leads to the increase of the silicon utilization and to the improvement of the initial capacity, is confirmed by the measured capacity value. Since there is no proper battery operation for MgO added composite, the effect of MgO as additive cannot be investigated in this work.

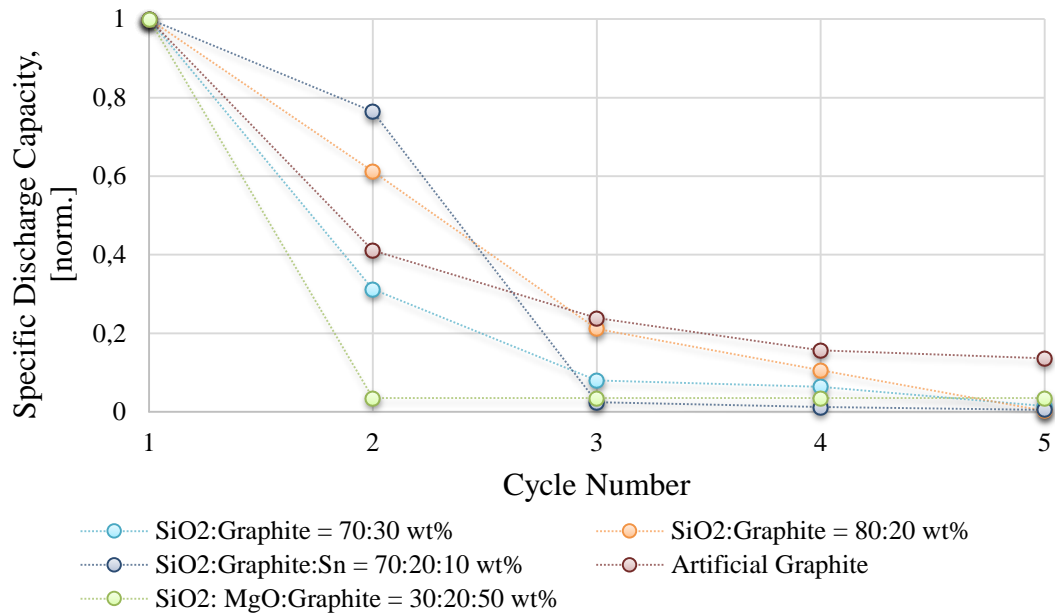


Figure 6.10 : Normalized specific capacity comparison of SiO₂ mixed graphite

When the absolute values were investigated, it can be seen that discharge capacities were doped to zero in 4 to 5 cycles, which is linked with solid electrolyte interphase (SEI) formation. This mechanism is explained in detail by Zhang [62]: In graphite, stable SEI film formation normally developed in the first cycle and contributes mostly to the first-cycle irreversible capacity. On the contrary, in alloy anodes, SEI formation is more like a dynamic process of cracking and reforming due to the volume change of active particle in cycling. This leads to the decrease of later cycle capacity on top of first-cycle irreversible capacity.

Figure 6.11 and Figure 6.12 show the charge and discharge curves of SiO₂:Graphite samples (SiO₂:Graphite = 80:20 wt% and SiO₂:Graphite:Sn = 70:20:10 wt% samples, respectively) for the first 2 cycles in the voltage range of 0.01-4.5V. Black lines indicate charge and red lines indicate the discharge. After the first cycle, capacity loss observed for both composites. This type of behavior has been commonly observed for metal included anodes.

The discharge profile can be divided into 3 regions: “Before the constant voltage plateau”, “the constant voltage plateau” and “after the constant voltage plateau” [63]. In Figure 6.11, for the first discharge curve, “the constant voltage plateau” can be seen for $V > 3.3V$, also known as biphasic domain, in which phase transition occurs.

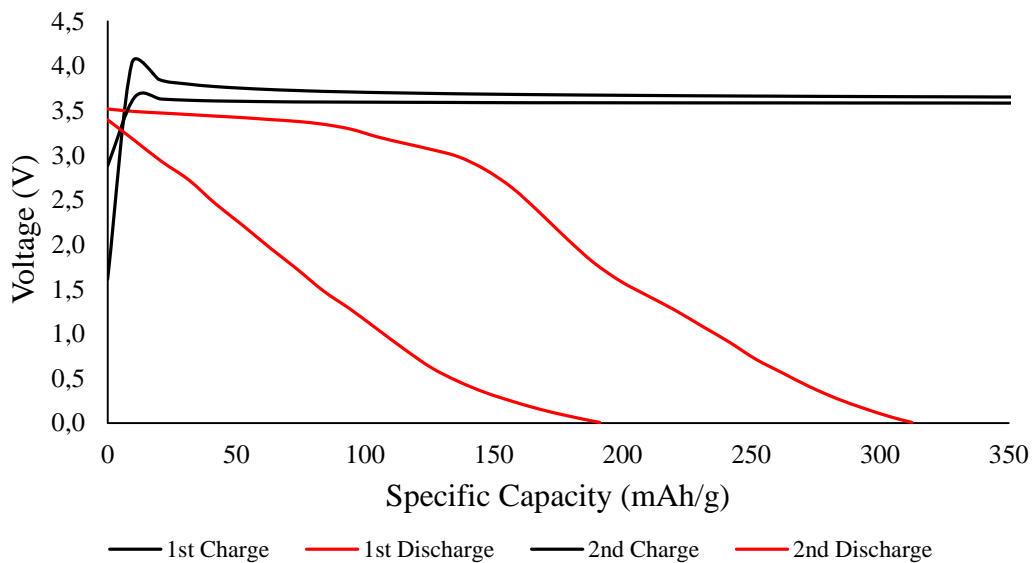


Figure 6.11 : Specific capacity vs voltage for SiO₂:graphite = 80:20 wt%.

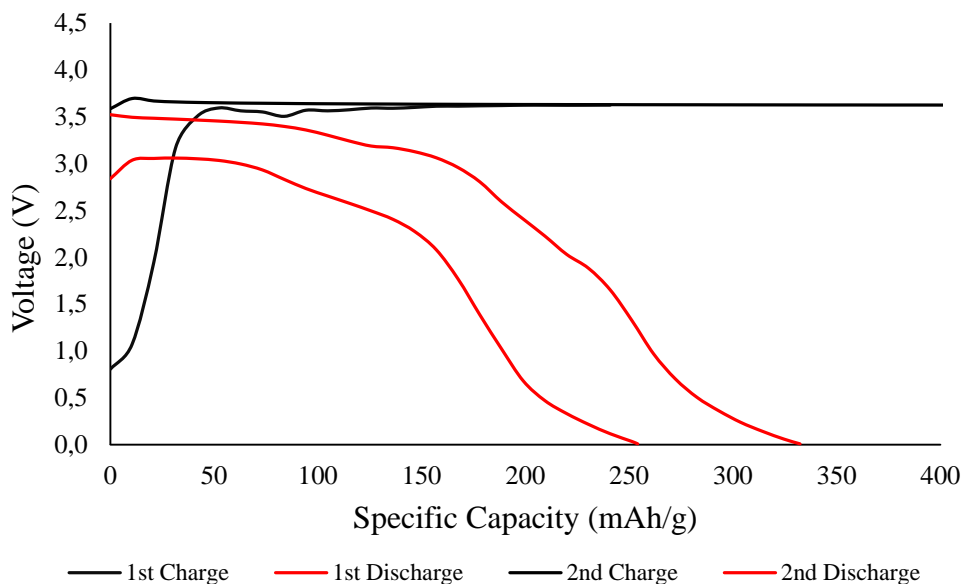


Figure 6.12 : Specific capacity vs voltage for SiO₂:graphite:Sn = 70:20:10 wt%.

This area corresponds to the amorphization process induced by the total reduction of all the cations. The “after the constant voltage plateau” for $V < 3V$, where the shoulder was observed, corresponds to the formation of lithium metal alloys at low potentials. However, in the second discharged curve, neither “before the constant voltage plateau” region, nor “the constant voltage plateau” itself can be observed. This can be explained with the decrease of the amorphization process with charge/discharge cycles. The decrease results also in the decline of the capacity, related to this chemical process. The final intercalation region, the so-called “after the constant voltage plateau” corresponds the reversible part of the lithium insertion

mechanism in the anode materials. The first sample (based on SiO₂:graphite = 80:20 wt%) features only the final Li-insertion mechanism after the first cycle, since the first two regions declined below a negligible value. In contrast to that, the second sample (based on SiO₂:graphite:Sn = 70:20:10 wt%) exhibits “the constant voltage plateau” also at the second charge/discharge cycle. Thus, it can be interpreted that Sn is responsible for the preservation of the biphasic region, where amorphization takes place. As a result, the second sample features a higher capacity due to the contribution of the second region. In both samples, the first region cannot be observed.

6.2 Results of Tin Mixed Graphite

To improve the capacity of lithium ion batteries, there is a particular interest for Sn due to its large theoretical specific capacity (990 mAh/g), which is much higher than the traditional anode material: graphite. However, one of the critical problems is the volume expansion during the lithiation process in lithium ion batteries. Different sample preparation processes are investigated to minimize the volume change [64].

Wang et al. [65] investigated graphite/Sn composite as anode material for lithium ion batteries, which was prepared by mixing via ballmiller. In their study, electrochemical tests showed that Sn/graphite composite could deliver a theoretical capacity of 800-1250 mAh/g, which is two or three times higher than that of graphite. Nevertheless, capacity loss was occurred after the first cycle due to the passivation layer formation, which may be prevented by optimizing the sample preparation conditions.

Wang et al. [52] investigated the characterization of Sn/graphite/Ag composite as anode material for lithium ion battery. In their study, cyclic voltammetry (CV) and galvanostatic discharge/charge tests were carried out to characterize the electrochemical properties of the composite. The composite electrodes exhibited an initial capacity of 1154 mAh/g and maintained a reversible capacity of above 380 mAh/g for more than 100 cycles [52].

In this study, different mass ratio of Sn and graphite composites were prepared. Furthermore, addition of AgNO₃ to composites were investigated. Anode material characterization has been undertaken by means of SEM and TGA analyses. Then,

galvanostatic tests were conducted for battery performances. Results were discussed in details in Sections 6.2.1 and 6.2.2 .

6.2.1 Results of anode material properties

6.2.1.1 Results of scanning electron microscopy (SEM)

Figure 6.13 shows the SEM images of silver nitrate powder. Silver nitrate has a slightly agglomerated structure.

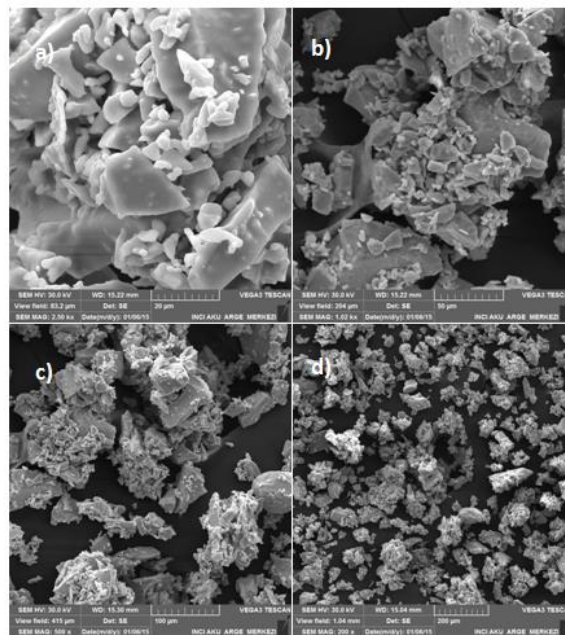


Figure 6.13 : SEM images of AgNO_3 powder: a) 2.5kx, b) 1.02kx, c) 500x, d) 200x.

Figure 6.14 and Figure 6.15 show the SEM images of tin:graphite composites which were mixed with a ratio of 50:50 and 60:40 weight percentages, respectively. Images show that tin is evenly mixed in graphite.

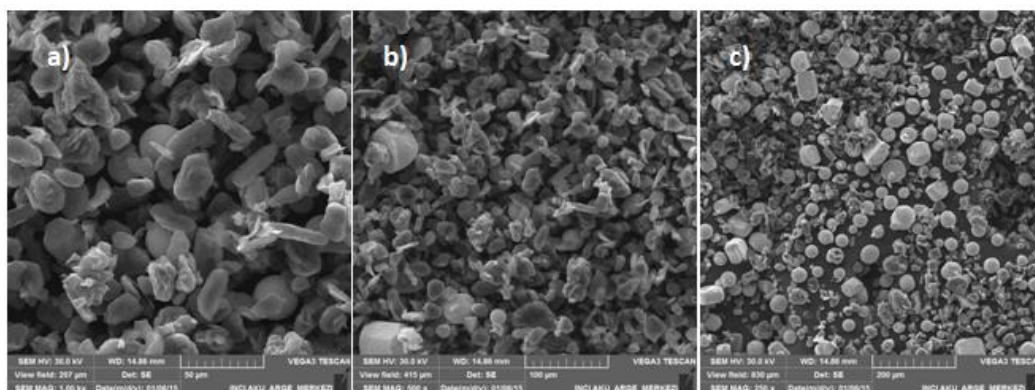


Figure 6.14 : SEM images of Sn:graphite composite = 50:50 wt%:
a) 1.0kx, b) 500x, c) 250x.

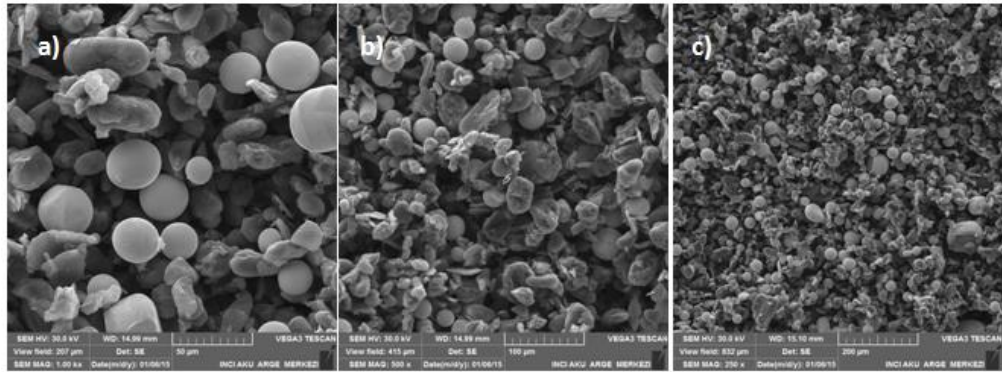


Figure 6.15 : SEM images of Sn:graphite composite = 60:40 wt%:
 a) 1.0kx, b) 500x, c) 250x.

Figure 6.16 and Figure 6.17 show the SEM images of tin/graphite/silver nitrate composites, which were mixed with a ratio of 60:30:10 and 45:45:10 weight percentages, respectively. Images show that tin and silver nitrate are evenly mixed in graphite.

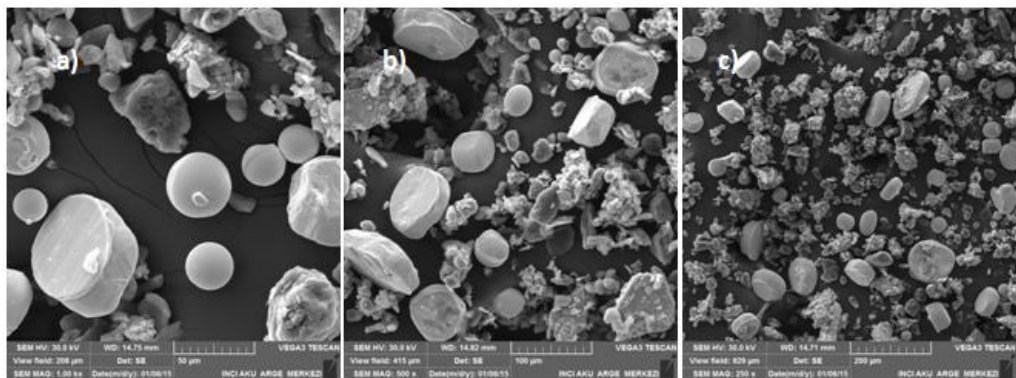


Figure 6.16 : SEM images of Sn:graphite:AgNO₃ composite = 60:30:10 wt%: a) 1.0kx, b) 500x, c) 250x.

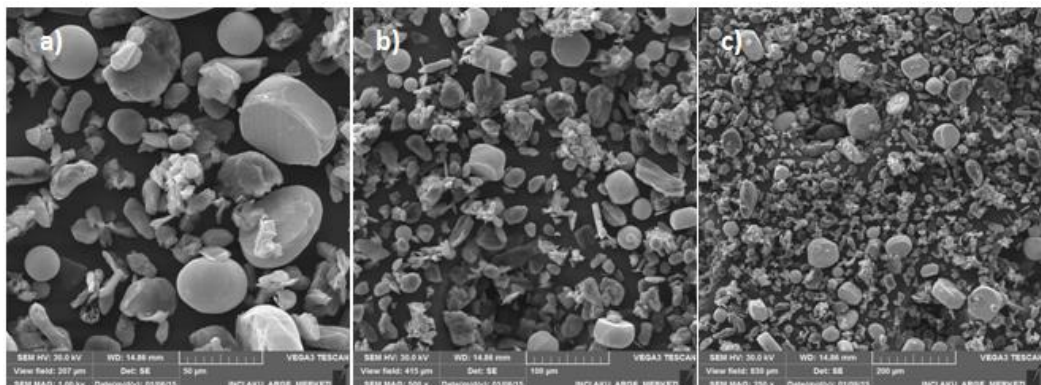


Figure 6.17 : SEM images of Sn:graphite:AgNO₃ composite = 45:45:10 wt%: a) 1.0kx, b) 500x, c) 250x.

6.2.1.2 Results of thermogravimetric analyses (TGA)

Tin content of tin/graphite composites were determined from TGA measurements. The weight loss at temperatures between 300-950 °C in the TGA graphs was attributed to the oxidation of graphite in the composite and the results were given in Table 6.2 by comparing targetted inclusion levels. All results show that inclusion levels are at target level.

Table 6.2 : TGA results of Sn mixed graphite samples.

Sample Name	Sample Content	SnO ₂ Content, %	SnO ₂ +Ag Content, %
Sn 1	Sn:Graphite = 50:50 wt%	67	-
Sn 2	Sn:Graphite = 60:40 wt%	63	-
Sn 3	Sn:Graphite:AgNO ₃ = 60:30:10 wt%	-	78
Sn 4	Sn:Graphite:AgNO ₃ = 45:45:10 wt%	-	53

6.2.2 Results of coin battery performances

At the galvanostatic measurements, no proper battery operation can be performed. This can be explained by the fact that the investigated tin powder consists of particles with a mean diameter of about 600 µm. Compared to other materials, such as graphite with a diameter of 119 µm as well as silicon dioxide and boron with diameters in the order of magnitude of 10⁻⁹ m, tin particles have the greatest surface area among all materials. It leads to a low surface tension between the tin mixed slurry and the copper band. During drying process of the slurry coated on copper, the different expansion coefficients of slurry and copper result in a strain between the surface of the coating and the surface of the copper band, which cannot be balanced with the low surface tension of tin mixed slurry in contrast to other mixtures. As a result, a flaking occurred at every coating of the tin mixed slurry. Since the diameter of the tin particles could not be reduced further with agate mortar, the qualitative research of tin mixed graphite could not be performed.

6.3 Results of Aluminum and Aluminium Oxide Mixed Graphite

Extensive studies have been undertaken with silicon and tin, where aluminum is not investigated in detail yet. Aluminum has a theoretical capacity of 990 mAh/g, which

is similar to tin, however, considerable lower than silicon. Nevertheless, compared to tin and silicon, which have have at least three-phase transitions for full lithiation, aluminum has only one transition, which leads to a flat voltage profile. In due consideration of this fact, aluminum may be more electrochemically suitable for alloyin/dealloying [48].

Hamon et al. [66] found out in their study that three different chemical reactions occurre, when aluminum is used as anode in lithium ion batteries. These reactions are oxidation of aluminum and two-step of lithiations, which were recognized on discharge curves as voltage regions. Even though the capacity loss was observed, they concluded that aluminum is a good candidate as an anode for lithium ion batteries, if the capacity fade and stability can be optimized.

Chena et al. [67] investigated addition of aluminum to silicon film to improve the electrochemical performance. It was found out that significant improvement is achieved on cycle performance and rate capability due to the less severe volume expansion of Si-Al thin film.

Zhou et al. [53] investigated impact of adding silicon (Si) and aluminum (Al) to graphite on specific capacity. Regarding to their study, the reversible capacity of Al/Si/graphite composite remained above 650 mAh/g after 10 cycles, corresponding to 310 mAh/g, almost double of that of graphite alone. Moreover, when capacities of Al/graphite and Al/graphite/Si were compared, they found out that Al/graphite/Si delivers 50% more.

In this study, samples were prepared by mixing graphite with different mass ratio of Al and Al₂O₃. Moreover, addition of SiO₂ to Al₂O₃/graphite composite was investigated. Anode material characterization has been undertaken by means of SEM and TGA analyses and galvanostatic tests were conducted for battery performances. Results were presented and discussed in detail in Sections 6.3.1 and 6.3.2 .

6.3.1 Results of anode material properties

6.3.1.1 Results of scanning electron microscopy (SEM)

Figure 6.18 and Figure 6.19 show the scanning electron microscopy (SEM) images of aluminum and aluminum oxide. Both aluminium powder and aluminium oxide powder have an irregular shape. Aluminum powder is composed of smaller grains,

where aluminum oxide powder is composed of bigger grains and has a more compact structure.

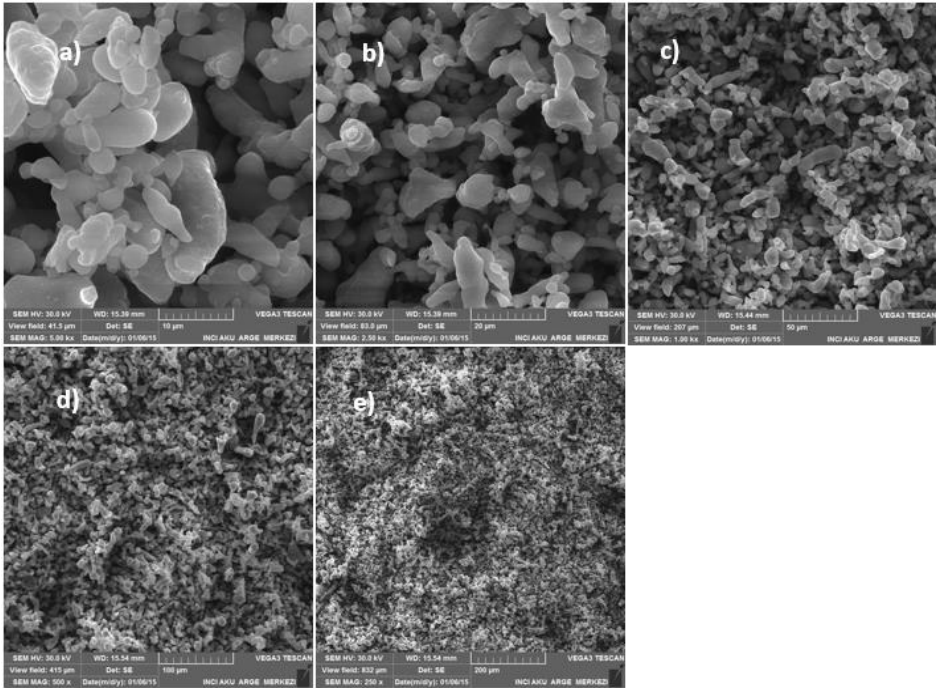


Figure 6.18 : SEM images of Al: a) 5.0kx, b) 2.5kx, c) 1.0kx, d) 500x, e) 250x.

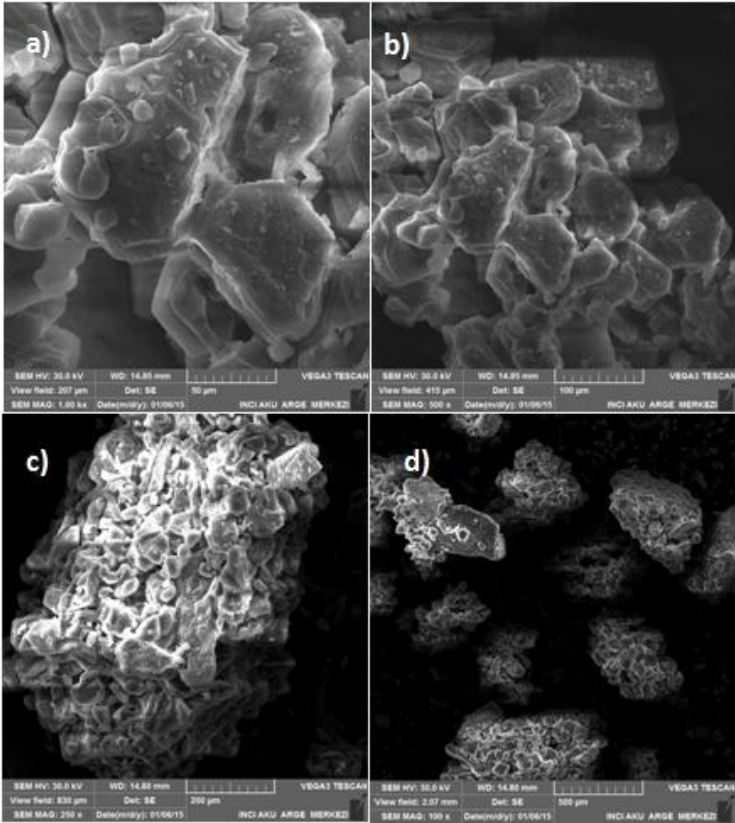


Figure 6.19 : SEM images of Al₂O₃: a) 1.0kx, b) 500x, c) 250x, d) 100x.

Figure 6.20 and Figure 6.21 exhibit the images of aluminium oxide/silicon dioxide/graphite composite, which are mixed with a ratio of 54:15:31 and 27:39:33 weight percentages, respectively. The eutectic Al–Si exhibits a very different hardness and mechanical property than that of Al. Eutectic Al–Si is used to make engine blocks due to its high fatigue strength and good wear resistance. In both composites, some of the spheres of the Al–Si could still be found. The local microstructure of the Al–Si is maintained and simply buried in the carbon matrix after milling.

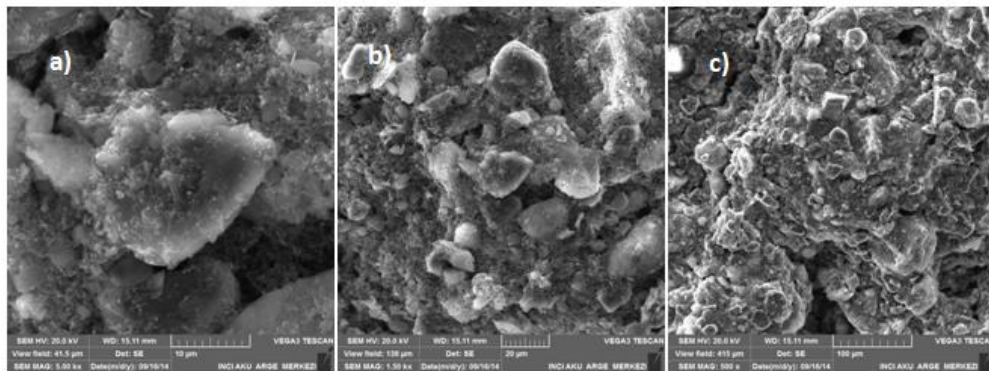


Figure 6.20 : SEM images of Al₂O₃:SiO₂:graphite composite at 54:15:31 wt%: a) 5.0kx, b) 1.5kx, c) 500x.

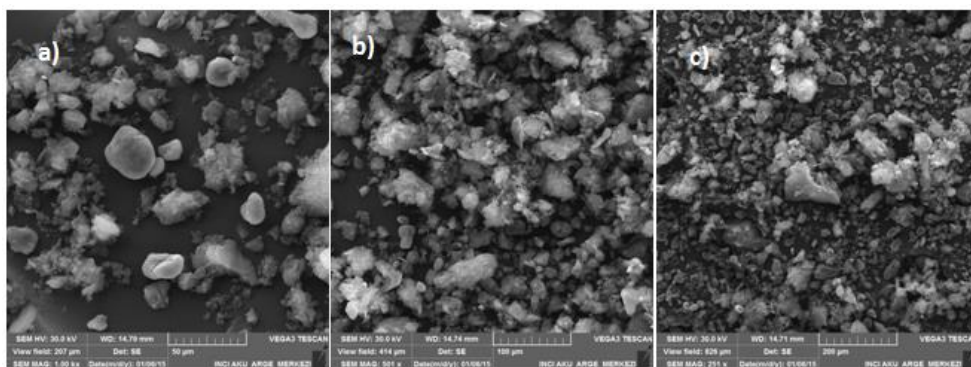


Figure 6.21 : SEM images of Al₂O₃:SiO₂:graphite composite at 27:39:33 wt%: a) 1.0kx, b) 501x, c) 251x.

Figure 6.22 and Figure 6.23 exhibit SEM images of composite of aluminium oxide and aluminium with graphite, both with a mixing ratio of Al:Graphite = 67:33 weight percentages. Structures of composites are very different.

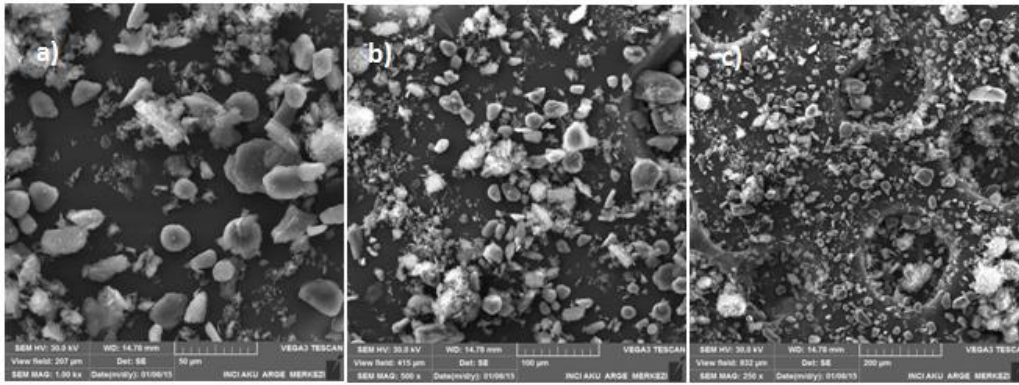


Figure 6.22 : SEM images of Al:graphite = 67:33 wt% by using Al_2O_3 : a) 1.0kx, b) 500x, c) 250x.

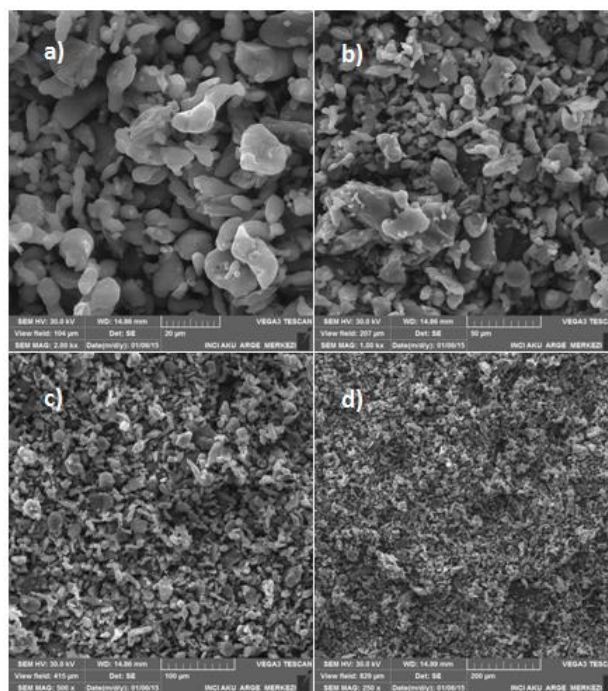


Figure 6.23 : SEM images of Al:graphite = 67:33 wt% by using Al: a) 2.0kx, b) 1.0kx, c) 500x, d) 210x.

6.3.1.2 Results of thermogravimetric analyses (TGA)

Aluminum oxide and aluminum contents of the composites were also determined from TGA measurements. The weight loss at temperatures between 300-950 °C in the TGA graphs was attributed to the oxidation of graphite in the composite and the results were given in Table 6.3 by comparing with the targetted inclusion levels. TGA results show that aluminum oxide and aluminum inclusion levels for Al 2, Al 3, Al 4 samples were similar to targetted levels. For sample Al 1, aluminum oxide inclusion level was found higher than expected. Sample Al 1 was mixed with IKA

universal mill M20 and it may be possible that aluminum oxide powder loss from the composite occurred during milling.

Table 6.3 : TGA results of Al₂O₃ and Al mixed graphite samples.

Sample Name	Sample Content	Al ₂ O ₃ Content, %	Al ₂ O ₃ + SiO ₂ Content, %
Al 1	Al ₂ O ₃ :SiO ₂ :Graphite = 54:15:31 wt%	-	85
Al 2	Al ₂ O ₃ :SiO ₂ :Graphite = 27:39:33 wt%	-	67
Al 3	Al:Graphite = 67:33 wt% by using Al ₂ O ₃	85	-
Al 4	Al:Graphite = 67:33 wt% by using Al	79	-

Table 6.4 shows the TGA results comparison of sample Al 3, which was both prepared via agate mortar and ball miller. Both results are similar to targetted level.

Table 6.4 : TGA results comparison of sample prepared by agate mortar and ball miller.

Sample Name	Sample Content	Prepared by Using	Al ₂ O ₃ Content, %
Al 3	Al:Graphite = 67:33 wt% by using Al ₂ O ₃	Agate Mortar	85
		Ball Miller	77

6.3.2 Results of coin battery performances

Same approach, as stated in section 6.1.2 applied for aluminum and aluminum oxide mixed graphite samples as well.

The comparison of capacity decrease slop of different mixing mass ratio of aluminum and aluminum oxide mixed graphite samples was shown in Figure 6.24 with regard to artificial graphite as reference.

Figure 6.24 shows discharge capacities of Al 3 and 4 samples (Al:graphite = 67:33 wt% by using aluminum and aluminum oxide) for the first 5 cycles, which were charged at C/4 ratio and discharged at C/3 ratio. Moreover, specific discharge capacity of SiO₂ added Al₂O₃/graphite composites and artificial graphite is shown for comparison.

Accordingly, it can be concluded that except Al 3 sample (Al:graphite = 67:33 wt% by using Al₂O₃), all samples showed superior initial capacity versus artificial

graphite. It is obvious that addition of Al rather than Al₂O₃ has a greater impact on improving the battery performance. Moreover, when capacities of Al₂O₃ mixed graphite composites were compared, the benefit of SiO₂ addition to composites can be seen clearly. Eventhough the greatest initial capacity was reached with the sample containing the highest SiO₂ level, most stable profile was achieved Al 1 sample (Al₂O₃:SiO₂:graphite = 54:15:31 wt%). This can be directly linked with the volume change of SiO₂ during cycling. Zhang [62] introduced an explanation for volume change and its effect: The volume expansion triggers the cracking and pulverization of active particles as well as the surrounding of the carbon matrix. These lead to the disconnection of active particles from the conductive carbon. Due to the disconnection of active particles and the carbon matrix, internal resistance of anode during de-intercalation is increased and the reaction cannot be completed. It results in an irreversible loss, which can also be seen in Figure 6.24.

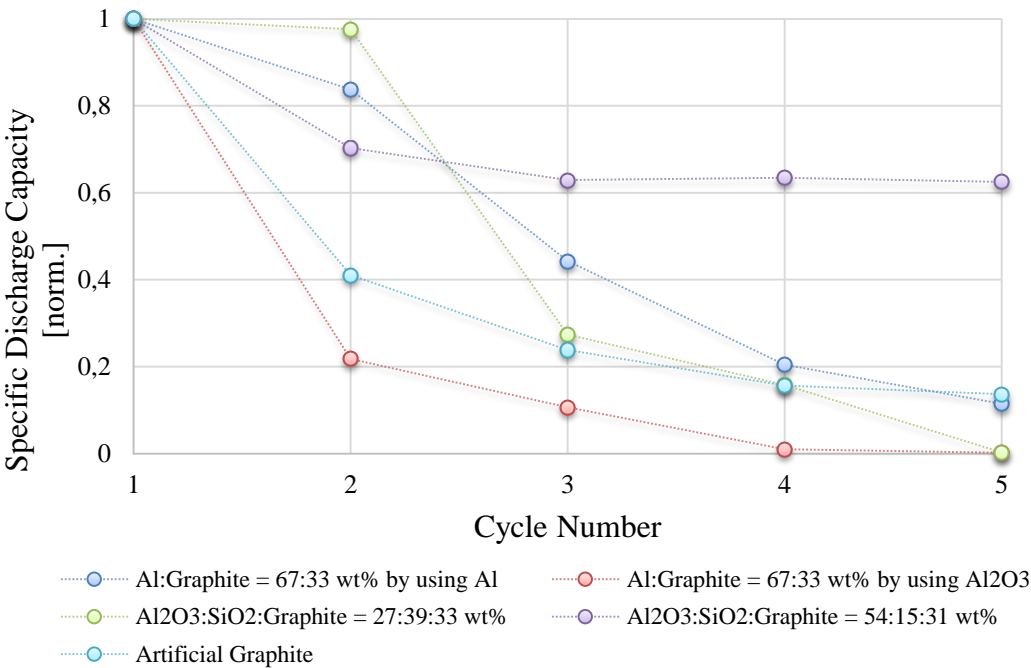


Figure 6.24 : Normalized specific capacity comparison of Al₂O₃ mixed graphite.

Figure 6.25, Figure 6.12, Figure 6.26 and Figure 6.27 show the charge and discharge curves of Al 1 (Al₂O₃:SiO₂:Graphite = 54:15:31 wt%), Al 2 (Al₂O₃:SiO₂:graphite = 27:39:33 wt%) and Al 4 sample (Al:graphite = 67:33 wt% by using Al samples), respectively, for the first 2 cycles in the voltage range of 0.01-4.5V. Black lines indicate charge and red lines indicate the discharge. In Figure 6.25, capacity loss can

be observed in A 1 sample ($\text{Al}_2\text{O}_3:\text{SiO}_2:\text{graphite} = 54:15:31$ wt%) after the 1st cycle, while for both Al 2 ($\text{Al}_2\text{O}_3:\text{SiO}_2:\text{Graphite} = 27:39:33$ wt%) and Al 4 ($\text{Al}:\text{graphite} = 67:33$ wt% by using Al) samples feature a constant specific capacity.

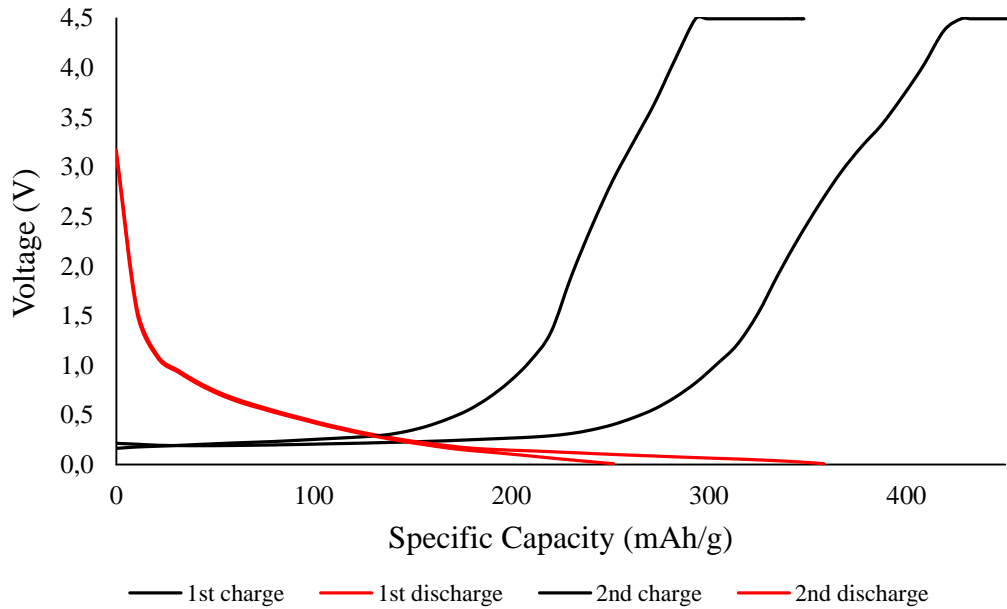


Figure 6.25 : Specific capacity vs voltage for $\text{Al}_2\text{O}_3:\text{SiO}_2:\text{graphite} = 54:15:31$ wt%.

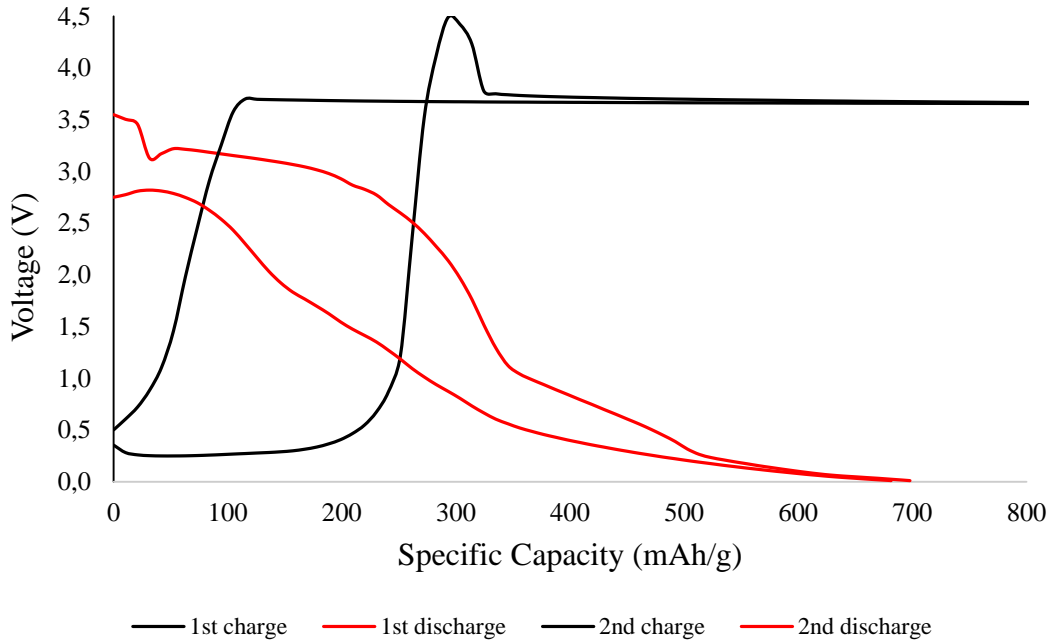


Figure 6.26 : Specific capacity vs voltage for $\text{Al}_2\text{O}_3:\text{SiO}_2:\text{graphite} = 27:39:33$ wt%.

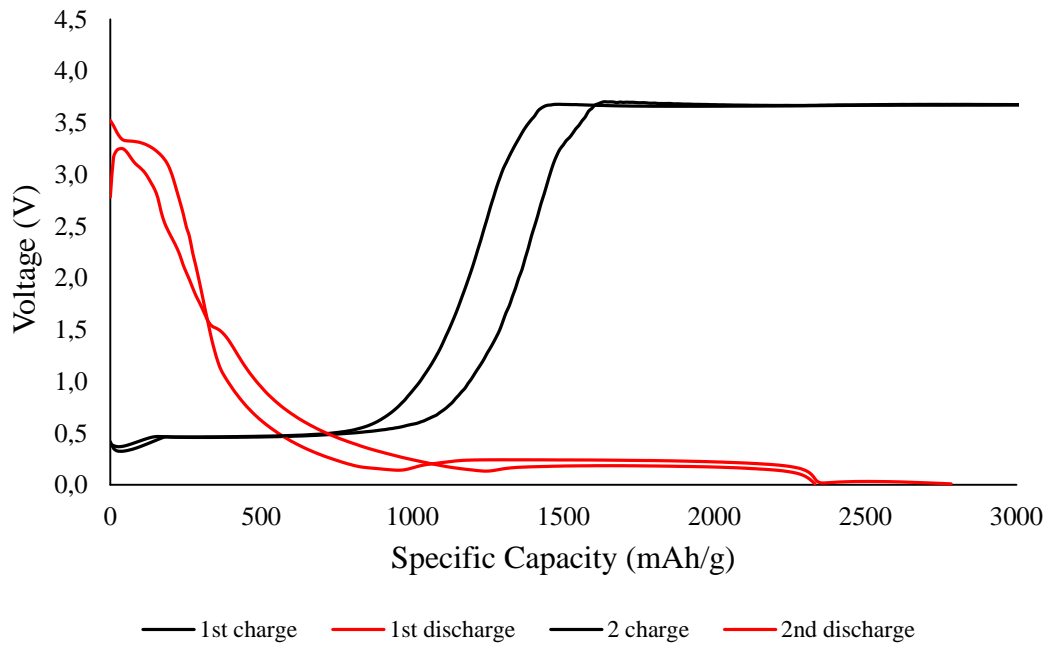


Figure 6.27 : Specific capacity vs voltage for Al:graphite = 67:33 wt% by using Al.

As mentioned in section 6.1.2 the discharge profile can be divided into 3 regions. While SiO₂-mixed samples from section 6.1.2 only feature so-called “the constant voltage plateau” and “after the constant voltage plateau” region, aluminum and aluminum oxide mixed graphite samples exhibit the “before” and “after the constant voltage plateau” characteristics. “Before the constant voltage plateau” region corresponds to the solid-solution reaction from one amorphous alloy structure to another amorphous alloy structure without a phase change, which causes in the constant voltage plateau. As a result, the discharge profile is a sloping voltage curve.

However, an increase in the mixing mass ratio of SiO₂ in the mixture leads to a phase changing characteristic, also known as the biphasic domain, as can be seen in Figure 6.26. Furthermore, a decline of the starting voltage can be observed with Al 1 sample (Al₂O₃:SiO₂:graphite = 54:15:31 wt%) after the 1st cycle. The reason of both the voltage and the specific capacity decline can be identified as the SiO₂, since the same behavior can also be observed with the SiO₂-mixed samples from section 6.1.2, but not with the Al 1 (Al₂O₃:SiO₂:graphite = 54:15:31 wt%) and Al 4 (Al:graphite = 67:33 wt% by using Al) samples. It can be interpreted that the amorphization process in the biphasic domain leads to a structural degradation of the anode material mixture, which results in a capacity loss. Thus, for a stable operation, optimum level of SiO₂ should be considered in the composite to increase the capacity and minimize the volume expansion.

Table 6.5 shows the specific discharge capacities at 1st, 5th and 10th of cycles and conservation of capacity at 5th and 10th cycles. According to the results, while discharge capacity was conserved at 63% and 38% after 5 and 10 cycles for Al 1 (Al₂O₃:SiO₂:graphite = 54:15:31 wt%), discharge capacity was only conserved at 11% and 1% after 5 and 10 cycles for Al 4 (Al:graphite = 67:33 wt% by using Al), respectively.

Table 6.5 : Specific discharge capacities of Al and Al₂O₃ mixed graphite and conservation of it.

Sample	Specific Discharge Capacity, mAh/g			Conservation of Capacity, %	
	1 st Cycle	5 th Cycle	10 th Cycle	5 th Cycle	10 th Cycle
Al ₂ O ₃ :SiO ₂ :Graphite = 54:15:31 wt%	358	224	135	63	38
Al:Graphite = 67:33 wt% by using Al	2783	318	23	11	1

6.4 Results of Boron Mixed Graphite Materials

To improve the performance of lithium ion batteries, researches have been going on to develop new anode materials with metals, which have a higher lithium storage capacity. Boron doping into carbon is one of the well-known methods to improve discharge capacity characteristics and coulombic efficiency of the carbon anode materials. The variation of the chemical potential of intercalated lithium in graphite and boron mixed graphite has been shown and it was suggested that boron doping affects charge-discharge profile around 1.2V [68, 69].

Tanaka et al. [68] investigated the anode property of boron mixed graphite materials for rechargeable lithium ion batteries by means of electrochemical measurements. It was found out that in terms weight, 5% boron mixed anode delivers the most promising discharge capacity of 315 mAh/g in the investigated range between 0% and 10% boron mixing ratio, while that of 10% boron mixed anode delivers 265 mAh/g, which is almost the same as that of boron-free sample.

Zhou et al. [69] investigated the properties of graphitized boron doped coal-based coke powders as anode for lithium ion batteries. Furthermore, effects of boron content and graphitization temperature on the anode for lithium ion batteries were

investigated in their study. It was found out that the reversible capacity of boron doped coal-based sample is about 360.3 mAh/g, while that of unboron doped is 292.9 mAh/g.

Wu et al. [70] investigated boron-doped graphene, used as an anode in lithium ion batteries. The study showed that superior charge/discharge performances can be achieved by boron doping. The reversible capacity of the boron doped graphene in first cycle and after 30 cycles were measured as 1549 mAh/g and 1227 mAh/g, respectively, which are much higher than pristine graphene (955 mAh/g in the first cycle and 638 mAh/g after 30 cycles).

In this study, samples were prepared by mixing graphite with different mass ratio of B. Anode material characterization has been undertaken by means of SEM and TGA analyses. Then, galvanostatic tests were conducted for battery performances. Results were presented and discussed in detail in Sections 6.4.1 and 6.4.2 .

6.4.1 Results of anode material properties

6.4.1.1 Results of scanning electron microscopy (SEM)

Figure 6.28 shows the SEM images of boron powder. It has an agglomerated structure.

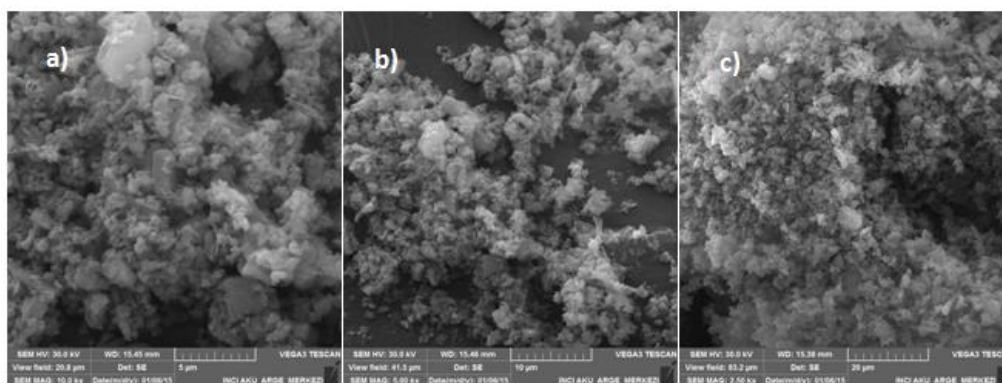


Figure 6.28 : SEM images of B powder: a) 10kx, b) 5.0kx, c) 2.5kx.

Figure 6.29 - Figure 6.31 exhibit SEM images of boron/graphite composites, which were mixed with a ratio of 2.5:97.5, 5:95 and 7.5:92.5 weight percentages, respectively. SEM images show that boron was observed on graphite surface and it dispersed homogenously.

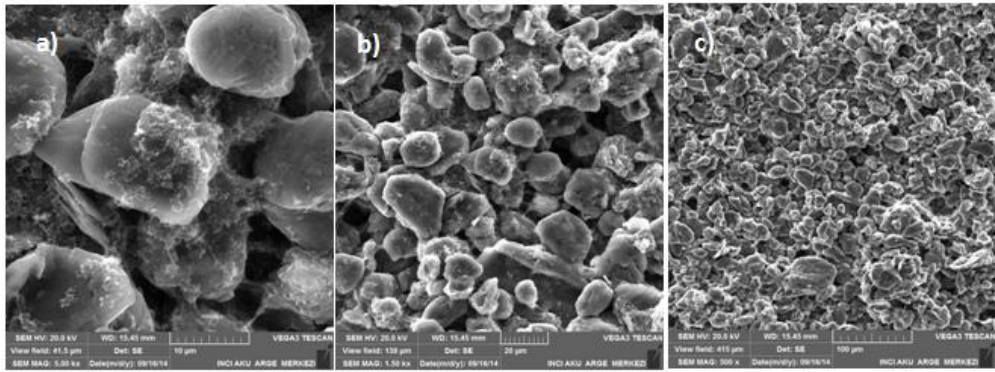


Figure 6.29 : SEM images of B:graphite = 2.5:97.5 wt%: a) 5.0kx, b) 1.5kx, c) 500x.

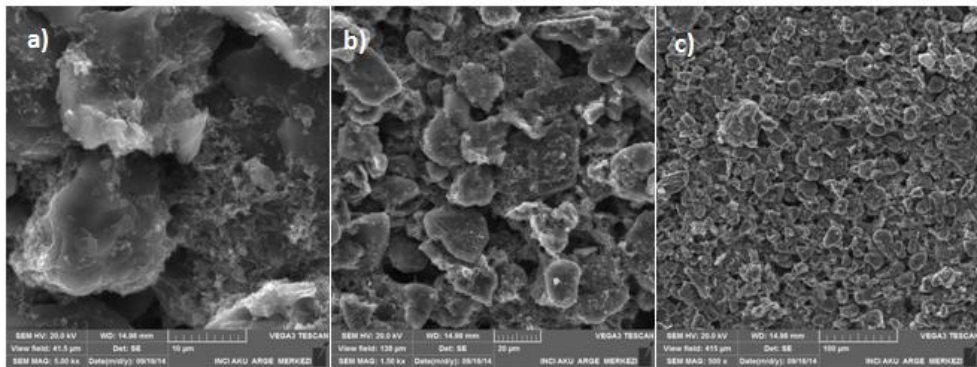


Figure 6.30 : SEM images of B:graphite = 5:95 wt%: a) 5.0kx, b) 1.5kx, c) 500x.

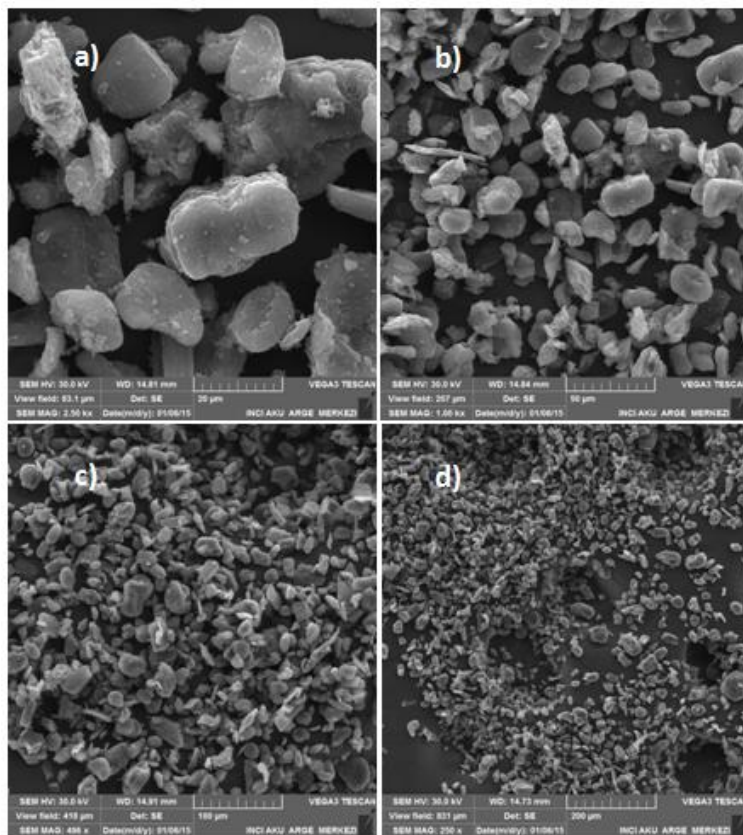


Figure 6.31 : SEM images of B:graphite = 7.5:92.5 wt%: a) 2.5kx, b) 1.0kx, c) 496x, d) 250x.

6.4.1.2 Results of thermogravimetric analyses (TGA)

Boron contents of the boron/graphite composites were determined from TGA measurements. The weight loss at temperatures between 300-950 °C in the TGA graphs was attributed to the oxidation of graphite in the composite and the results were given in Table 6.6 by comparing targetted inclusion levels. TGA results show that boron inclusion level for sample B 1 is lower than expected and for sample B 2 higher than expected. These samples were mixed with IKA universal mill M20 and it may be possible that boron or graphite loss from the composite occurred during milling. The boron inclusion level for sample B 3, which was mixed by using agate mortar, is at the target level.

Table 6.6 : TGA results of B mixed graphite samples.

Sample Name	Sample Content	B ₂ O ₃ Content, %
B 1	B:Graphite = 2.5:97.5 wt%	6
B 2	B:Graphite = 5:95 wt%	17
B 3	B:Graphite = 7.5:92.5 wt%	24

6.4.2 Results of coin battery performances

Same approach, as stated in section 6.1.2 is applied for boron mixed graphite samples as well.

The comparison of capacity decrease slop of different mixing mass ratio of aluminum and aluminum oxide mixed graphite samples was shown in Figure 6.32 with regard to artificial graphite as reference.

Figure 6.32 shows discharge capacities of 2.5 wt%, 5 wt% and 7.5 wt% boron mixed graphite samples and artificial graphite for the first 5 cycles, which were charged at C/4 ratio and discharged at C/3 ratio. For the first cycle, discharge capacities of samples are 893 mAh/g, 1077 mAh/g and 957 mAh/g for 2.5 wt%, 5 wt% and 7.5 wt% boron mixed graphite, respectively. In agreement with literature data, 5 wt% boron mixed graphite delivers the highest discharge capacity among all samples and is also greater than that of the artificial graphite.

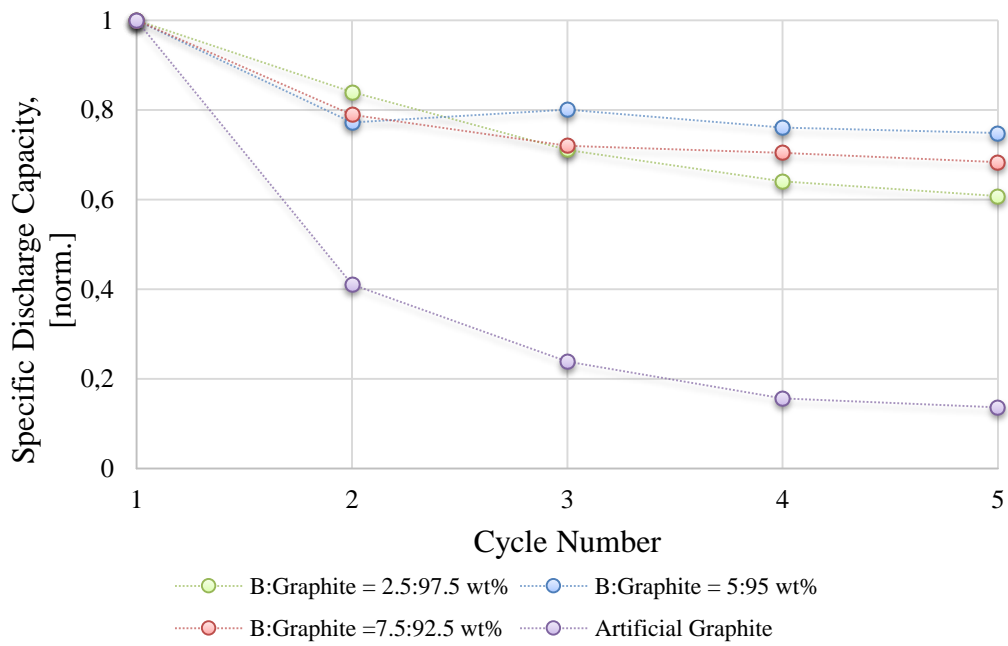


Figure 6.32 : Normalized specific capacity comparison of B mixed graphite samples.

Figure 6.33 shows the charge and discharge curves of 5 wt% boron mixed graphite sample for the first 2 cycles in the voltage range of 0.01-4.5V. Black lines indicate charge and red lines indicate the discharge. After 1st cycle, the capacity drops from 1077 to 832 mAh/g, which can be explained with the formation of the solid electrolyte interphase (SEI) films.

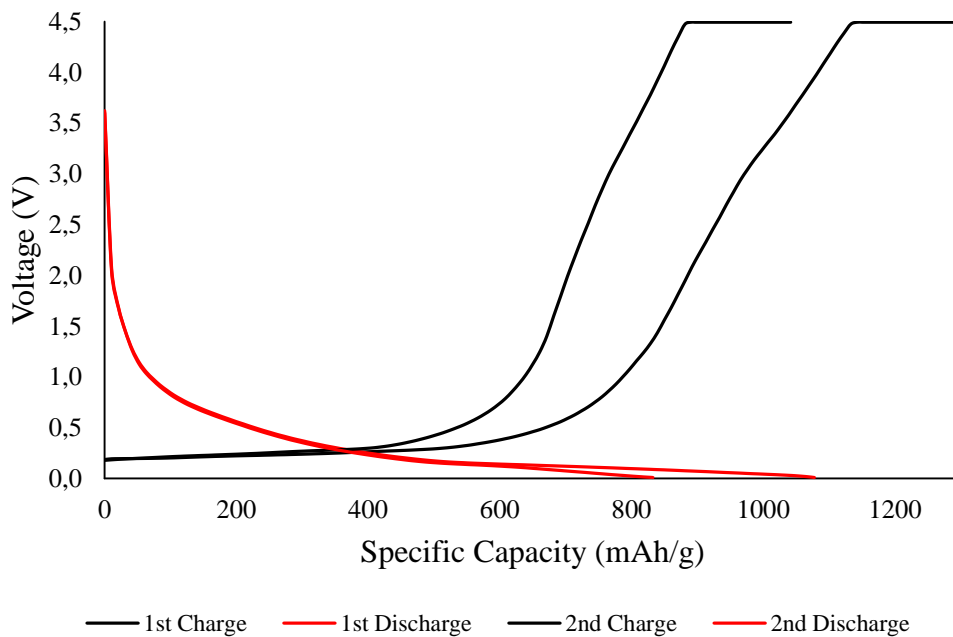


Figure 6.33 : Specific capacity vs voltage for 5 wt% B mixed graphite.

As mentioned in section 6.1.2 the discharge profile can be divided into 3 regions. While SiO₂-mixed samples from section 6.1.2 only feature so-called “the constant voltage plateau” and “after the constant voltage plateau” region, boron mixed graphite samples exhibit the “before” and “after the constant voltage plateau” characteristics. “Before the constant voltage plateau” region corresponds to the solid-solution reaction from one amorphous alloy structure to another amorphous alloy structure without a phase change, which causes in the constant voltage plateau. As a result, the discharge profile is a sloping voltage curve.

Table 6.7 shows the specific discharge capacities at 1st, 8th and 23rd cycles, and conservation of capacity at 8th and 23rd cycles. According to the results, discharge capacity was conserved at 74% and 43% after 8 and 23 cycles, respectively.

Table 6.7 : Specific discharge capacities of 5% wt B mixed graphite and conservation of capacity.

Sample	Specific Discharge Capacity, mAh/g			Conservation of Capacity, %	
	1 st Cycle	8 th Cycle	23 rd Cycle	8 th Cycle	23 rd Cycle
B:Graphite = 5:95 wt%	1077	792	466	74	43

7. OVERALL RESULTS AND RECOMMENDATION

In this work, properties and battery performances of metal or metal oxide mixed graphite anode for lithium ion batteries have been investigated. Silicon dioxide, tin, aluminum, aluminium oxide and boron were used as additives. In addition to that, MgO and AgNO₃ were used to enhance the battery performance. Samples were prepared by mixing mechanically. No other treatment has been applied. Samples' characterizations have been conducted via scanning electron microscopy (SEM) and thermogravimetric analyses (TGA). After the fabrication of coin lithium ion batteries with prepared samples, galvanostatic measurements were undertaken to investigate the battery performances.

At the early stage of sample preparation, IKA universal mill M20 was used for the mechanical mixing. During milling, sample loss was observed, which was also confirmed by the TGA results. For this reason, Hi-Quality natural agate mortar was used for the following sample preparation, where the composition content was confirmed by TGA measurements. Furthermore, one of the samples was prepared via ball miller to make a correlation with the sample prepared by agate mortar. TGA results affirmed that the compositions' contents of both samples are similar and agreeing with target level.

All metals and metal oxides' structures were investigated individually and on the graphite surface by means of SEM. In the light of SEM images, it can be concluded that mixing was done homogeneously and each structure can be detected on graphite surface.

The battery performances were investigated by means of galvanostatic measurements. At the galvanostatic measurement of some samples, systematic measurement errors occurred. Although the absolute values of some samples cannot be used directly, conservation of specific capacity can be compared for all samples by normalizing measurement data to their corresponding start value.

When battery performance of silicon dioxide mixed graphite samples were examined, it can be commented that certain amount of SiO_2 addition increases the initial discharge capacity compared to artificial graphite. Addition of Sn to SiO_2 /graphite composite delivers the highest initial discharge capacity among all samples. However, due to loss of active matter and SEI formation at the initial cycles, stable discharge capacity cannot be met for all samples.

At the galvanostatic measurement of Sn mixed graphite, no proper battery operation can be performed resulting from using a mean diameter of about 600 μm particle sized Sn powder, which leads flaking at every coating of the tin mixed slurry. Since the diameter of the tin particles could not be reduced further with agate mortar, the qualitative research of tin mixed graphite could not be undertaken. The use of nanosized particle Sn is recommended for appropriate sample preparation and accurate galvanostatic measurements.

When aluminum and aluminum oxide mixed graphite composites' battery performances were investigated, the addition of Al and Al_2O_3 at certain level to graphite resulted in higher initial specific capacity than that of pure artificial graphite. In spite of the fact that even the highest initial discharge capacity could not be reached, dual usage of Al_2O_3 and SiO_2 delivered the most stable discharge capacity profile among all samples. However, none of the samples showed proper running battery profile due to the irreversible capacity losses during first cycle.

During the investigation of battery performances of boron mixed graphite, it can be clearly observed that all samples showed superior initial capacity compared to that of artificial graphite. In addition to that, after irreversible capacity loss at the first cycle, the capacity stayed stable at the following cycles with minor changes.

In summary, within the framework of the thesis, SiO_2 , Sn, Al, Al_2O_3 and B were mixed with graphite to improve the battery performance of lithium ion batteries. This study confirms that initial discharge capacities can be improved by preparing the anode as composites, which consists of metals or metals oxides and graphite, as long as the size of the used particles is in nm-region. Among all samples, B-mixed graphite samples showed most stable capacity profile at cycling, which makes the B-mixed graphite a good candidate as anode material in lithium ion batteries. For a more stable battery performance, further investigation on optimization of irreversible

capacity loss at initial cycles should be examined, which would be considered as a new subject for next studies.

REFERENCES

- [1] **Linden, D. and Reddy, T. B.** (2002). Handbook of batteries, McGraw-Hill..
- [2] **Berndt, D.** (1993). A Handbook of Battery Technology, Research Studies Press.
- [3] **Dell, R. M. and Rand, D. A. J.** (2001). Understanding batteries, Royal Society of Chemistry (Great Britain).
- [4] **Tarkoma, S., Siekkinen, M., Lagerspetz, E. and Xiao, Y.** (2014). Smartphone Energy Consumption: Modeling and Optimization, Cambridge University Press.
- [5] **Fransson, L.** (2002). Design and characterisation of new anode materials for lithium-ion batteries, Uppsala: Acta Universitatis Upsaliensis (dissertation).
- [6] **Williamson, S. S.** (2013). Energy Management Strategies for Electric and Plug-in Hybrid Electric Vehicles, Springer.
- [7] **Team, M. E. V.** (2008). "A Guide to Understanding Battery Specification", MIT.
- [8] **Akkus, N., Saban, H., Göktepe, H., Kilic, F. and Patat, S.** (2010). "Şarj edilebilir lityum iyon bataryalarda katot aktif madde olarak kullanılan LiMn_2O_4 bileşiğine değişik metal katkılamının elektrokimyasal performansına etkisi", Erciyes Üniversitesi (ERÜ) Fen Fakültesi (master's thesis).
- [9] **Pistoia, G.** (2008). Battery Operated Devices and Systems: From Portable Electronics to Industrial Products, Elsevier Science.
- [10] **Pistoia, G.** (2005). Batteries for Portable Devices, Elsevier Science.
- [11] **Kiehne, H. A.** (2003). Battery Technology Handbook, CRC Press.
- [12] **Broussely, M. and Pistoia, G.** (2007). Industrial applications of batteries: from cars to aerospace and energy storage, Elsevier Science.
- [13] **Paravasthu, R.** (2012). Synthesis and characterization of lithium-ion cathode materials in the system $(1-x-y) \text{LiNi/Mn/3Co/3O}_2 \cdot x\text{Li}_2\text{MnO}_3 \cdot y\text{LiCoO}_2$, Mechanical Engineering of Colorado State University (master's thesis).
- [14] **Patey, T. J.** (2009). Oxide nanoparticles for electrodes in lithium-ion batteries, Eidgenössische Technische Hochschule ETH Zürich, (dissertation).
- [15] **Yao, Y.** (2008). A study of electro materials for lithium-ion batteries, Institute for Superconducting and Electronic Materials, University of Wollongong (dissertation).
- [16] **Url-1** <<http://www.sony.com.cn/products/ed/battery/download.pdf>>, date retrieved: 03.09.2014.

- [17] **Nazri, G. A. and Pistoia, G.** (2003). *Lithium Batteries*, Springer.
- [18] **Tarascon, J. M. and Armand, M.** (2001). "Issues and challenges facing rechargeable lithium batteries," *Nature*, vol. 414, pp. 359-367, 11.
- [19] **Yang, M.** (2012). Strategies to improve the electrochemical performance of electrodes for Li-ion batteries, University of Florida (dissertation).
- [20] **Ozawa, K.** (2009). *Lithium Ion Rechargeable Batteries*, 1. Edition ed., Wiley-VCH.
- [21] **Gullbrekken, Ø.** (2012). Thermal characterisation of anode materials for Li-ion batteries, Institutt for materialteknologi of Norwegian University of Science and Technology (dissertation).
- [22] **Zhao, M.** (2001). Electrochemical studies of lithium-ion battery anode materials in lithium-ion battery electrolytes, College of Arts and Sciences of Ohio University (dissertation).
- [23] **Wakihara, M.** (2001). "Recent developments in lithium ion batteries," *Materials Science and Engineering*, vol. R33, pp. 109-134, February.
- [24] **Patterson, M. L.** (2009). "Anode Materials for Lithium Ion Batteries, November (dissertation).
- [25] **DiLeo, R.** (2012). The development of nanomaterials for high performance lithium ion battery anodes, Rochester Institute of Technology (dissertation).
- [26] **van Schalkwijk, W.** (2002). *Advances in Lithium-Ion Batteries*, B. Scrosati, Ed., Springer.
- [27] **Simpson, C.** (2011). Texas Instruments, "Characteristics of Rechargeable Batteries".
- [28] **Daniel, C.** (2011). *Handbook of battery materials*, 2., vollst. überarb. u. erw. Auflage ed., J. O. Besenhard, Ed., Weinheim: Wiley-VCH.
- [29] **Park, J.-K.** (2012). *Principles and Applications of Lithium Secondary Batteries*, J. Park, Ed., Wiley-VCH Verlag GmbH & Co. KGaA.
- [30] **Zhong, C.** (2010). Development of new electrode materials for lithium ion batteries, Research thesis ed., Institute for Superconducting & Electronic Materials - Faculty of Engineering, University of Wollongong (dissertation).
- [31] **Huang, R. and Ikuhara, Y.** (2012). "STEM characterization for lithium-ion battery cathode materials," *Current Opinion in Solid State & Materials Science*, vol. 16, no. 1, pp. 31-38.
- [32] **Eckert, M.** (2012). "Max von Laue and the discovery of X-ray diffraction in 1912," *Annalen der Physik*, vol. 524, no. 5, p. A83–A85, May.
- [33] **Röntgen, W. C.** (1986). "On a new kind of rays," *Science*, vol. 3, no. 59, pp. 227-231, 2.
- [34] **Leng, Y.** (2009). *Materials characterization: Introduction to microscopic and spectroscopic methods*, John Wiley & Sons.
- [35] **von Ardenne, M.** (1938). "Das Elektronen-Rastermikroskop," *Zeitschrift für Physik*, vol. 109, no. 9-10, pp. 553-572.

- [36] **Boucher, A., Ducey, M. and McNeff, N.** (2009). Synthesis, characterization and electrochemical performance of $\text{Li}_2\text{Fe}_x\text{Mn}_{1-x}\text{SiO}_4/\text{C}$ as cathode material for thin-film lithium-ion batteries, Major Qualifying Project Report ed., Worcester: Worcester Polytechnic Institute (bachelor's thesis).
- [37] **Url-2** <<http://www.tescan.com/en/products/vega-sem/vega3-sb.>>, date retrieved: 03.09.2014.
- [38] **Knoll, M. and Ruska, E.** (1932). "Das Elektronenmikroskop," *Zeitschrift für Physik*, vol. 78, no. 5-6, pp. 318-339.
- [39] **Raman, C. V.** (1928). "A new radiation," *Indian Journal of physics*, vol. 2, pp. 387-398.
- [40] **Brunauer, S., Emmett, P. H. and Teller, E.** (1938). "Adsorption of gases in multimolecular layers," *J. Am. Chem. Soc.*, vol. 60, no. 2, p. 309-319.
- [41] **Url-3** <<http://www.tainstruments.com/product.>>, date retrieved: 13.12.2014.
- [42] **Kissinger, P. T. and Heineman, W. R.** (1983). "Cyclic voltammetry," *J. Chem. Educ.*, vol. 60, no. 9, p. 702.
- [43] **Reece, C.** (2008). "An Introduction to Electrochemical Impedance Spectroscopy".
- [44] **Url-4** <<http://www.mtixtl.com/8ChannelsBatteryAnalyzer-BST8-WA.aspx.>>, date retrieved: 13.12.2014.
- [45] **Breitkopf, C.** (2012). "Impedance spectroscopy: old technique new applications," Dresden.
- [46] **Yoshino, A.** (2014). "Development of the Lithium-Ion Battery and Recent Technological Trends," in *Lithium-Ion Batteries Advances and Applications*, Oxford, Elsevier, pp. 1-20.
- [47] **Zhou, W., Upreti, S. and Whittingham, M. S.** (2011). "High performance Si/MgO/graphite composite as the anode for lithium-ion batteries," *Electrochemistry Communications*, vol. 13, no. 10, pp. 1102-1104.
- [48] **Huber, N. S. and Hudak, D. L.** (2011). "Nanostructured lithium-aluminum alloy electrodes for lithium-ion batteries," *ECS Transactions*, pp. 1-13.
- [49] **Wu, J., Zhu, Z., Zhang, H., Fu, H., Li, H., Wang, A. and Zhang, H.** (2014). "A novel nano-structured interpenetrating phase composite of silicon/graphite-tin for lithium-ion rechargeable batteries anode materials," *Journal of Alloys and Compounds*, pp. 86-91, 5 May.
- [50] **Url-5** <http://www.ika.de/owa/ika/catalog.product_detail.>, date retrieved: 12.01.2015.
- [51] **Url-6** <<http://www.mtixtl.com/5hi-qualitynatureagatemortarandpestlebestdeal-opmta-5.aspx.>>, date retrieved: 12.01.2015.
- [52] **Wang, X., Wen, Z., Lin, B., Wu, X and Xu, X.,** (2008) "Preparation and electrochemical characterization of tin/graphite/silver composite as anode materials for lithium-ion batteries," *Journal of Power Sources*, vol. 184, no. 2, p. 508-512, 10.
- [53] **Zhou, W., Upreti, S. and Whittingham, M. S.** (2011). "Electrochemical

performance of Al–Si–graphite composite as anode for lithium-ion batteries," *Electrochemistry Communications*, vol. 13, no. 2, pp. 158-161.

- [54] **Url-7** <<http://www.mtixtl.com/CompactTapeCastingFilmCoater-MSK-AFA-III.aspx>>, date retrieved: 13.12.2014.
- [55] **Url-8** <<http://www.binder-world.com/en/vacuum-drying-oven/vdl-series/vdl-23/>>, date retrieved: 13.12.2014.
- [56] **Url-9** <<http://www.mtixtl.com/PrecisionDiscCutter-MSK-T-06.aspx>>, date retrieved: 13.12.2014.
- [57] **Sakamoto, K. M.** (2011). Development of nanoporous carbide-derived carbon electrodes for high performance lithium ion batteries, California: Naval Postgraduate School (dissertation).
- [58] **Url-10** <<http://www.mtixtl.com/CompactHydraulicCoinCellDisassemblingMachine-MSK-110D.aspx>>, date retrieved: 13.12.2014.
- [59] **Sun, Q., Zhang, B. and Fu, Z. W.** (2008). "Lithium electrochemistry of SiO₂ thin film electrode for lithium ion batteries," *Applied Surface Science*, vol. 254, pp. 3774-3779.
- [60] **Guo, B., Shu, J., Wang, Z., Yang, H., Shi, L., Liu, Y. and Chen L.** (2008). "Electrochemical reduction of nano-SiO₂ in hard carbon as anode material for lithium ion batteries," *Electrochemical Communications*, vol. 10, pp. 1876-1878.
- [61] **Zuo, P., Yin, G., Yang, Z., Wang, Z., Cheng, X., Jia, D. and Du, C.** (2009). "Improvement of cycle performance for silicon/carbon composite used as anode for lithium ion batteries," *Materials Chemistry and Physics*, vol. 115, no. 2-3, p. 757–760, 6.
- [62] **Zhang, W. J.** (2011). "A review of the electrochemical performance of alloy anodes for lithium-ion batteries," *Journal of Power Sources*, vol. 196, pp. 13-24.
- [63] **Lafont, U., Carta, D., Mountjoy, G., Chadwick, A. V. and Kelder, E. M.** (2010). "In situ structural changes upon electrochemical lithium insertion in nanosized anatase TiO₂," *Journal of Phy. Chem.*, vol. 114, p. 1372–1378.
- [64] **Morishita, T., Hirabayashi, T., Okuni, T., Ota, N. and Inagaki, M.** (2006). "Preparation of carbon-coated Sn powders and their loading onto graphite flakes for lithium ion secondary battery," *Journal of Power Sources*, vol. 160, p. 638–644.
- [65] **Wang, G. X., Ahn, J., Lindsay, M. J., Sun, L., Bradhurst, D. H., Dou, S. X. and Liu, H. K.** (2001). "Graphite–Tin composites as anode materials for lithium-ion batteries," *Journal of Power Sources*, Vols. 97-98, pp. 211-215, 7.
- [66] **Hamon, Y., Brousse, T., Jousse, F., Topart, P., Buvat, P. and Scheich, D. M.** (2001). "Aluminum negative electrode in lithium ion batteries," *Journal of Power Sources*, Vols. 97-98, pp. 185-187.
- [67] **Chena, L. B., Xieb, J. Y., Yua, H. C. and Wanga, T. H.** (2008). "Si–Al thin film anode material with superior cycle performance and rate capability for lithium ion batteries," *Electrochimica Acta*, vol. 53, pp. 8149 - 8153.

- [68] **Tanaka, U., Sogabe, T., Sakagoshi, H., Ito, M. and Tojo, T.** (2001). "Anode property of boron-doped graphite materials for rechargeable lithium-ion batteries," *Carbon*, vol. 39, no. 6, p. 931–936, 5.
- [69] **Zhou, X., Ma, L., Yang, J., Huang, B., Zou, Y., Tang, J., Xie, J., Wang, S. and Chen, G.** (2013). "Properties of graphitized boron-doped coal-based coke powders as anode for lithium-ion batteries," *Journal of Electroanalytical Chemistry*, vol. 698, no. 1, p. 39–44, 6.
- [70] **Wu, Z. S., Ren, W., Xu, L., Li, F. and Cheng, H. M.** (2011). "Doped graphene sheets as anode materials with superhigh rate and large capacity for lithium ion batteries," *ACS Nano*, vol. 5, no. 7, pp. 5463-5471.

CURRICULUM VITAE



Name Surname: Handan Bakalci

Place and Date of Birth: Bergama/Izmir and 20 March 1986

E-Mail: handanbakalci@gmail.com

EDUCATION:

2009 – 2015 Istanbul Technical University (ITU), Istanbul, Turkey
Department: Energy Institute
Degree: *M.Sc in Energy Science & Technology (pending)*

2004 – 2009 Istanbul Technical University (ITU), Istanbul, Turkey
Department: Chemical Engineering
Degree: *B.Sc in Chemical Engineering*

2007 - 2008 Karlsruhe Institute of Technology (KIT), Karlsruhe, Germany
Department: Chemical Engineering
Degree: *B.Sc in Chemical Engineering (Erasmus Exchange Program)*

PROFESSIONAL EXPERIENCE:

04/2014 – present Unilever R&D Home Care
Powder Detergent Product Development Technologist
North Africa, Middle East & Turkey Region
Unilever, Istanbul, Turkey

03/2010 – 03/2014 Unilever R&D Home Care
Fabric Conditioner Product Development Technologist
North Africa, Middle East & Turkey Region
Unilever, Istanbul, Turkey